“EXPLORING THE STIM–ORAI INTERFACE IN THE ACTIVATION OF THE CRAC CHANNEL IN HELMINTH PARASITES”

“EXPLORANDO A INTERFACE STIM-ORAI NA ATIVAÇÃO DO CANAL CRAC EM PARASITOS HELMINTOS”

YHONY SUMARI MISAICO

STATE UNIVERSITY OF NORTHERN RIO DE JANEIRO DARCY RIBEIRO

CAMPOS DOS GOYTACAZES-RJ

FEBRUARY, 2026

“EXPLORING THE STIM–ORAI INTERFACE IN THE ACTIVATION OF THE CRAC CHANNEL IN HELMINTH PARASITES”

“EXPLORANDO A INTERFACE STIM-ORAI NA ATIVAÇÃO DO CANAL CRAC EM PARASITOS HELMINTOS”

YHONY SUMARI MISAICO

Thesis presented to the Center for Biosciences and Biotechnology at the State University of Northern Rio de Janeiro Darcy Ribeiro, as part of the requirements for obtaining the title of Master in Biosciences and Biotechnology.

ADVISOR: Prof. Dra. Ana Eliza Zeraik

STATE UNIVERSITY OF NORTHERN RIO DE JANEIRO DARCY RIBEIRO

CAMPOS DOS GOYTACAZES-RJ

FEBRUARY, 2026

FICHA CATALOGRÁFICA
UENF - Bibliotecas
Elaborada com os dados fornecidos pelo autor.

M678 Misaico, Yhony Sumari.

"EXPLORANDO A INTERFACE STIM-ORAI NA ATIVAÇÃO DO CANAL CRAC EM PARASITOS HELMINTOS". / Yhony Sumari Misaico. - Campos dos Goytacazes, RJ, 2026.

95 f. : il.
Inclui bibliografia.

Dissertação (Mestrado em Biociências e Biotecnologia) - Universidade Estadual do Norte Fluminense Darcy Ribeiro, Centro de Biociências e Biotecnologia, 2026.
Orientadora: Ana Eliza Zeraik.

1. CRAC channel. 2. STIM/Orai. 3. Ascaris lumbricoides . 4. Schistosoma mansoni. 5. calcium signaling. I. Universidade Estadual do Norte Fluminense Darcy Ribeiro. II. Título.

CDD - 570

“EXPLORING THE STIM–ORAI INTERFACE IN THE ACTIVATION OF THE CRAC CHANNEL IN HELMINTH PARASITES”

YHONY SUMARI MISAICO

Thesis submitted to the Center for Biosciences and Biotechnology at the State University of Northern Rio de Janeiro Darcy Ribeiro (UENF), as part of the requirements for obtaining the title of Master in Biosciences and Biotechnology.

Approved on February 11th, 2026.

Examination Committee:

Documento assinado digitalmente
gov.br
ANNA LVOVNA OKOROKOVA FACANHA
Data: 12/02/2026 17:06:57-0300
Verifique em https://validar.iti.gov.br

Prof. Dr. Anna Lvovna Okorokova Façanha
(Ph.D. in Biological Chemistry) – LFBM/UENF

Documento assinado digitalmente
gov.br
ERICA DE OLIVEIRA MELLO
Data: 12/02/2026 17:33:50-0300
Verifique em https://validar.iti.gov.br

Prof. Dr. Érica de Oliveira Mello
(Ph.D. in Biosciences and Biotechnology) – LFBM/UENF

Documento assinado digitalmente
gov.br
WALLANCE MOREIRA PAZIN
Data: 13/02/2026 08:03:43-0300
Verifique em https://validar.iti.gov.br

Prof. Dr. Wallance Moreira Pazin
(Ph.D. in Applied Physics to Medicine and Biology) – DFMFC/UNESP

Documento assinado digitalmente
gov.br
ANA ELIZA ZERAIK
Data: 12/02/2026 11:55:35-0300
Verifique em https://validar.iti.gov.br

Prof. Dr. Ana Eliza Zeraik
(Ph.D. in Biomolecular Applied Physics) – LQFPP/UENF
Advisor

To Almighty God, my parents Marisol, Amelia, Efrain and my siblings, who with great dedication help me become a better person.

ACKNOWLEDGMENTS

I am infinitely grateful to God Almighty for granting me wisdom, strength, and perseverance throughout this journey. I also deeply thank my family, who have been a constant source of motivation, encouragement, and unconditional support, inspiring me to move forward and never give up.

I would like to express my sincere gratitude to Professor Dr. Ana Eliza Zeraik for her patience, dedication, and unwavering support. Her guidance was fundamental to the development of this work and to my immersion in the fascinating world of membrane proteins, particularly the CRAC channel. Through her mentorship, I was able to understand its function from the most fundamental principles, which further strengthened my passion for scientific research.

I am profoundly grateful to Dr. Diego Antonio Leonardo Cabrejos, without whom pursuing graduate studies in Brazil would not have been possible. I consider him not only a mentor, but also a friend, whose trust and support have played a decisive role in making my dream of becoming a scientist a reality.

I would like to thank the members of the Biophysics and Biochemistry research group for their constant support and collaborative spirit. This group operates under the supervision of Dr. Ana Eliza Zeraik and Dr. Luis Mansor Basso, whose leadership and scientific rigor foster an inspiring research environment.

I am also thankful to the professors, technicians, and colleagues of the Laboratório de Biologia Celular e Tecidos for their support and assistance with confocal microscopy experiments. I am especially grateful to Prof. Jorge Hernández Fernández for his support in the *in silico* analyses, as well as to the other members of the Laboratório de Química e Função de Proteínas e Peptídeos. I also thank all professors of the Centro de Biociências e Biotecnologia at the Universidade Estadual do Norte Fluminense Darcy Ribeiro for their invaluable contributions to my academic training and scientific development.

I would like to acknowledge the coordination and administrative staff of the Programa de Pós-Graduação em Biociências e Biotecnologia for their availability, support, and patience throughout my graduate studies. A special acknowledgment is extended to the Universidade Estadual do Norte Fluminense Darcy Ribeiro for providing the laboratory infrastructure and equipment essential for the execution of this research.

Finally, I gratefully acknowledge the financial support that made this work possible. I thank the Coordenação de Aperfeiçoamento de Pessoal de Nível Superior (CAPES) – *Finance Code 001* for the scholarship support. This research was conducted using funding from the Fundação Carlos Chagas Filho de Amparo à Pesquisa do Estado do Rio de Janeiro (FAPERJ) through processes E-26/200.177/2023, E-26/211.860/2021, and E-26/210.094/2022. This research was also conducted using infrastructure funded by Finep under the FINEP/MCTI/FNDCT/PROINFRA 2021 program (Agreement No. 0.1.22.0442.00).

TABLE OF CONTENTS

LIST OF ABBREVIATIONS

Abbreviation	Definition
Al	*Ascaris lumbricoides*
*Al*Orai	*Ascaris lumbricoides* Orai
*Al*STIM	*Ascaris lumbricoides* STIM
*Al*STIM-CT	C-terminal domain of *Ascaris lumbricoides* STIM
ATP	Adenosine Triphosphate
Ca^{2+}	Calcium ion
$CaCl_2$	Calcium chloride
CAD	CRAC Activation Domain
CC	Coiled-Coil
CC2–CC3	Coiled-coil domains 2 and 3
CDC	Centers for Disease Control and Prevention
COILS	Coiled-coil prediction algorithm
CRAC	Calcium Release-Activated Calcium
CT	C-terminal
DMEM	Dulbecco's Modified Eagle Medium
DNA	Deoxyribonucleic Acid
DOPE	Discrete Optimized Protein Energy
DS	Drug Score
EGFP	Enhanced Green Fluorescent Protein
EGTA	Ethylene glycol-bis(β-aminoethyl ether)-N,N,N′,N′-tetraacetic acid
EF–SAM	EF-hand and Sterile Alpha Motif domain
ER	Endoplasmic Reticulum
ER–PM	Endoplasmic Reticulum–Plasma Membrane
FASTA	Text-based format for nucleotide or peptide sequences
FBS	Fetal Bovine Serum
FDA	Food and Drug Administration
Fpocket	Pocket detection and druggability prediction software
GFP	Green Fluorescent Protein
GRAVY	Grand Average of Hydropathicity
HEK293	Human Embryonic Kidney 293 cells
HEPES	4-(2-hydroxyethyl)-1-piperazineethanesulfonic acid
*Hs*Orai	*Homo sapiens* Orai
*Hs*STIM	*Homo sapiens* STIM
ID	Inhibitory Domain
KCl	Potassium chloride
kDa	Kilodalton
MD	Molecular Dynamics
mCherry	Monomeric red fluorescent protein
$MgCl_2$	Magnesium chloride
MES	2-(N-morpholino)ethanesulfonic acid
MODELLER	Comparative protein structure modeling software
MSA	Multiple Sequence Alignment

Abbreviation	Definition
NFAT	Nuclear Factor of Activated T cells
NMR	Nuclear Magnetic Resonance
NaCl	Sodium chloride
ORAI	Calcium channel pore-forming subunit
PBD	Polybasic Domain
pH	Potential of Hydrogen
PM	Plasma Membrane
RMSD	Root Mean Square Deviation
RMSF	Root Mean Square Fluctuation
SAM	Sterile Alpha Motif
*Sm*Orai	*Schistosoma mansoni* Orai
*Sm*STIM	*Schistosoma mansoni* STIM
SOAR	STIM-Orai Activating Region
SOCE	Store-Operated Calcium Entry
SERCA	Sarcoplasmic/Endoplasmic Reticulum Ca^{2+}-ATPase
STIM	Stromal Interaction Molecule
TG	Thapsigargin
TIRF	Total Internal Reflection Fluorescence
TM	Transmembrane
TMHMM	Transmembrane Hidden Markov Model
Tris	Tris(hydroxymethyl)aminomethane

LIST OF FIGURES

LIST OF TABLES

ABSTRACT

Store-operated calcium entry (SOCE), mediated by the STIM–Orai complex, represents a fundamental Ca^{2+} signaling pathway in metazoans, yet its molecular organization and regulatory mechanisms in helminth parasites remain poorly understood. In this study, we investigated the structural, functional, and regulatory features of STIM and Orai proteins from *Ascaris lumbricoides* and *Schistosoma mansoni*, with emphasis on CRAC channel activation, species-specific coupling, intracellular pH sensitivity, and the identification of parasite-selective inhibitory sites. Comparative sequence and structural analyses revealed that helminth STIM and Orai proteins preserve the core architectural elements required for CRAC channel function, including the EF–SAM Ca^{2+}-sensing domain, SOAR/CC2–CC3 activation region, and the four transmembrane helices forming the Orai pore. However, pronounced divergence was observed in regulatory regions, particularly the C-terminal polybasic domain of STIM, which is absent in *A. lumbricoides*. Confocal imaging using fluorescently tagged constructs demonstrated that *A. lumbricoides* EGFP-STIM fails to form puncta upon ER Ca^{2+} depletion when expressed alone, but efficiently clusters at ER–plasma membrane junctions when co-expressed with its cognate mCherry-Orai, indicating that direct STIM–Orai interaction compensates for reduced intrinsic membrane tethering. The experimental combinations performed demonstrated that helminth STIM proteins are unable to activate human Orai, whereas helminth Orai can be efficiently activated by human STIM. NFAT nuclear translocation assays confirmed that the A. *lumbricoides* EGFP-STIM–mCherry-Orai complex forms a functional CRAC channel capable of sustaining Ca^{2+}-dependent transcriptional signaling. Intracellular pH modulation further showed that *A. lumbricoides* STIM functions as a pH-sensitive regulator, albeit with an activation range shifted toward alkaline conditions, likely reflecting species-specific adaptation linked to the distribution of histidine residues outside the SOAR core. Finally, homology modeling of the *A. lumbricoides* Orai homohexamer identified druggable transmembrane cavities within the pore. Structure-based virtual screening and molecular dynamics simulations prioritized three candidate ligands with stable pore binding, supporting the feasibility of selectively targeting helminth CRAC channels. Collectively, these findings establish the CRAC channel as a conserved yet selectively regulatable signaling system in helminths and highlight STIM–Orai interfaces as promising antiparasitic drug targets.

Keywords: CRAC channel; STIM–Orai coupling; *Ascaris lumbricoides*; *Schistosoma mansoni*; calcium signaling; pH regulation; structure-based drug discovery

RESUMO

A entrada de cálcio operada por estoques (SOCE), mediada pelo complexo STIM–Orai, constitui uma via fundamental de sinalização por Ca^{2+} em metazoários; entretanto, sua organização molecular e mecanismos regulatórios em parasitos helmintos permanecem pouco compreendidos. Neste estudo, investigamos as características estruturais, funcionais e regulatórias das proteínas STIM e Orai de *Ascaris lumbricoides* e *Schistosoma mansoni*, com ênfase na ativação do canal CRAC, no acoplamento espécie-específico, na sensibilidade ao pH intracelular e na identificação de sítios inibitórios seletivos ao parasito. As análises comparativas de sequência e estrutura demonstraram que STIM e Orai de helmintos preservam os elementos arquitetônicos centrais necessários para a função do canal CRAC, incluindo o domínio sensor de Ca^{2+} EF–SAM, a região ativadora SOAR/CC2–CC3 e as quatro hélices transmembrana que formam o poro de Orai. No entanto, divergências marcantes foram observadas em regiões regulatórias, particularmente na ausência do domínio polibásico C-terminal de STIM em *A. lumbricoides*. Ensaios de microscopia confocal empregando construções fluorescentes revelaram que EGFP-STIM de *A. lumbricoides* não forma puncta após a depleção de Ca^{2+} do retículo endoplasmático quando expresso isoladamente, mas se organiza eficientemente em junções retículo endoplasmático–membrana plasmática quando coexpresso com seu mCherry-Orai cognato, indicando que a interação direta STIM–Orai compensa a menor capacidade intrínseca de ancoragem à membrana. As combinações experimentais realizadas demonstraram que as proteínas STIM de helmintos não são capazes de ativar a Orai humana, enquanto a Orai de helmintos pode ser eficientemente ativada pela STIM humana. Ensaios de translocação nuclear de NFAT confirmaram que o complexo EGFP-STIM–mCherry-Orai de *A. lumbricoides* constitui um canal CRAC funcional, capaz de sustentar sinalização transcricional dependente de Ca^{2+}. A modulação do pH intracelular demonstrou ainda que STIM de *A. lumbricoides* atua como regulador sensível ao pH, porém com uma faixa de ativação deslocada para valores mais alcalinos, possivelmente refletindo adaptações espécie-específicas associadas à distribuição de resíduos de histidina fora do núcleo SOAR. Por fim, a modelagem estrutural do Orai homohexamérico de *A. lumbricoides* permitiu a identificação de cavidades transmembrana farmacologicamente relevantes no poro do canal. Triagens virtuais baseadas em estrutura e simulações de dinâmica molecular priorizaram três ligantes candidatos com ligação estável ao poro, sustentando a viabilidade do canal CRAC como alvo terapêutico seletivo em helmintos. Em conjunto, estes resultados estabelecem o canal CRAC como um sistema de sinalização conservado, porém regulável de forma seletiva, e destacam as interfaces STIM–Orai como alvos promissores para o desenvolvimento de novas estratégias antiparasitárias.

Palavras-chave: canal CRAC; acoplamento STIM–Orai; *Ascaris lumbricoides*; *Schistosoma mansoni*; sinalização por cálcio; regulação por pH; descoberta de fármacos baseada em estrutura.

1. INTRODUCTION

1.1. Helminthiasis

Constitute one of the most widespread groups of parasitic diseases affecting humans and represent a significant public health burden worldwide. According to epidemiological estimates, more than one billion people are infected with helminths, particularly in regions characterized by inadequate sanitation, limited access to clean water, and favorable climatic conditions for parasite development (King, 2019; Siqueira et al., 2020).

Helminths are multicellular parasitic organisms adapted to long-term survival within vertebrate hosts. Unlike protozoan or microbial pathogens, helminths are relatively large organisms, commonly ranging from a few millimeters to several centimeters in length, and establish complex biological interactions with their hosts. These interactions involve not only mechanical damage to tissues but also sophisticated modulation of the host immune response, allowing chronic infections to persist for years (Brooker et al., 2006; Hotez et al., 2008; King, 2019).

The biological cycles of helminths are generally complex and include multiple developmental stages, such as eggs, larval forms, and adult parasites. In most species of medical importance, reproduction does not occur within the human host (King, 2019). Instead, infection depends on continuous exposure to infective stages present in contaminated soil, water, food, or intermediate hosts. Human infection may occur through ingestion of embryonated eggs or larvae, active skin penetration by infective larvae, or, in some cases, through insect vectors (Oliveira de Freitas & Oliveira, 2015).

Based on their taxonomic classification and primary anatomical site of infection, the major human helminths can be grouped into nematodes and platyhelminths, including gastrointestinal and tissue-dwelling parasites, as summarized in Table 1.

Environmental and ecological factors play a central role in the transmission of helminth infections. In tropical and subtropical regions, where temperature and humidity favor parasite survival, repeated exposure is common and often leads to

high parasite burdens (Brooker et al., 2006; J. Chen et al., 2024; Melo et al., 2004).

Table 1. Classification of the major human helminths. According to phylum, class, and primary anatomical localization, highlighting gastrointestinal and tissue-dwelling parasites.

Phylum	Class	Primary site of infection	Representative genera/species
Nematoda	Nematodes	Tissue	*Onchocerca*, *Brugia*, *Wuchereria*, *Dracunculus*, *Loa loa*, *Trichinella*, *Toxocara*
	Nematodes	Gastrointestinal tract (GI)	*Ascaris lumbricoides*, *Strongyloides stercoralis*, *Trichuris trichiura*, *Enterobius vermicularis*, Hookworms
Platyhelminthes	Trematodes	Tissue	*Schistosoma mansoni*, *Paragonimus spp.*, *Fasciola hepatica*
	Trematodes	Gastrointestinal tract / liver	*Clonorchis sinensis*, *Opisthorchis spp.*, *Fasciola hepatica*, *Heterophyes spp.*
	Cestodes	Tissue (larval stages)	*Echinococcus spp.*, *Cysticercus* (*Taenia solium*), Coenurus
	Cestodes	Intestinal (adult stages)	*Taenia saginata*, *Taenia solium*, *Diphyllobothrium latum*, *Hymenolepis nana*

Source adapted (King, 2019; Siqueira et al., 2020)

In addition to climatic determinants that favor the global distribution of helminthiasis, socioeconomic factors play a critical role in shaping the distribution of helminth infections. Poverty, inadequate sanitation, limited access to clean water, and overcrowded living conditions significantly increase the risk of exposure and reinfection. Consequently, helminthiasis prevalence often overlaps with regions experiencing broader structural inequities in health and development. Notably, although helminth infections are most prevalent in tropical regions (Figure 1), transmission may also occur outside these zones, including temperate, sub-arctic, and arctic areas, particularly in contexts where sanitation infrastructure is insufficient (King, 2019).

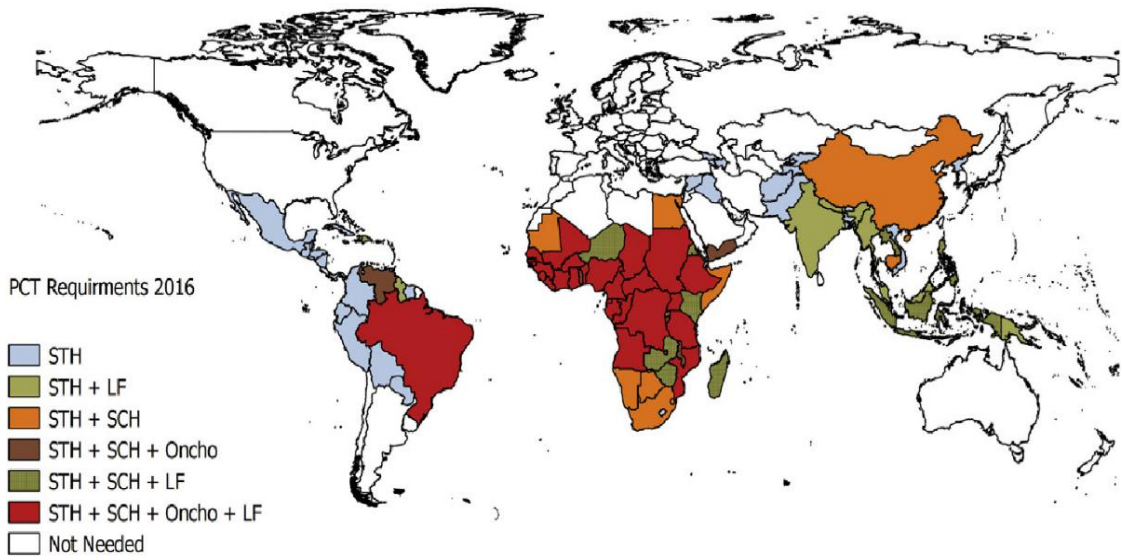

Figure 1. Global distribution of helminth infections and preventive chemotherapy requirements.

World map illustrating the global distribution of helminth burden based on requirements for preventive chemotherapy (PCT) interventions. Shaded regions represent countries requiring PCT for soil-transmitted helminths (STH), lymphatic filariasis (LF), onchocerciasis (Oncho), schistosomiasis (SCH), or combinations of these infections. Data are derived from disease mapping surveys and compiled by the World Health Organization (WHO) (King, 2019).

1.2. Nematodes

Nematodes are non-segmented, cylindrical worms belonging to the phylum Nematoda and represent one of the most diverse and abundant groups of metazoans. Although the majority of nematode species are free-living and inhabit aquatic or terrestrial environments, a significant number have adapted to parasitic lifestyles affecting plants, animals, and humans. In parasitology, nematodes are of particular importance due to their high prevalence, broad geographic distribution, and capacity to establish chronic infections, especially in regions with inadequate sanitary conditions (Urbano, 2020). These parasites exhibit a strong biological dependence on their hosts and are often unable to survive or reproduce outside specific ecological niches, a feature that contributes to their persistence in endemic areas (Despommier et al., 2019).

From a morphological and anatomical perspective, nematodes are characterized by an elongated, cylindrical body with tapered ends and bilateral symmetry. Unlike flatworms, they possess a complete digestive tract extending from the mouth to the anus, allowing continuous ingestion and processing of nutrients (Urbano, 2020). Their body is covered by a thin but highly resistant cuticle, an acellular multilayered structure that provides mechanical protection and

resistance to host digestive enzymes while also participating in selective molecular exchange. Beneath the cuticle lies a well-developed longitudinal musculature that enables the characteristic serpentine movement observed in both free-living and parasitic species (Despommier et al., 2019).

Reproduction in nematodes is typically sexual, with separate sexes and marked sexual dimorphism, particularly among species of medical importance. Females are generally larger than males and allocate a substantial proportion of their body volume to reproductive organs, resulting in high fecundity and efficient transmission. Most parasitic nematodes are oviparous, releasing large numbers of eggs into the environment, although some species exhibit viviparity (Oliveira de Freitas & Oliveira, 2015; Urbano, 2020). In humans, infections caused by intestinal nematodes such as *Ascaris lumbricoides*, *Trichuris trichiura*, and hookworms are among the most prevalent soil-transmitted helminthiases worldwide and are closely associated with malnutrition, impaired physical growth, and reduced cognitive performance, particularly in children from endemic regions (Despommier et al., 2019; Siqueira et al., 2020).

1.2.1. Ascariasis

Is an intestinal helminth infection caused primarily by *Ascaris lumbricoides* (large human roundworm), acquired through ingestion of embryonated eggs from fecally contaminated soil, food, or hands (Siqueira et al., 2020; Urbano, 2020). After hatching, larvae migrate through tissues (notably the lungs) before returning to the small intestine, where adults may establish chronic infections; morbidity is strongly related to worm burden and is most pronounced in children living in settings with poor sanitation (Krücken et al., 2017). In endemic regions, ascariasis remains a major component of soil-transmitted helminthiasis and a key target of preventive chemotherapy and WASH interventions (WHO, 2023b).

Recent global estimates indicate that between approximately 772–892 million to around 1.2 billion people are infected with *Ascaris lumbricoides* worldwide, making ascariasis one of the most prevalent human parasitic infections; prevalence tends to be highest in tropical and subtropical regions with inadequate sanitation, and children bear the highest burden of infection. The global number of infected individuals can vary depending on the methodology used — from ~732 million based on systematic analysis of prevalence surveys to

estimates exceeding 1 billion in public health reports (CDC, 2024a; Despommier et al., 2019; Maia et al., 2015).

1.2.2. Taxonomy

Ascaris lumbricoides is a nematode (Phylum Nematoda) within the order Ascaridida and the family Ascarididae, a group that includes large-bodied gastrointestinal parasites of vertebrates (Schoch et al., 2020a; Zeibig, 2014). Its complete taxonomic classification is summarized in Table 2. Within the genus Ascaris, the relationship between *A. lumbricoides* (humans) and *A. suum* (pigs) has been extensively debated; several genetic and paleoparasitological analyses support very close affinity and even synonymy in some taxonomic interpretations, which matters for zoonotic and transmission discussions (Leles et al., 2012).

Table 2. Taxonomic classification of *Ascaris lumbricoides*

Taxonomic rank	Classification
Kingdom	Animalia
Phylum	Nematoda
Class	Secernentea
Order	Ascaridida
Family	Ascarididae
Subfamily	Ascarinae
Genus	*Ascaris*
Species	*Ascaris lumbricoides*

(Schoch et al., 2020a; Siqueira et al., 2020)

1.2.3. Morphological aspects

Ascaris lumbricoides is a large intestinal nematode with an elongated, cylindrical, and unsegmented body that gradually tapers at both ends and is covered by a smooth, thick, and highly resistant cuticle adapted to the intestinal environment (Siqueira et al., 2020; Urbano, 2020). Adult worms exhibit a pale white to light pink coloration and present a terminal mouth surrounded by three prominent lips—one dorsal and two ventrolateral—bearing fine denticles and sensory papillae, which are involved in feeding and attachment (Murray et al., 2005). Marked sexual dimorphism is observed, with females being larger and more robust (20–40 cm in length) and males smaller (15–30 cm), characterized by a curved posterior extremity with paired copulatory spicules (Urbano, 2020).

Egg morphology represents a key diagnostic and epidemiological feature of *A. lumbricoides*. Fertilized eggs are oval to round (45–75 µm × 35–50 µm) and

possess a thick, trilaminar shell composed of an inner vitelline membrane, a chitinous middle layer, and an external mammillated albuminous coat, conferring high resistance to environmental conditions (Urbano, 2020). In contrast, infertile eggs are more elongated, have thinner and irregular shells, and lack the characteristic mammillated outer layer (Figure 2) (CDC, 2019).

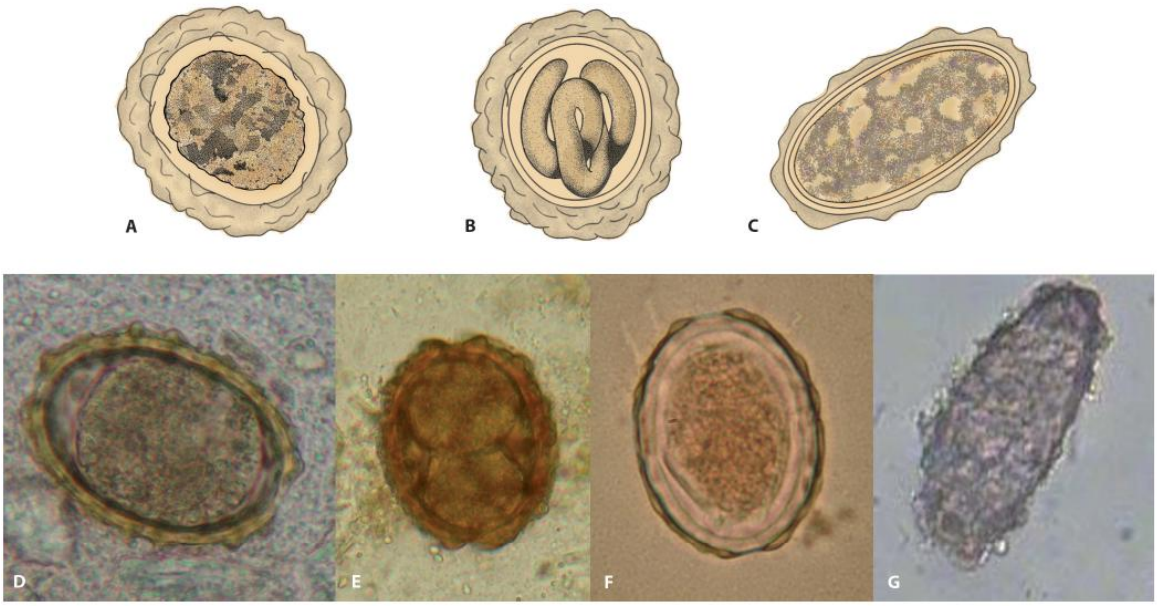

Figure 2. Eggs of *Ascaris lumbricoides*.
Eggs eliminated in feces (**A**) become embryonated (**B**) in approximately three weeks; some infertile eggs containing an amorphous mass of protoplasm are also eliminated (**C**). The images show three fertilized eggs (**D**, **E**, and **F**); the third (**F**) is decorticated, and an infertile egg of *A. lumbricoides* (**G**) (Urbano, 2020).

1.2.4. Life cycle

The life cycle of *Ascaris lumbricoides* is monoxenous and involves a single human host. Non-embryonated eggs are eliminated with feces and, under favorable environmental conditions—adequate temperature (around 25–30 °C), humidity, and oxygen—develop into embryonated eggs containing infective larvae within approximately 2–3 weeks (CDC, 2019). Human infection occurs through ingestion of these embryonated eggs via contaminated food, water, or hands. After hatching in the small intestine, larvae penetrate the intestinal wall, migrate through the lymphatic and circulatory systems to the liver and lungs, where they undergo further development, and then ascend the bronchial tree to the pharynx to be swallowed back into the gastrointestinal tract (Murray et al., 2005; Siqueira et al., 2020). Once returned to the small intestine, larvae mature into adult worms,

establish themselves in the intestinal lumen, and begin egg production, completing the biological cycle within approximately 6–8 weeks after infection (CDC, 2019).

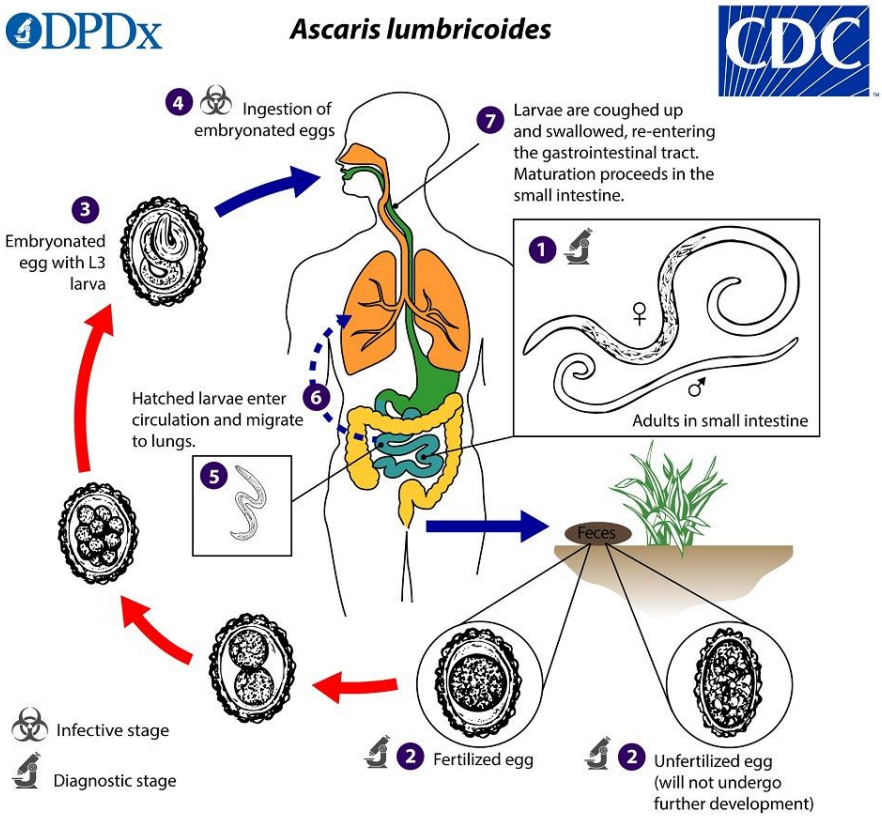

Figure 3. Life cycle of *Ascaris lumbricoides* (CDC - DPDx - Ascariasis, 2019).

1.2.5. Clinical presentation

The clinical manifestations of ascariasis depend largely on parasite burden and the stage of infection. Most infected individuals, particularly those with low worm loads, remain asymptomatic or present mild, nonspecific symptoms, especially in immunocompetent hosts (Zeibig, 2014). During the larval migratory phase, pulmonary involvement may occur as larvae pass through the lungs, giving rise to transient respiratory symptoms such as cough, wheezing, dyspnea, fever, and eosinophilia, a presentation classically known as Löffler's syndrome (CDC, 2019; Murray et al., 2005; Silva Teixeira et al., 2018).

In the chronic intestinal phase, adult worms inhabit the small intestine and may cause abdominal pain, nausea, diarrhea, vomiting, malnutrition, and growth impairment, particularly in children with heavy infections (Siqueira et al., 2020; Zeibig, 2014). Severe complications result from aberrant migration or high parasite burden and include intestinal obstruction, appendicitis, biliary and pancreatic

involvement (cholangitis, cholecystitis, pancreatitis), and, in rare cases, intestinal perforation or peritonitis (Murray et al., 2005). The severity of disease is therefore closely related to worm load, nutritional status, and age of the host (Siqueira et al., 2020).

1.2.6. Treatment

The treatment of ascariasis is primarily based on the use of broad-spectrum anthelmintic drugs, particularly albendazole and mebendazole (Utzinger & Keiser, 2004; WHO, 2011). These benzimidazoles disrupt microtubule polymerization and glucose uptake by binding to β-tubulin, resulting in parasite immobilization and death, but their lack of molecular selectivity highlights the need for the identification of parasite-specific therapeutic targets (Murray et al., 2005; Siqueira et al., 2020). Alternative agents such as pyrantel pamoate or levamisole may be used in specific clinical settings, although benzimidazoles are generally avoided during the first trimester of pregnancy due to potential embryotoxic effects (WHO, 2011). In severe infections with high parasite burden, supportive management and, in rare cases, surgical intervention may be required (Conterno et al., 2020; Siqueira et al., 2020).

1.3. Trematodes

Trematodes are parasitic flatworms belonging to the phylum Platyhelminthes and the class Trematoda, a group recognized since Antiquity due to their medical and veterinary relevance. They are dorsoventrally flattened helminths, generally leaf-shaped, and equipped with two muscular suckers—oral and ventral—which play essential roles in attachment and feeding within the definitive host. Most trematodes of medical importance belong to the subclass Digenea, characterized by obligate parasitic life cycles that require at least two hosts for completion, typically a mollusk as the first intermediate host and a vertebrate as the definitive host. These parasites are widely distributed worldwide and are particularly prevalent in regions with limited sanitation, where they contribute significantly to the burden of neglected tropical diseases (Despommier et al., 2019; Urbano, 2020).

From a biological and epidemiological perspective, digenean trematodes exhibit complex developmental cycles involving both sexual and asexual reproduction. Sexual reproduction occurs in the definitive vertebrate host, whereas

asexual multiplication takes place within the molluscan intermediate host, generating large numbers of infective stages. The typical larval sequence includes miracidium, sporocyst, redia, cercaria, and, in many species, metacercaria, which serves as the infective stage for the vertebrate host (Urbano, 2020). Clinically relevant trematodes infect diverse organ systems—such as the hepatobiliary tract, intestines, lungs, and blood vessels—leading to chronic inflammatory processes and tissue damage, as observed in infections caused by *Schistosoma spp*. and *Fasciola hepatica* (Murray et al., 2005).

1.3.1. Schistosomiasis

Is a chronic parasitic disease caused by blood flukes of the genus Schistosoma, among which *Schistosoma mansoni* is the main etiological agent of intestinal schistosomiasis in Africa and the Americas. Human infection occurs through direct skin contact with freshwater contaminated by cercariae released from infected aquatic snails of the genus Biomphalaria, which act as intermediate hosts (Colley et al., 2014; Siqueira et al., 2020). Once inside the host, the parasites migrate through the bloodstream and mature within the mesenteric veins, where paired adult worms produce eggs that are responsible for most of the pathological manifestations. The disease is widely distributed in endemic regions and is strongly associated with poverty, inadequate sanitation, and water resource development projects, remaining a major neglected tropical disease with significant morbidity and socioeconomic impact (Despommier et al., 2019; Murray et al., 2005; WHO, 2023).

Schistosomiasis remains one of the most prevalent neglected tropical diseases worldwide, representing a major public health challenge in low- and middle-income countries. Current estimates indicate that more than 280 million people are infected globally, with transmission reported in 78 countries, of which approximately 52 are considered endemic. According to the World Health Organization, at least 251 million people required preventive treatment in 2021, reflecting the extensive population at risk and the persistence of transmission in endemic regions (WHO, 2023a, 2024). The disease is responsible for an estimated 200,000 to 280,000 deaths annually, largely due to chronic complications affecting the liver, intestines, and urogenital system, as well as its interaction with poverty, inadequate sanitation, and limited access to healthcare.

Consequently, schistosomiasis ranks among the most frequently recorded tropical diseases worldwide, underscoring the urgent need for sustained control, surveillance, and elimination strategies (Despommier et al., 2019; Molehin, 2020).

Brazil bears one of the highest burdens of schistosomiasis in the Americas and remains a key endemic country for *Schistosoma mansoni*. Estimates indicate that between 1 and 1.5 million people are currently infected, while more than 25 million individuals live in areas at risk of transmission, particularly in the Northeast and Southeast regions of the country (Ministério da Saúde do Brasil, n.d.; WHO, 2023a).

1.3.2. Taxonomy

Schistosoma mansoni is a parasitic trematode belonging to the phylum Platyhelminthes and the class Trematoda, subclass Digenea. Its complete taxonomic classification is summarized in Table 3. It is a member of the family Schistosomatidae, a group of blood flukes characterized by dioecious adults and a life cycle that requires freshwater snails as intermediate hosts. Within the genus *Schistosoma*, *S. mansoni* is taxonomically classified among the intestinal schistosomes and represents the main etiological agent of intestinal schistosomiasis in Africa and the Americas, showing distinct morphological, biological, and epidemiological features compared to urogenital and Asian species (CDC, 2024b; Schoch et al., 2020b).

Table 3. Taxonomic classification of *Schistosoma mansoni.*

Taxonomic rank	Classification
Kingdom	Animalia
Phylum	Platyhelminthes
Class	Trematoda
Subclass	Digenea
Order	Strigeidida
Superfamily	Schistosomatoidea
Family	Schistosomatidae
Genus	*Schistosoma*
Species	*Schistosoma mansoni*

(Schoch et al., 2020b; Siqueira et al., 2020)

1.3.3. Morphological aspects

Schistosoma mansoni is a dioecious trematode, a distinctive trait within the class Trematoda, as males and females exhibit marked sexual dimorphism (CDC,

2024b). Adult worms are elongated and cylindrical rather than leaf-shaped, reflecting their adaptation to an intravascular habitat. The male measures approximately 6–12 mm in length and is shorter and more robust, presenting a ventral longitudinal groove known as the gynecophoral canal, which accommodates the female during copulation and migration within the host's mesenteric veins. In contrast, the female is longer and more slender, reaching up to 15 mm, with a cylindrical body morphology optimized for oviposition in the venous circulation (Urbano, 2020).

The tegument of *S. mansoni* adults consists of a dynamic syncytial layer enriched with spines and tubercles, particularly pronounced in males, facilitating attachment to the vascular endothelium and contributing to immune modulation (Murray et al., 2005). Both sexes possess two muscular suckers—an oral sucker and a ventral sucker (acetabulum) which play essential roles in fixation and hematophagy. The digestive system is incomplete, comprising a mouth, esophagus, and bifurcated intestinal ceca that terminate blindly, as no anus is present (CDC, 2024b). The eggs are oval, non-operculated, and measure approximately 114–180 µm in length, bearing a characteristic lateral spine that is fundamental for species identification in parasitological diagnosis. Larval stages, including miracidia and cercariae, display specialized morphologies - ciliated surfaces and bifurcated tails, respectively - adapted to host penetration and transmission (Figure 4) (Siqueira et al., 2020; Zeibig, 2014).

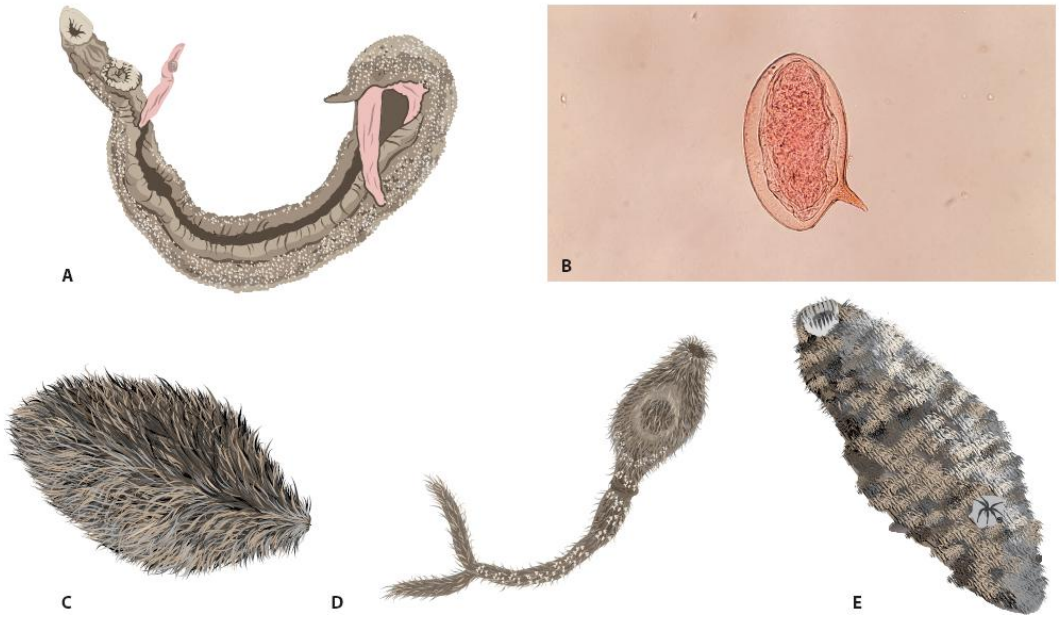

Figure 4. Developmental stages of *Schistosoma mansoni*.
(**A**) Adult helminths, in which the female is seen lodged in the male's gynecophoric canal. (**B**) Egg, with emphasis on the lateral spicula. (**C**) Miracidium. (**D**) Cercaria. (**E**) Schistosomulum. (Siqueira et al., 2020)

1.3.4. Life cycle

The life cycle of *Schistosoma mansoni* is complex and heteroxenous, involving a definitive human host and a freshwater snail of the genus Biomphalaria as the intermediate host. Adult male and female worms reside paired within the mesenteric veins of the human host, where eggs are deposited and subsequently migrate through the intestinal wall, being eliminated with feces into freshwater environments (CDC, 2024c). Under suitable conditions, the eggs hatch, releasing ciliated miracidia that actively seek and penetrate the snail host, initiating asexual development into sporocysts that generate large numbers of cercariae. These free-swimming cercariae are released into the water and represent the infective stage for humans, penetrating intact skin during contact with contaminated freshwater and transforming into schistosomula (Siqueira et al., 2020; Urbano, 2020). The schistosomula migrate via the bloodstream through the lungs to the portal venous system, where they mature into adult worms and complete the cycle approximately 4–6 weeks after infection, ensuring continuous transmission in endemic areas (Figure 5) (CDC, 2024c; Murray et al., 2005).

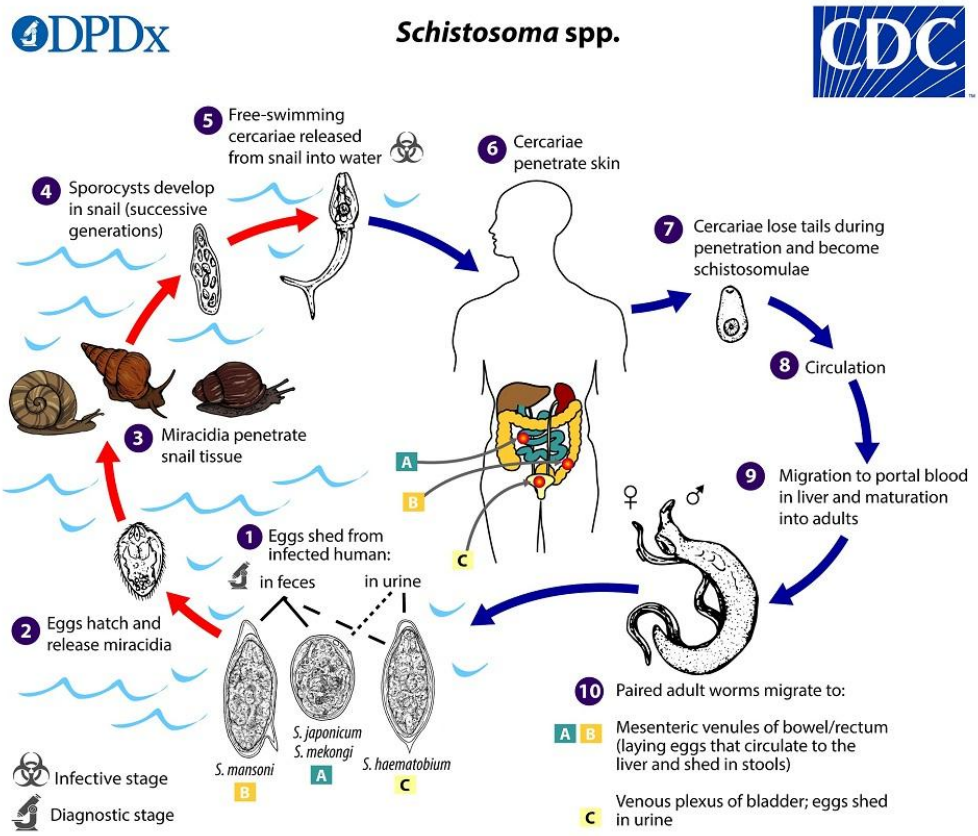

Figure 5. Life cycle of *Schistosoma mansoni* (CDC - DPDx - Schistosomiasis, 2024).

1.3.5. Clinical presentation

Human infection by *Schistosoma mansoni* presents a wide clinical spectrum, ranging from asymptomatic or mild disease to severe chronic manifestations associated with significant morbidity (CDC, 2024c; WHO, 2024). The acute phase, which may occur weeks after exposure, is characterized by cercarial dermatitis at the site of skin penetration and, in non-immune individuals, by acute schistosomiasis or Katayama syndrome. This systemic hypersensitivity reaction is marked by fever, malaise, cough, diarrhea, hepatosplenomegaly, and pronounced eosinophilia, reflecting an intense immune response against migrating schistosomula and newly deposited eggs. In endemic populations, however, acute manifestations are often mild or absent due to partial immune tolerance developed after repeated exposures (Siqueira et al., 2020; Urbano, 2020; Zeibig, 2014).

Chronic schistosomiasis results primarily from the host's inflammatory and fibrotic response to parasite eggs retained in tissues, especially the liver and intestines. The most common clinical forms include the intestinal and hepatointestinal presentations, characterized by abdominal pain, diarrhea, anemia,

and hepatomegaly, while the hepatosplenic form represents the most severe outcome, associated with periportal fibrosis, portal hypertension, splenomegaly, and risk of gastrointestinal bleeding (CDC, 2024c). Less frequent but clinically significant complications include pulmonary vascular involvement, neuroschistosomiasis, and schistosomal nephropathy due to immune complex deposition in the glomeruli. Disease severity is closely related to parasite burden, duration of infection, reinfection rates, and host immunological factors (Siqueira et al., 2020; WHO, 2024).

1.3.6. Treatment

The treatment of schistosomiasis mansoni is based primarily on chemotherapy with praziquantel, which remains the drug of choice due to its high efficacy, broad antiparasitic spectrum, and favorable safety profile (CDC, 2024b, 2024c; Doenhoff et al., 2002; Siqueira et al., 2020). Praziquantel acts mainly against adult worms by inducing severe tegumental damage and sustained muscular paralysis, leading to parasite dislodgement, exposure to host immune responses, and eventual death. At the molecular level, praziquantel has been shown to disrupt calcium homeostasis by increasing Ca^{2+} influx through voltage-gated calcium channels and transient receptor potential (TRP)-like channels, resulting in spastic paralysis and contraction of the parasite musculature (Park et al., 2019; Thomas & Timson, 2018). Standard regimens achieve cure or significant reduction of egg excretion in most patients, although treatment does not reverse established fibrotic lesions in advanced chronic disease. Oxamniquine represents an alternative option with activity restricted to *S. mansoni*, but its use has declined due to limited availability and narrower spectrum. In acute disease, symptomatic management may be required to control hypersensitivity reactions, while in chronic hepatosplenic forms, treatment must be complemented by clinical management of complications such as portal hypertension and gastrointestinal bleeding. Despite its effectiveness, reliance on a single drug underscores the need for new therapeutic targets and strategies, particularly in endemic areas with repeated exposure and concerns about emerging drug tolerance (Murray et al., 2005; Siqueira et al., 2020; Urbano, 2020; Zeibig, 2014).

1.4. The Calcium Release-Activated Calcium (CRAC) Channel

Calcium (Ca^{2+}) is a ubiquitous second messenger essential for controlling a vast array of cellular processes. Among the various pathways for (Ca^{2+}) entry into the cell, the Calcium Release-Activated Calcium (CRAC) channel represents the most archetypical and well-characterized form of Store-Operated Calcium Entry (SOCE). Unlike voltage-gated or ligand-gated channels that respond to electrical changes or external chemical signals, CRAC channels are uniquely defined by their activation mechanism: they open specifically in response to the depletion of (Ca^{2+}) stores within the endoplasmic reticulum (ER). This distinct mode of operation ensures that the cell can replenish its intracellular stores while simultaneously sustaining prolonged (Ca^{2+}) signaling necessary for complex cellular functions (Hogan & Rao, 2015; Prakriya & Lewis, 2015).

The concept of this signaling pathway is often described as "inside-out" signaling (Hogan & Rao, 2015), where an event occurring deep within the cell (in the ER) triggers an event at the cell surface (the plasma membrane). This remarkable inter-organelle communication is coordinated by two principal protein families identified in the mid-2000s: the stromal interaction molecules (STIM), which act as (Ca^{2+}) sensors located in the ER membrane, and the Orai proteins, which form the highly (Ca^{2+}) selective pore within the plasma membrane (Tiffner & Derler, 2020). As broadly outlined by various studies, the reduction of ER luminal calcium causes the STIM proteins to reorganize and move toward the plasma membrane, where they physically engage with Orai proteins to open the channel pore (Baraniak et al., 2020; Fröhlich et al., 2024; Hogan & Rao, 2015).

The influx of calcium mediated by CRAC channels is critical for numerous physiological systems across virtually all metazoan cells. It is perhaps best understood in the context of the immune system, where CRAC channel activation is indispensable for gene expression, proliferation, and the effector functions of T lymphocytes (Prakriya & Lewis, 2015). Consequently, the precise regulation of this channel is vital; as noted by Tiffner & Derler, (2020), dysregulation of the CRAC channel machinery is implicated in a spectrum of diseases, ranging from severe immunodeficiencies to conditions involving pathological cell migration and proliferation, such as cancer (Waldherr et al., 2020). The following sections will

detail the specific molecular mechanics and the roles of the individual protein components that orchestrate this vital cellular process.

1.4.1. Orai protein

Orai proteins constitute the pore-forming subunits of the CRAC channel and represent the central molecular element of SOCE. Their identification as the molecular correlate of the highly Ca^{2+}-selective CRAC current resolved a long-standing question in calcium signaling and established Orai as a channel family fundamentally distinct from voltage or ligand-gated Ca^{2+} channels (Feske et al., 2006; Prakriya et al., 2006; Prakriya & Lewis, 2015). In mammals, three homologs Orai1, Orai2 and Orai3 have been described, with Orai1 being the predominant isoform underlying canonical CRAC currents in immune and non-excitable cells (Amcheslavsky et al., 2015; Hogan & Rao, 2015).

Structurally, each Orai subunit is composed of four transmembrane helices (TM1–TM4), with cytosolic N- and C-terminal regions that play critical roles in channel gating and interaction with STIM proteins. High-resolution structural and biophysical studies revealed that functional Orai channels assemble as hexameric complexes, forming a narrow central pore primarily lined by the TM1 helices (Figure 6) (Hou et al., 2020). A conserved ring of acidic residues within TM1, most notably E106 in human Orai1, constitutes the Ca^{2+} selectivity filter, while downstream hydrophobic and basic regions contribute to permeation control and gating, allowing sustained Ca^{2+} influx with exceptionally low unitary conductance (Amcheslavsky et al., 2015; Prakriya et al., 2006; Prakriya & Lewis, 2015).

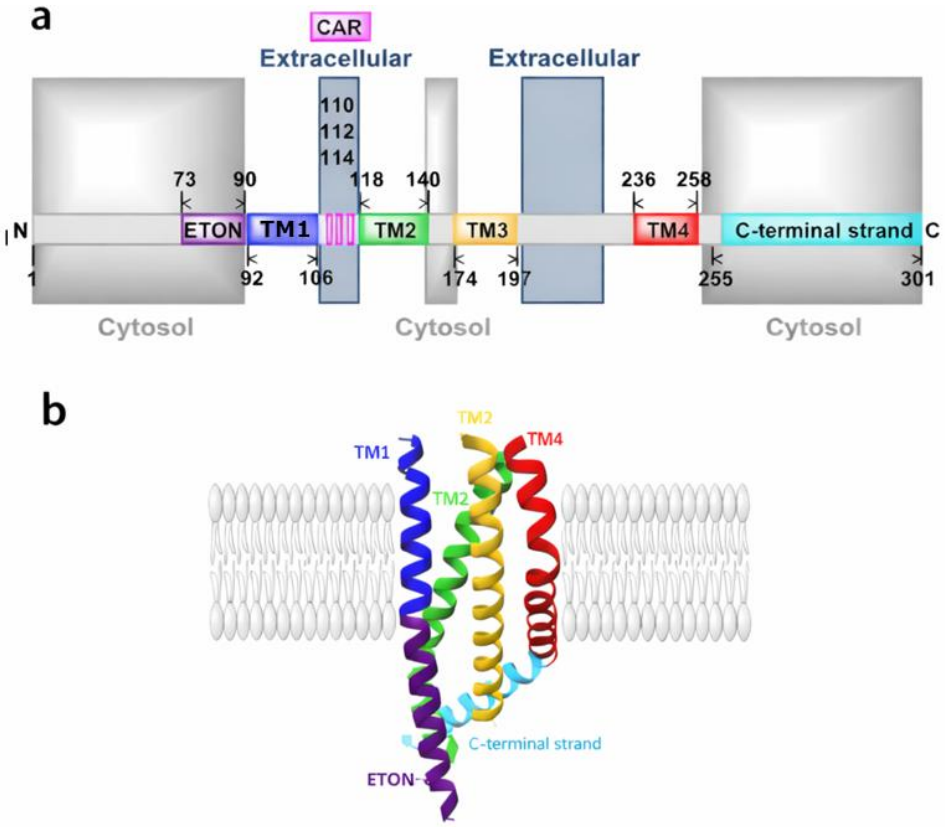

Figure 6. Structural organization of the Orai1 protein.
(**A**) Schematic representation of the full-length human Orai1 showing the four transmembrane helices (TM1–TM4), the cytosolic N- and C-terminal regions, and key structural segments involved in channel architecture. (**B**) Cartoon representation of a single Orai1 subunit embedded in the plasma membrane, illustrating the spatial arrangement of the four transmembrane helices and the cytosolic C-terminal strand (Tiffner & Derler, 2020).

Beyond forming a passive ion-conducting pore, Orai functions as an allosterically regulated channel whose activation strictly depends on direct coupling to STIM proteins. The cytosolic C-terminus of Orai1 represents the primary binding interface for STIM1; however, accumulating evidence indicates that the N-terminus and intracellular loop regions also play essential roles in transmitting and stabilizing the conformational changes required for pore opening (Baraniak et al., 2020; Stathopulos et al., 2013). Structural, mutational, and molecular dynamics studies support a gating mechanism involving coordinated rearrangements across all four transmembrane helices, rather than a localized gate, enabling efficient signal propagation from STIM binding to pore dilation (Fröhlich et al., 2024; Tiffner & Derler, 2020).

Functionally, the unique architecture of Orai channels allows cells to generate long-lasting, spatially restricted Ca^{2+} signals essential for transcriptional activation, immune responses, and metabolic regulation. Dysregulation of Orai-

mediated Ca^{2+} entry has been linked to immunodeficiency, autoimmunity, cancer, and neurodegeneration, highlighting the channel's physiological and pathological relevance (Hogan & Rao, 2015; Tiffner & Derler, 2020). Importantly, comparative and evolutionary analyses indicate that Orai homologs are conserved across metazoans, including helminth parasites, although sequence and structural divergences may influence channel regulation and pharmacological sensitivity. These features provide a strong rationale for exploring parasite Orai channels as potential selective therapeutic targets, as discussed in subsequent sections.

1.4.2. STIM protein

STIM (Stromal Interaction Molecule) proteins function as endoplasmic reticulum (ER) resident Ca^{2+} sensors that initiate store-operated calcium entry (SOCE) by coupling ER Ca^{2+} depletion to activation of plasma membrane Orai channels. STIM1, the best-characterized isoform, is a single-pass transmembrane protein with an N-terminal luminal region containing canonical and non-canonical EF-hand motifs followed by a sterile α motif (SAM), which together form the EF - SAM domain responsible for Ca^{2+} sensing (Liou et al., 2005; Prakriya & Lewis, 2015; Stathopulos et al., 2008). Under resting conditions, Ca^{2+} binding to the EF-hand stabilizes STIM1 in a compact, inactive conformation distributed throughout the ER membrane, preventing premature activation of SOCE (Hogan & Rao, 2015).

Upon ER Ca^{2+} store depletion, Ca^{2+} dissociates from the EF-hand, triggering destabilization of the EF–SAM domain and promoting STIM1 oligomerization through SAM–SAM interactions (Ma et al., 2015; Stathopulos et al., 2008). This luminal conformational change is transmitted across the membrane, leading to extensive rearrangements in the cytosolic portion of STIM1, which contains three coiled-coil domains (CC1–CC3), a serine/proline-rich region, and a polybasic C-terminal tail (Tiffner & Derler, 2020). Central to this process is the exposure of the STIM1 Orai-activating region—also referred to as CAD, SOAR, or Ccb9—which spans residues approximately 344–442 and forms a dimeric coiled-coil structure essential for Orai binding and activation (Figure 7) (Baraniak et al., 2020; Stathopulos et al., 2013).

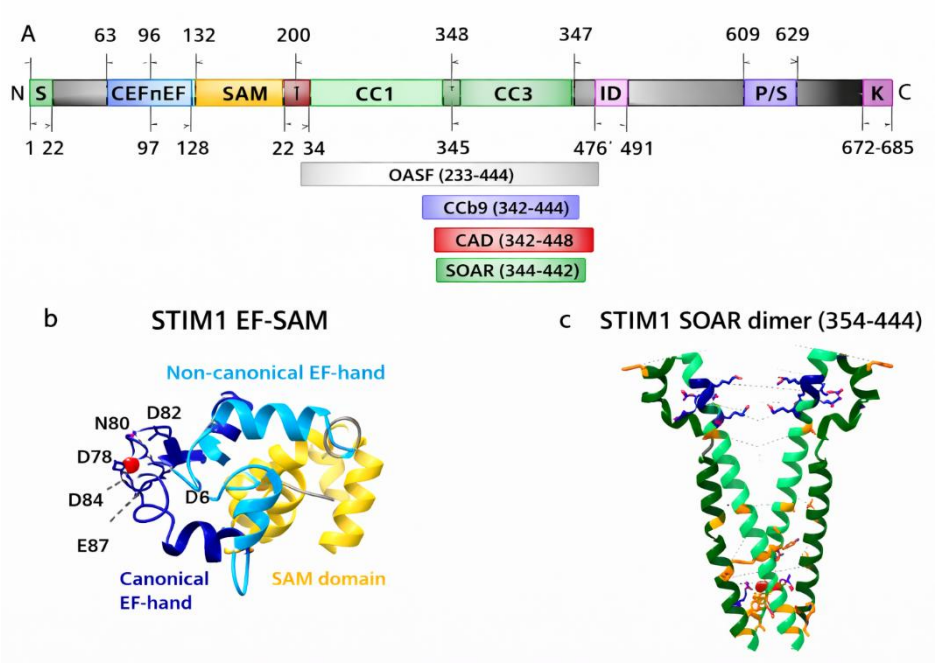

Figure 7. The structural features of Stromal interaction molecule 1 (STIM1).
(**A**) Schematic representation of the full-length human STIM1 highlighting the major functional domains involved in Ca^{2+} sensing and Orai1 activation, including the EF-hand, SAM, coiled-coil regions, and the SOAR/CAD signaling module. (**B**) Structural model of the EF–SAM domain of STIM1 illustrating the canonical and non-canonical EF-hand motifs responsible for Ca^{2+} binding. (**C**) Crystallographic structure of the STIM1 SOAR dimer showing its characteristic V-shaped architecture formed by the CC2 and CC3 domains (Tiffner & Derler, 2020).

Following oligomerization and extension, STIM1 translocates to ER-plasma membrane (ER-PM) junctions, where its polybasic C-terminal region interacts with phosphoinositides in the inner leaflet of the plasma membrane, stabilizing ER-PM contacts and positioning STIM1 for productive coupling to Orai channels (Chang et al., 2018; Liou et al., 2005). Recent studies further indicate that STIM1 activity is finely tuned by additional regulatory inputs, including interactions with cytoskeletal elements, modulation by cytosolic pH, and isoform-specific structural differences, underscoring its role as a dynamic integrator of cellular Ca^{2+} homeostasis rather than a simple binary switch (Figure 8) (Y. Chen et al., 2024; Gao et al., 2009; Narayanasamy et al., 2024)

1.4.3. Mechanism of STIM-Orai signaling activation

Store-operated calcium entry (SOCE) is initiated when extracellular stimuli activate receptor-dependent signaling pathways that reduce Ca^{2+} levels within the endoplasmic reticulum (ER), most commonly through GPCR- or RTK-mediated activation of phospholipase C (PLC), generation of IP_3, and Ca^{2+} release via IP_3 receptors (Hogan & Rao, 2015; Prakriya & Lewis, 2015). The resulting depletion of

ER Ca^{2+} stores is sensed by STIM proteins through the luminal EF–SAM domain, enabling STIM to act as a molecular transducer that converts ER Ca^{2+} loss into a plasma membrane Ca^{2+} influx signal (Prakriya & Lewis, 2015; Stathopulos et al., 2008). This mechanism allows cells to generate sustained Ca^{2+} signals while maintaining tight spatial and temporal control over cytosolic Ca^{2+} concentrations (Figure 8).

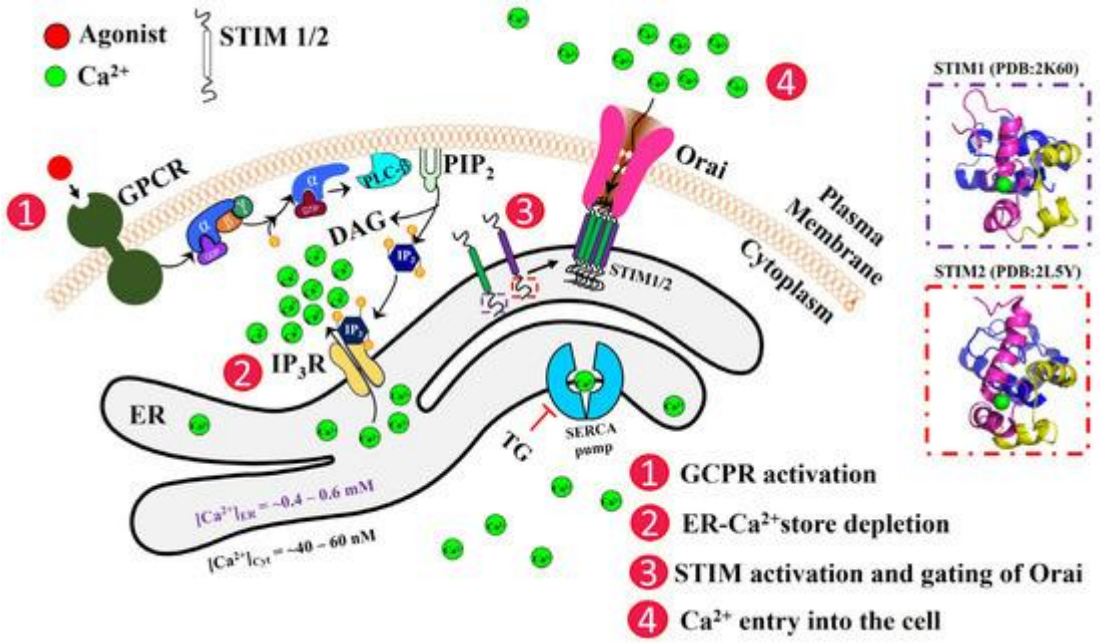

Figure 8. Schematic overview of STIM–Orai–mediated store-operated Ca^{2+} entry (SOCE). Receptor activation triggers phospholipase C–dependent signaling and IP_3-mediated Ca^{2+} release from the endoplasmic reticulum (ER), leading to ER Ca^{2+} store depletion. STIM proteins sense ER Ca^{2+} loss, undergo conformational activation, and accumulate at ER–plasma membrane junctions, where they gate Orai channels. Subsequent Ca^{2+} influx across the plasma membrane restores cytosolic Ca^{2+} signaling and contributes to ER Ca^{2+} refilling via SERCA activity (Narayanasamy et al., 2024).

Following ER Ca^{2+} depletion, dissociation of Ca^{2+} from the STIM1 EF-hand destabilizes the EF–SAM domain and triggers STIM1 oligomerization and conformational extension, leading to exposure of the SOAR/CAD region within the cytosolic coiled-coil core (Ma et al., 2015; Stathopulos et al., 2013). Activated STIM1 accumulates at ER–plasma membrane (ER–PM) junctions, where its polybasic C-terminal tail interacts with phosphoinositides to stabilize membrane contacts and promote efficient coupling to Orai channels (Baraniak et al., 2020; Chang et al., 2018). Upon Orai activation, Ca^{2+} enters the cytosol and rapidly engages downstream Ca^{2+} sensors, including calmodulin (CaM), which binds to cytosolic regions of Orai and contributes to Ca^{2+}-dependent inactivation (CDI),

thereby preventing excessive Ca^{2+} influx (Fröhlich et al., 2024; Li et al., 2017; Prakriya & Lewis, 2015). In parallel, Ca^{2+} pumps such as SERCA, located in close proximity to ER–PM junctions, actively transport Ca^{2+} back into the ER, promoting store refilling and facilitating termination or modulation of CRAC channel activity (Figure 9) (Hogan & Rao, 2015; Narayanasamy et al., 2024).

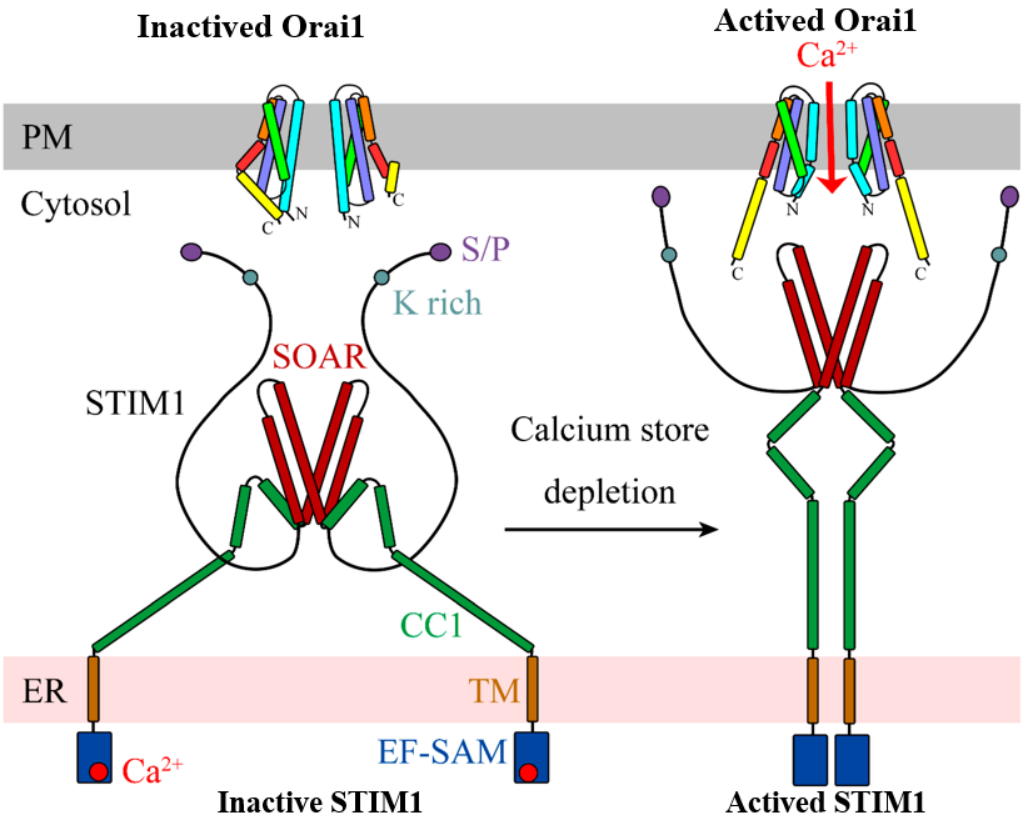

Figure 9. Conformational transition of STIM1 and Orai1 during CRAC channel activation. Schematic representation of the inactive and active states of STIM1 and Orai1 following ER Ca^{2+} store depletion. In the resting state, STIM1 adopts a compact conformation and Orai1 remains closed. ER Ca^{2+} depletion induces STIM1 extension and exposure of the SOAR domain, enabling coupling to Orai1, channel opening, and Ca^{2+} influx across the plasma membrane (Prakriya & Lewis, 2015; Stathopulos et al., 2013).

At the molecular level, STIM–Orai coupling induces coordinated allosteric rearrangements across the Orai transmembrane helices, resulting in pore opening and highly Ca^{2+}-selective conductance (Baraniak et al., 2020; Prakriya & Lewis, 2015). The balance between channel activation, CaM-mediated inactivation, and ER Ca^{2+} refilling ensures that CRAC signaling remains sustained yet self-limiting. Downstream, Ca^{2+} influx through CRAC channels activates Ca^{2+}/calmodulin-dependent pathways and the calcineurin–NFAT (nuclear factor of activated T cells) signaling axis, where Ca^{2+}-dependent dephosphorylation of NFAT drives its

nuclear translocation and transcriptional activity. Owing to this direct coupling, NFAT nuclear translocation is widely used as a functional readout of SOCE/CRAC activity in cellular systems (Hogan & Rao, 2015; Prakriya & Lewis, 2015).

1.5. CRAC channel on helminths

To date, *Caenorhabditis elegans* represents the only characterized helminth model for which functional evidence of the STIM–Orai–mediated store-operated calcium entry (SOCE) pathway has been reported. Genetic, electrophysiological, and imaging studies have unequivocally shown that *C. elegans* expresses bona fide homologues of STIM1 (C.STIM1) and Orai1 (C.Orai1), which together reconstitute a classical Ca^{2+} release-activated Ca^{2+} (CRAC) current upon endoplasmic reticulum Ca^{2+} store depletion. Loss-of-function approaches, including RNAi-mediated silencing of either component, abolish CRAC currents and lead to severe physiological defects such as sterility, highlighting the essential role of SOCE in nematode reproductive biology and Ca^{2+} homeostasis. These studies firmly establish *C. elegans* as a validated in vivo system for CRAC channel function in helminths and demonstrate strong evolutionary conservation of the STIM–Orai signaling axis across metazoans (Gao et al., 2009; Strange et al., 2007).

Beyond genomic evidence, functional characterization of the CRAC channel machinery has been achieved for the parasitic trematode *Schistosoma mansoni* through heterologous expression approaches. Seminal work demonstrated that *S. mansoni* encodes bona fide orthologues of STIM and ORAI, and that these proteins are capable of recapitulating the essential molecular mechanisms of store-operated calcium entry (SOCE) when expressed in mammalian cells. Recombinant *Sm*STIM functions as an endoplasmic reticulum Ca^{2+} sensor, undergoes Ca^{2+}-dependent conformational rearrangements, and targets ER–plasma membrane junctions, while *Sm*ORAI forms a plasma membrane Ca^{2+} channel with conserved pore architecture and gating properties. Biochemical, imaging, Ca^{2+} influx assays, and mutational analyses collectively demonstrate that *Sm*ORAI is a STIM-gated calcium channel, establishing the first functional CRAC channel characterized from a parasitic helminth. Importantly, comparative analyses between schistosome and human STIM–ORAI systems revealed subtle but

significant mechanistic and pharmacological differences, including differential sensitivity to CRAC channel inhibitors, highlighting the potential for selective therapeutic targeting of parasite Ca^{2+} signaling. While these studies were necessarily performed in heterologous cell systems due to the lack of stable schistosome cell lines, they provide compelling evidence that a functional STIM–ORAI-dependent Ca^{2+} entry pathway operates in *S. mansoni* and may play critical roles in parasite physiology (Zeraik et al., Submitted article).

1.6. Therapeutic implications of CRAC channel modulation

Beyond mammalian systems (Waldherr et al., 2020), the identification of conserved STIM-Orai signaling components across metazoans provides a strong conceptual framework for rational drug design targeting CRAC channels in parasitic helminths. Comparative genomic and functional studies indicate that key elements of store-operated Ca^{2+} entry are evolutionarily conserved, suggesting that helminth Orai channels retain fundamental structural and biophysical features required for Ca^{2+} permeation and regulation (Prakriya & Lewis, 2015). This conservation supports the feasibility of structure-guided approaches aimed at selectively targeting helminth CRAC channels while minimizing host toxicity. High-resolution structural and mechanistic insights obtained from mammalian Orai1, including the identification of druggable regions such as the pore selectivity filter and extracellular transmembrane interfaces, provide a valuable template for homology modeling and *in silico* screening of helminth Orai homologs (Derler et al., 2013; Waldherr et al., 2020). Importantly, the growing recognition of Ca^{2+} signaling as a central regulator of parasite motility, development, neuromuscular function, and host–parasite interaction further reinforces CRAC channels as attractive pharmacological targets in helminthiasis (Greenberg, 2005; McVeigh, 2020). Collectively, these findings position helminth CRAC channels as promising candidates for rational drug discovery pipelines that integrate comparative genomics, structural modeling, and selective pore-targeted inhibition to develop next-generation antiparasitic therapies.

2. OBJECTIVES

2.1. General objective

To investigate the molecular, functional, and structural mechanisms underlying STIM–Orai coupling in helminth parasites, with emphasis on CRAC channel activation, pH-dependent regulation, and the identification of parasite-selective inhibitory sites.

2.2. Specific objectives

2.2.1. To perform a comparative sequence and structural analysis of STIM and Orai proteins from *Ascaris lumbricoides*, *Schistosoma mansoni, Homo sapiens*, and selected orthologs in order to identify conserved and parasite-specific molecular features involved in CRAC channel activation.

2.2.2. To evaluate the functional coupling between helminth-derived STIM and Orai proteins using confocal microscopy, focusing on puncta formation and ER–plasma membrane junction dynamics.

2.2.3. To assess CRAC channel activation mediated by helminth STIM–Orai complexes through NFAT nuclear translocation assays as a Ca^{2+}-dependent functional readout.

2.2.4. To investigate the role of *A. lumbricoides* STIM proteins as intracellular pH sensors and determine how pH variations modulate STIM activation and CRAC channel coupling.

2.2.5. To generate a three-dimensional structural model of *A. lumbricoides* Orai and identify and characterize potential small-molecule inhibitors targeting transmembrane druggable pockets through structure-based virtual screening, redocking, and molecular dynamics simulations.

3. METHODOLOGY

3.1. Multiple sequence alignment and comparative analysis of STIM and Orai proteins from *Ascaris lumbricoides, Schistosoma mansoni,* and selected orthologs

A comparative sequence analysis of STIM and Orai proteins was performed using homologous sequences from *Ascaris lumbricoides*, *Schistosoma mansoni*, *Homo sapiens*, and selected representative orthologs from metazoans. Amino acid sequences were retrieved from the National Center for Biotechnology Information

(NCBI) (Sayers et al., 2021) and the UniProt databases (Bateman et al., 2023), ensuring full-length annotations and curated entries whenever available (Table 4).

Multiple sequence alignments were generated using Jalview (Waterhouse et al., 2009), allowing detailed comparison of primary sequences, detection of conserved residues, and assessment of evolutionary relationships across species. The alignments were manually inspected and refined to ensure accurate positioning of functionally relevant regions. Conserved motifs and domains were highlighted directly within the multiple sequence alignment to facilitate cross-species comparison.

Functional and structural features of STIM and Orai proteins were further annotated using complementary bioinformatic prediction tools. Signal peptides were predicted using SignalP (version 5.0) (Almagro Armenteros et al., 2019), while domain architecture was analyzed with SMART (Letunic & Bork, 2025). Transmembrane helices were identified using TMHMM (version 2.0) (Krogh et al., 2001), and coiled-coil regions were predicted using the COILS algorithm (Lupas, 1997). In parallel, three-dimensional structural predictions were obtained from the AlphaFold platform to support domain localization and guide structural interpretation (Jumper et al., 2021).

Table 4. Amino acid sequences of STIM and Orai proteins from helminth parasites in FASTA format.

Protein	FASTA (sequence)
Ascaris lumbricoides	
STIM*	>SAM domain-containing protein OS=Ascaris lumbricoides OX=6252 PE=4 SV=2 MFARRIDFRLKRVMCPRWGTHLELLSASAPLIASVVITADDEKFRDPEGYAAIMQLHRQM DDDHSGSIDRFESNDFLKEDMKFGGSDREKREKAFHHNNDEQITVDDLWEAWFGSEERAW TTAEVVAWLENSVRLPQYSNNLIVKNVDGRALPRMAVANSTYLATELGIKNAVHKHKIHL KALDVVLFGFSGDGSSRMKDIALSILLCVLIAVLVLYKRQRSRSRNEMEQLTSKLRQLKS MESDFEDVQQKFEEERKKRQSVSEAIVAENAQMETLRSQLMEAERLLESSSSAPLALQPL LRRTCELEMSYVGQQRLECIAEMREAIELIDKLRKKQSSLMSSIKLATGGSTGTDQVDSR IFSLKARMEKISLAMEECQQRWIEIESLCGFPLMVQPNGAELTFMGHTMPASGSSHLPRT PSMCSSFYRSSGICSTLATSAPPSYSSASALSTLALLDTSVAPKRPTTVFSLTSASTSRL SSSSHSHSSSSSEDRPYPLPSPSEFQLLTSAEHRNPGSTLYGALENRIQQQTGTLRFFAH EYFFGMRLSRSLHPARFCSS
Orai**	>Protein orai OS=Ascaris lumbricoides OX=6252 PE=3 SV=1 MVSSSPLHLDTSAPRRKGITEAYPLSGWITDVKLASRLAASNRMLNESRSANDICTNAFE GGTRHDFMHEHDDVKSLLQESRHRGELTILEKYRYDLSRAQLKASSRTSALLAGFAMVAL VELQYESNTPPYLLILLGVVTTLLVSVHLLALMMSTCILPYIEANGCTQDSPHIRLKFYI DLSWLFSTCIGLVLFLVEIGVIFFVKFNAVNYELAAYITTAMLIPVLIIFTVFSCLIHKN RFIHSMDRVDTKVNDLQKFLSENESAVALPNATSVQRHLVGAGLQGITILR
Schistosoma mansoni	
	>SAM domain-containing protein OS=Schistosoma mansoni OX=6183 PE=4 SV=1 MICYIFGILFCTCMFSPTVCSDICSATDEILSCFTKILSYEAIEDLHRNLDGDKNGEVDH

STIM***	SETEKFLRKEFNPGDAAKKSRMLNSDDPLISLTDLWQMWRNNPAFNWTVRDTTQWLVNLV DLPQYADLFRQHNLDGRSLPRLAMQNMSYLVDVLGIQNPIHKKKLMLRALDIILFGPPRQ PVLVSGNVPLVTLSIGLLCVSFVSFSHWFYHTSSFSEKNSVGENQEKLNVAEQTLKQLQR RLDDVEQLRQTLNAYEINQHFASSSSSAPKGMKRDNLSSPHLKSMEALNEDSLNTRKQSY DHSSYIPSSITEFSLSTDLCNDSLHSNSSNNNNIYSANDPLTSDQIRTLQCRKILNLKGR NYGNEFCSSIALSRNPCNKYHLDEPHYELKHWLQVTYELELKRYCEKRMKAEKKLDFARQ SCKRFMRKRYGIFGSVRLVNAINLDELENRLISAKQALDQLEIEVQERINRWSRIEALTG HFIHTDIHNQYAKSTICETTKSIHCSMDMYRYCNGSMKSSDSDRLSSMIEETSLESNRFS KSTSNGLVNDFDCTHNKEIFNLKDSFQSNSETADTFRTSLPRNYSFVRPFATLWRRKTKS GRGKADSKQ
Orai1****	>OS=Schistosoma mansoni OX=6183 PE=3 SV=1 MSSDNVVTSSVLPDSYSLARRHLQLSRAKLKATSRVSALLAGFAMVAIIELQVAVGESKP PEGLLFAFTILSCLLVVVHIMAVMISTCILPHIDSYTVPQDCYLIEEAPHNRLRTFVEVA WICSTVVGIILFLAVVTLAFWVKFWSVSSLSAIAATIVLIPAMLIFVIFAILFYRALTTY KVERATEMIRNIDMRMSFLRSGVQKMYDEDNRKQHV

*(UniProt AlSTIM, n.d.) **(UniProt AlOrai, n.d.) ***(UniProt SmSTIM, n.d.) ****(UniProt SmOrai, n.d.)

3.2. Cloning of STIM and Orai from *Ascaris lumbricoides* and *Schistosoma mansoni*

Previously generated clones of *Schistosoma mansoni* STIM (*Sm*STIM) and Orai (*Sm*Orai), as well as human STIM (*Hs*STIM), Orai (*Hs*Orai), and NFAT, obtained from earlier studies, were used in this work together with *Ascaris lumbricoides* Orai (*Al*Orai) as templates for the generation of recombinant and chimeric constructs.

The first construct corresponded to full-length *Ascaris lumbricoides* STIM (*Al*STIM) excluding the predicted signal peptide. Specifically, the first 28 N-terminal residues were removed, and the construct comprised residues 29–560 of the *Al*STIM sequence. This fragment was cloned into the EGFP-pCMV6-XL5 expression vector using the HindIII and XhoI restriction sites. It is important to note that the EGFP-pCMV6-XL5 vector contains a human signal peptide located at the N-terminus, upstream of the EGFP tag, which directs the expressed fusion protein to the endoplasmic reticulum (ER), thereby ensuring appropriate subcellular targeting during heterologous expression. The second construct consisted of the C-terminal region of *A. lumbricoides* STIM (*Al*STIM-CT), comprising 333 amino acid residues corresponding to positions 227–560 of the *Al*STIM sequence. This fragment was subcloned into the EGFP-pcDNA3.1 expression vector using the BamHI and XhoI restriction sites. The third construct corresponded to isoform 2 of *S. mansoni* Orai, which was cloned into the pGEM vector using BamHI and XhoI restriction sites (Table 5).

In addition, a chimeric STIM construct was designed in which the C-terminal region of *S. mansoni* STIM was replaced by the corresponding C-terminal domain of *A. lumbricoides*. The resulting chimeric *Sm*STIM construct was cloned into the EGFP-pCMV6-XL5 expression vector. Specific primers were designed to amplify the regions of interest by PCR, incorporating overlapping sequences with the vector backbone to enable cloning via the Gibson Assembly method (Table 5). Following amplification, insert and vector fragments were assembled using the enzymes provided in the NEBuilder Assembly Tool kit according to the manufacturer's instructions. Restriction enzyme analysis using HindIII and XhoI was subsequently performed to verify successful replacement and correct insertion of the substituted C-terminal region.

Following confirmation of the recombinant clones by DNA sequencing, the plasmids were transformed into competent *Escherichia coli* DH5α cells for plasmid propagation. Cells were incubated with the recombinant plasmids for 30 min on ice and subsequently subjected to heat shock at 42 °C for 50 s in a water bath. Immediately after heat shock, 200 µL of Luria–Bertani (LB) medium were added, and the cells were returned to ice for 2 min. The transformed cells were then incubated under agitation at 37 °C for 1 h 30 min and plated onto LB agar plates supplemented with ampicillin or carbenicillin (50 µg/mL), depending on the plasmid construct. Plates were incubated at 37 °C for 16 h. Colonies corresponding to positive clones were selected and grown for approximately 16 h at 37 °C in LB medium containing ampicillin (50 µg/mL) and plasmid DNA were subsequently extracted using the Wizard® Plus SV Miniprep DNA Purification System (Promega), following the manufacturer's instructions.

Table 5. Primers used for cloning and generation of chimeric STIM.

Construct / Target	Primer name	Sequence (5'→3')	Restriction site	Tm (°C)
***Al*STIM full-length** (excluding predicted signal peptide) (EGFP-pCMV6-XL5)	*Al*STIM_F_HindIII	CCGAAGCTTAGCGCCCCTCTGATCGCC	HindIII	69
	*Al*STIM_R_XhoI	CCGCTCGAGTCAGCTGCTGCAGAATCTAGC	XhoI	68
***Al*STIM-CT** (C-terminal region) (EGFP-pcDNA3.1)	*Al*STIM_CT_F_BamHI	CCGGGATCCAAGCGGCAGCGGAGCAGAAG	BamHI	71
	*Al*STIM_R_XhoI	CCGCTCGAGTCAGCTGCTGCAGAATCTAGC	XhoI	68

Construct / Target	Primer name	Sequence (5'→3')	Restriction site	Tm (°C)
***Sm*Orai isoform 2** (pGEM)	*Sm*ORAI2_F_1_BamHI	CCGGGATCCATGAGTTCAGACAACGTTGTTACT	BamHI	65
	*Sm*ORAI2_R_1_XhoI	CCGCTCGAGTCAACTTTGTAGGTAGTAAGCGC	XhoI	66
Chimeric STIM (overlap/assembly primers)	Fw_vector_chimera	TAGATTCTGCAGCAGCTGAGCAGGATGGGGTGGCAGTAA	—	69
	Rv_vector_chimera	CTTCTGCTCCGCTGCCGCTTGTAAAACCAATGAGAAAAGG	—	68
	Fw_insert_chimera	GCTTTTCTCATTGGTTTTACAAGCGGCAGCGGAGCAGAAG	—	69
	Rv_insert_chimera	TTACTCCCACCCCATCCTGCTCAGCTGCTGCAGAATCTAGC	—	69

3.3. Confocal fluorescence imaging

3.3.1. STIM–Orai puncta formation upon ER Ca^{2+} depletion

Human embryonic kidney cells (HEK293) were transiently transfected with EGFP-tagged STIM and mCherry-tagged Orai constructs derived from *Ascaris lumbricoides* (EGFP-*Al*STIM/mCherry-*Al*Orai), *Schistosoma mansoni* (EGFP-*Sm*STIM/mCherry-*Sm*Orai), or *Homo sapiens* (EGFP-*Hs*STIM/mCherry-*Hs*Orai). HEK293 cells were selected due to their high transfection efficiency and suitability for heterologous protein expression and imaging assays (P. Thomas & Smart, 2005). Transfections were performed in six-well plates at a density of 3×10^5 cells per well using Lipofectamine 2000 (Thermo Fisher Scientific), following the manufacturer's instructions. Cells were maintained at 37 °C in a humidified atmosphere containing 5% CO_2.

Twenty-four hours after transfection, the medium was replaced with DMEM supplemented with 10% fetal bovine serum (FBS) and antibiotics (penicillin–streptomycin). Cells were then seeded onto poly-D-lysine–coated glass coverslips (Sigma) or 35-mm glass-bottom dishes and analyzed 48 hours post-transfection.

Confocal fluorescence imaging was performed using a Zeiss LSM 710 laser scanning confocal microscope (Carl Zeiss), equipped with a 488 nm laser for EGFP excitation and a 561 nm laser for mCherry excitation. Non-transfected cells present in the same cultures served as internal negative controls, as they showed no detectable EGFP fluorescence. For functional assessment of CRAC channel activation, transfected HEK293 cells were stimulated with thapsigargin (1 μM) to induce endoplasmic reticulum Ca^{2+} store depletion, and STIM–Orai puncta

formation was monitored by real-time confocal microscopy. (Gao et al., 2009; Zeraik et al., Submittend article).

3.3.2. NFAT-translocation assays

As a functional readout of CRAC channel activation mediated by helminth-derived STIM and Orai proteins in mammalian cells, nuclear translocation of NFAT (nuclear factor of activated T cells) was employed as a Ca^{2+}-dependent signaling assay. NFAT activation is triggered by sustained Ca^{2+} influx through CRAC channels, leading to calcineurin-dependent dephosphorylation and subsequent translocation of NFAT from the cytoplasm to the nucleus (Carretta et al., 2018).

HEK293 cells were transiently co-transfected with the following constructs: eGFP-*Al*STIM/mCherry-*Al*Orai, eGFP-*Sm*STIM/mCherry-*Sm*Orai or eGFP-*Hs*STIM/mCherry-*Hs*Orai, together with a GFP-tagged NFAT reporter plasmid. Transfections were performed using Lipofectamine 2000 according to the manufacturer's instructions. Cells were maintained at 37 °C in a humidified atmosphere containing 5% CO_2 and analyzed 48 h post-transfection.

To induce store-operated Ca^{2+} entry (SOCE), cells were treated with thapsigargin (1 µM; Sigma-Aldrich). NFAT translocation dynamics from the cytoplasm to the nucleus were monitored by confocal microscopy, with images acquired before and after TG stimulation in real-time mode. Image analyses were performed using Fiji/ImageJ. This approach enabled direct correlation between CRAC channel activation mediated by helminth-derived STIM–Orai complexes and downstream Ca^{2+}-dependent transcriptional signaling, providing functional evidence for SOCE-driven NFAT activation in mammalian cells expressing parasite CRAC channel components (Princen et al., 2024).

Image analysis was performed using Fiji/ImageJ software (Schindelin et al., 2012). Qualitative comparisons were conducted based on fluorescence redistribution patterns and puncta formation, with particular emphasis on the conservation and functional relevance of the C-terminal polybasic domain across species.

3.3.3. Evaluation of STIM as an intracellular pH sensor

To evaluate the role of STIM as an intracellular pH (pH_i) sensor, HEK293 cells were transiently co-transfected with the following constructs: EGFP-

*Al*STIM/mCherry-*Al*Orai or EGFP-*Hs*STIM/mCherry-*Hs*Orai. Cells were maintained at 37 °C in a humidified atmosphere containing 5% CO_2 and analyzed 48 h post-transfection.

Prior to pH manipulation, cells were washed and equilibrated in a standard recording solution containing (in mM): 140 NaCl, 5 KCl, 1 $MgCl_2$, 1 $CaCl_2$, 10 glucose, and 20 HEPES, adjusted to pH 7.5. This solution was used as the baseline condition for confocal imaging. Intracellular pH clamping were achieved using nigericin (10 μM; Sigma-Aldrich), a H^+/K^+ ionophore that equilibrates intracellular and extracellular pH in high-potassium buffers. Cells were incubated with calibration solutions of defined pH values (pH 6.0, 7.2, 7.5, 8.0, and 9.0), each containing 140 mM KCl, 1 mM $MgCl_2$, 0.2 mM EGTA, and 10 mM glucose. Buffer systems were selected according to the target pH: MES for pH 6.0, HEPES for pH 7.2, 7.5, and 8.0, and Tris for pH 9.0 (Y. Chen et al., 2024).

Confocal microscopy was performed before and after exposure to each pH condition to assess STIM redistribution and puncta formation at endoplasmic reticulum–plasma membrane (ER–PM) junctions. Changes in STIM activation in response to intracellular pH shifts were analyzed comparatively between AlSTIM and HsSTIM constructs.

3.4. *In silico* structural modeling, virtual screening, redocking and molecular dynamics simulations

The amino acid sequence of *Ascaris lumbricoides* Orai was retrieved from UniProt (Bateman et al., 2023) and used to generate a three-dimensional structural model. Homology modeling was performed using MODELLER (Webb & Sali, 2016), employing the open-state structure of *Drosophila melanogaster* Orai (PDB ID: 7KR5) as the template. A homohexameric assembly was constructed, and the best model was selected based on the lowest DOPE score. The selected structure was subsequently subjected to energy minimization and preliminary relaxation.

Virtual screening was carried out using a library of 3,400 small molecules obtained from the ZINC database (Irwin et al., 2020), corresponding to compounds classified as FDA-approved or in advanced clinical trial phases. Protein and ligand preparation for docking was performed using MGLTools (Morris et al., 2009). The

Orai model was prepared by adding polar hydrogens, assigning Gasteiger charges, and defining AutoDock4 atom types, followed by conversion to PDBQT format. Ligands were geometry-optimized and energy-minimized at physiological pH (7.4), with Gasteiger charges and AD4 atom types assigned prior to conversion to PDBQT format.

Docking calculations were performed using AutoDock Vina (Trott & Olson, 2010), executed via custom Bash scripts to enable batch processing. Docking poses were ranked according to binding affinity, and the three top-scoring ligands with the lowest binding energies were selected for further analysis. Binding modes were visually inspected using PyMOL (PyMOL, 2025).

To refine docking results, directed redocking was performed for each selected ligand using AutoDock Vina (Trott & Olson, 2010), with 30 independent docking runs per ligand. The most stable receptor–ligand complexes were selected based on consistently low binding energies and favorable interaction geometries. Protein–ligand interactions were subsequently analyzed using Discovery Studio Visualizer (BIOVIA, n.d.).

Molecular dynamics (MD) simulations were performed using Desmond-Maestro (Schrödinger) to evaluate the stability of the selected complexes under membrane-embedded conditions. Each protein–ligand complex was embedded in a DPPC lipid bilayer, solvated with explicit water molecules, and neutralized by the addition of Na^+ and Cl^- ions to achieve physiological ionic strength. Simulations were conducted using the OPLS (Optimized Potentials for Liquid Simulations) force field, which is the default force field implemented in Desmond for biomolecular and membrane systems (Higginbotham et al., 2025). The system was built using the Desmond System Builder and subjected to the standard Desmond relaxation protocol, including energy minimization and short equilibration phases under restrained conditions. Production MD simulations were carried out for 50 ns under the NPγT ensemble at 300 K, allowing for constant pressure, temperature, and membrane surface tension control. Trajectory analyses included root-mean-square deviation (RMSD), root-mean-square fluctuation (RMSF), secondary structure stability, protein–ligand contact profiles, and ligand conformational stability, as extracted from the Desmond simulation interaction reports (Friedrichs et al., 2009; Higginbotham et al., 2025).

4. RESULTS AND DISCUSSION

4.1. Multiple sequence alignment and comparative analysis of STIM and Orai proteins

The physicochemical properties of STIM and Orai proteins from *Ascaris lumbricoides* and *Schistosoma mansoni,* are summarized in Table 6, providing a comparative framework to evaluate structural features that may influence protein stability, membrane association, and functional coupling within the CRAC channel complex.

Table 6. General physicochemical properties of STIM and Orai proteins from helminth parasites.

Organism	Protein	Length (aa)	Molecular weight (kDa)	Theoretical pI	Extinction coefficient (280 nm, $M^{-1}\cdot cm^{-1}$)	GRAVY
Ascaris lumbricoides	STIM	560	62.92	6.96	48,400	−0.383
	Orai	291	32.48	7.14	24,660	0.260
Schistosoma mansoni	STIM	609	70.22	8.19	73,310	−0.584
	Orai1	216	24.16	8.72	25,690	0.687

Source (Expasy ProtParam, n.d.)

Multiple sequence alignment of STIM proteins from *Ascaris lumbricoides, Schistosoma mansoni, Homo sapiens*, and selected metazoan orthologs revealed a high degree of conservation across functionally critical regions (Figure 10). Pairwise comparative analysis indicated a moderate overall sequence identity between helminth STIM proteins and human STIM1. In this context, *A. lumbricoides* STIM displays 25.82% identity to human STIM1 at the full-length level, whereas *S. mansoni* STIM shows slightly higher identity, ranging from 24.51%. Notably, the luminal EF–SAM domain, the single transmembrane segment, and the cytosolic coiled-coil regions directly involved in Orai activation (CC2–CC3/SOAR) are well conserved between helminth STIM proteins and human STIM, suggesting strong evolutionary pressure to maintain the core mechanisms of Ca^{2+} sensing and STIM–Orai coupling. In contrast, greater sequence divergence is observed in low-complexity regions and in C-terminal regulatory segments, such as CC1 and the polybasic domain (PBD), which are enriched in proline and serine residues, potentially reflecting species-specific

regulatory adaptations without compromising the fundamental activation machinery (Cohen et al., 2023).

Analogous to the analysis performed for STIM, a multiple sequence alignment of Orai proteins from *Ascaris lumbricoides*, *Schistosoma mansoni*, representative helminths, vertebrates, and *Drosophila melanogaster* was conducted, with the latter used as a structural reference due to the availability of experimentally resolved structures in defined functional states (PDB: 4HKS, closed state; PDB: 7KR5, open state) (Hou et al., 2012a, 2020b). Comparative analysis revealed a moderate overall sequence identity between helminth Orai proteins and *D. melanogaster* Orai, with approximate values of 40.28% for *A. lumbricoides* Orai and 43.87% for *S. mansoni* Orai1.

Notably, the four transmembrane domains (TM1–TM4) display a high degree of conservation (Figure 11), preserving the alpha-helical organization characteristic of the Orai channel and consistent with its assembly as a homohexameric pore. This structural conservation suggests that the fundamental principles governing pore formation, ion selectivity, and Ca^{2+} permeation are maintained in helminth Orai proteins, despite divergence observed in extracellular and cytosolic regions, which may contribute to species-specific regulatory modulation (Hou et al., 2020b).

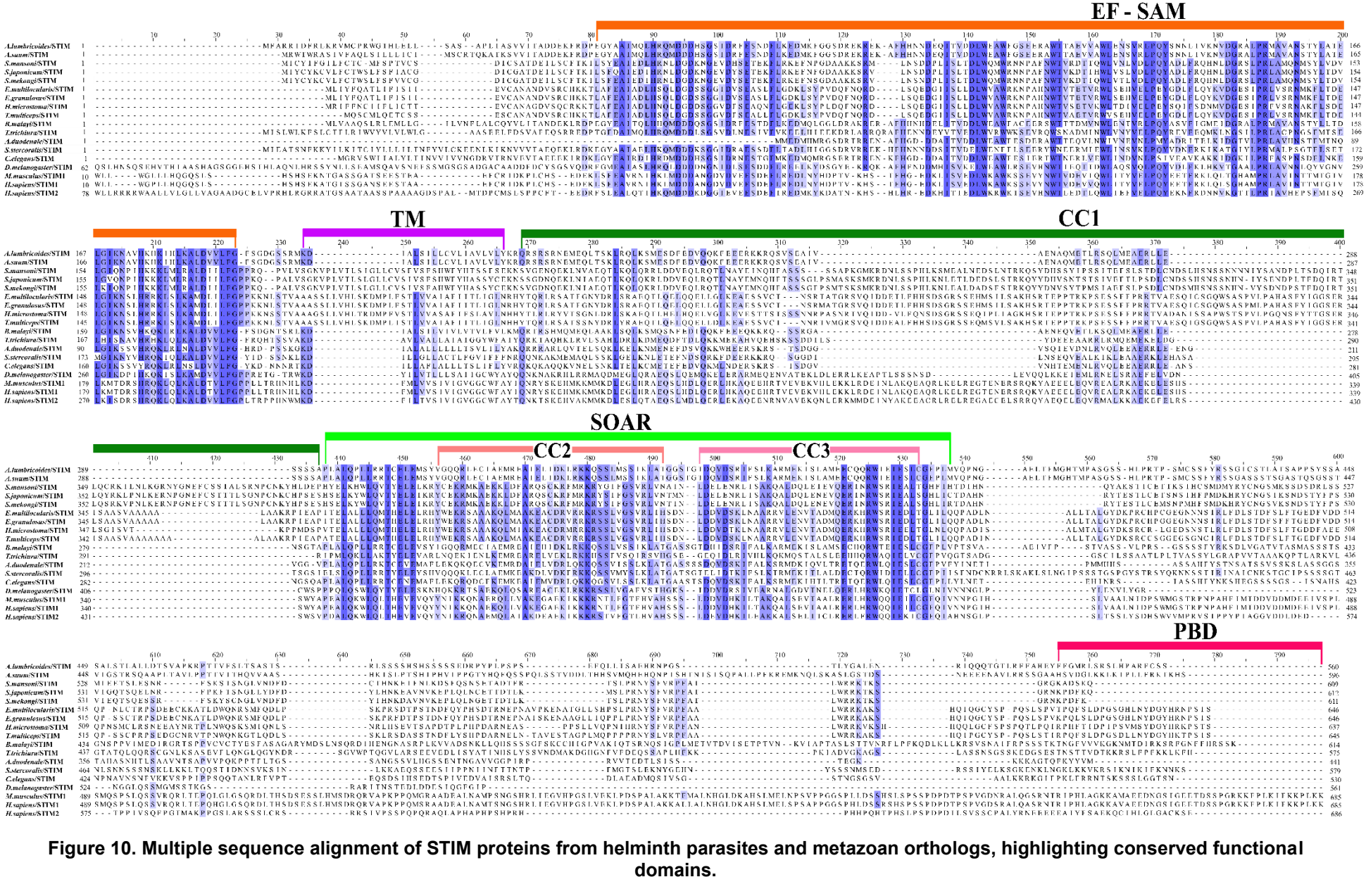

Figure 10. Multiple sequence alignment of STIM proteins from helminth parasites and metazoan orthologs, highlighting conserved functional domains.

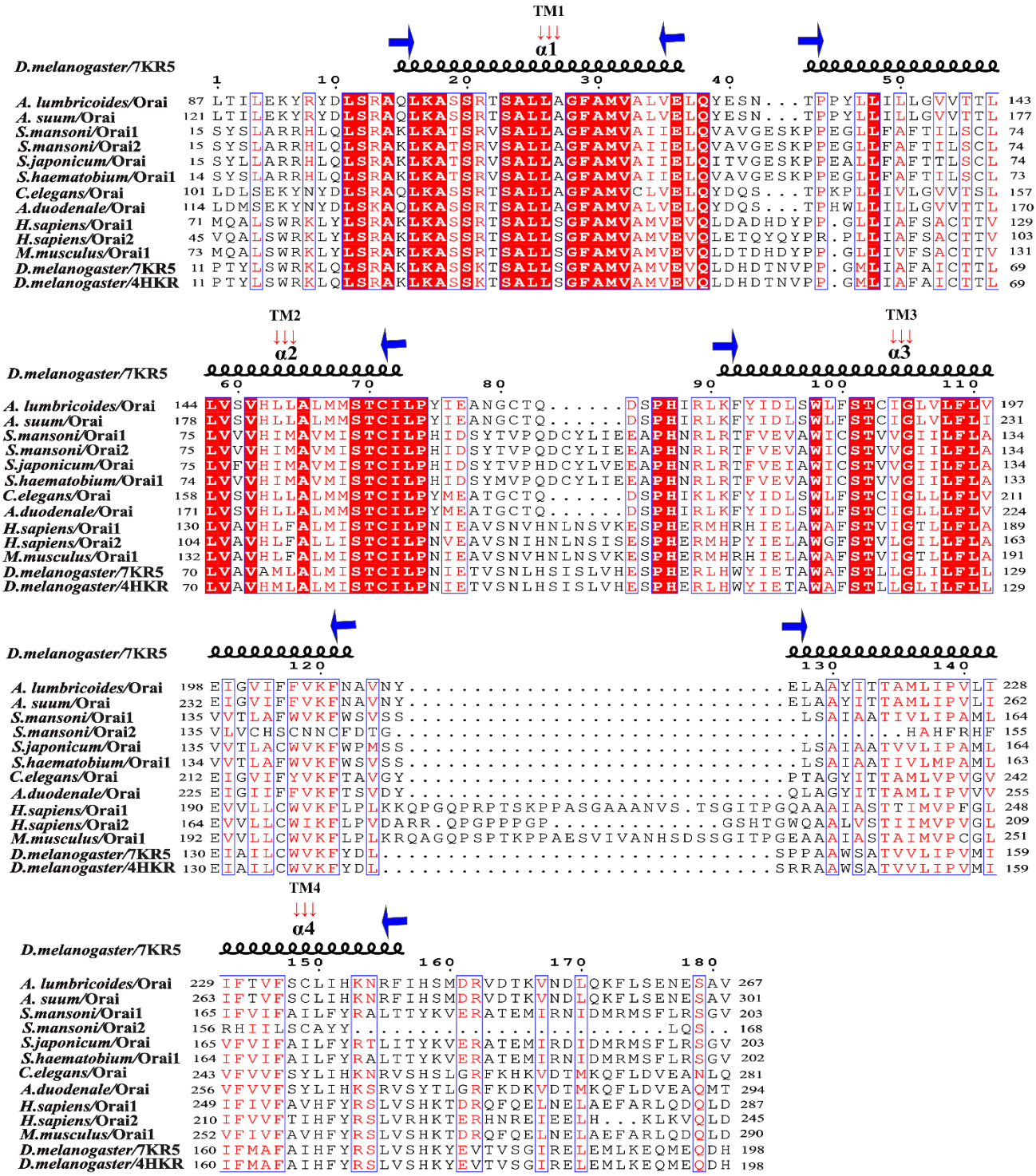

Figure 11. Multiple sequence alignment of Orai proteins from helminths, vertebrates, and *Drosophila melanogaster*, highlighting conservation of transmembrane domains.
The alignment highlights conservation of the four transmembrane segments (TM1–TM4) of Orai, as well as the predominantly alpha-helical secondary structure characteristic of the channel. *D. melanogaster* Orai structures in the closed (4HKS) and open (7KR5) states are included as structural references. The alignment was generated using ESPript 3.2.

Three-dimensional structure prediction of STIM using AlphaFold for *Ascaris lumbricoides* (Figure 12A) enabled clear identification of the canonical structural domains of STIM, including the luminal EF–SAM module, the single transmembrane segment, and the cytosolic coiled-coil regions involved in Orai activation. A notable finding is the absence of the polybasic domain (PBD) at the C-terminus of *A. lumbricoides* STIM, in contrast to what has been described for vertebrate STIM proteins. Similarly, structural prediction of STIM from *Schistosoma mansoni* (Figure 12B) revealed the presence of conserved domains but with a pronounced extension of disordered regions and cytosolic loops, particularly toward the C-terminal region, suggesting increased conformational flexibility relative to *A. lumbricoides* and other orthologs.

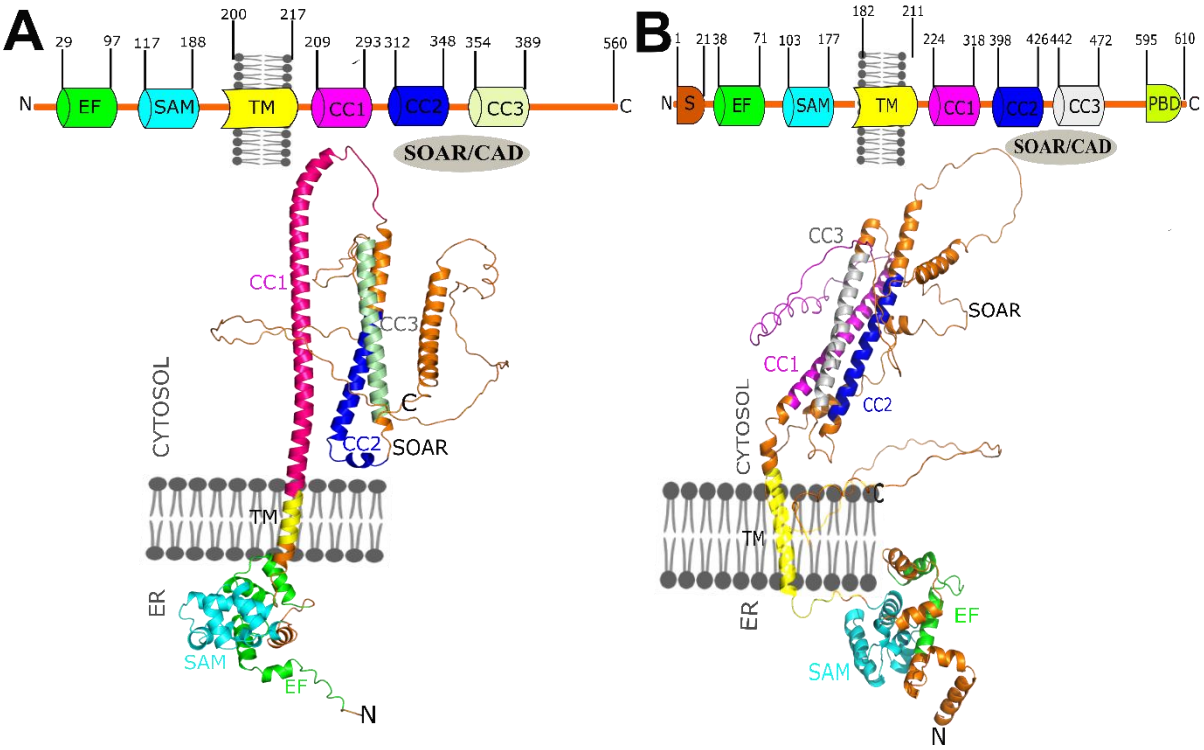

Figure 12. AlphaFold-based three-dimensional structural prediction of helminth STIM proteins.
Structural models of STIM generated by AlphaFold. **(A)** STIM from *Ascaris lumbricoides and* **(B)** STIM from *Schistosoma mansoni*. The EF–SAM domain, transmembrane segment (TM), CC1, CC2-CC3/SOAR regions, and the polybasic domain (PBD), when present, are indicated. Differences in the extent of disordered regions and cytosolic loops between both species are observed.

4.2. Cloning of STIM and Orai from *Ascaris lumbricoides* and *Schistosoma mansoni*

Successful generation of recombinant STIM constructs from *Ascaris lumbricoides* was confirmed by restriction analysis and agarose gel electrophoresis (Figure 13). Digestion of the pCMV6-XL5 expression vector harboring the full-length *A. lumbricoides* STIM sequence lacking the predicted signal peptide yielded a DNA fragment of approximately 1,625 bp, consistent with the expected size of the *Al*STIM insert. Similarly, restriction analysis of the pcDNA3.1-based construct containing the C-terminal region of *Al*STIM produced a fragment of approximately 1,043 bp, corresponding to the predicted length of the *Al*STIM-CT domain.

As shown in Figure 13, lanes I–IV display the recombinant clones containing full-length *Al*STIM, whereas lanes V–VII correspond to the *Al*STIM-CT construct. The presence of single, well-defined bands at the expected molecular sizes, together with the absence of non-specific amplification products, indicates high cloning specificity and structural integrity of the inserts. The reproducibility of the banding pattern across independent clones further supports the robustness of the cloning strategy and the efficiency of the restriction-based verification approach.

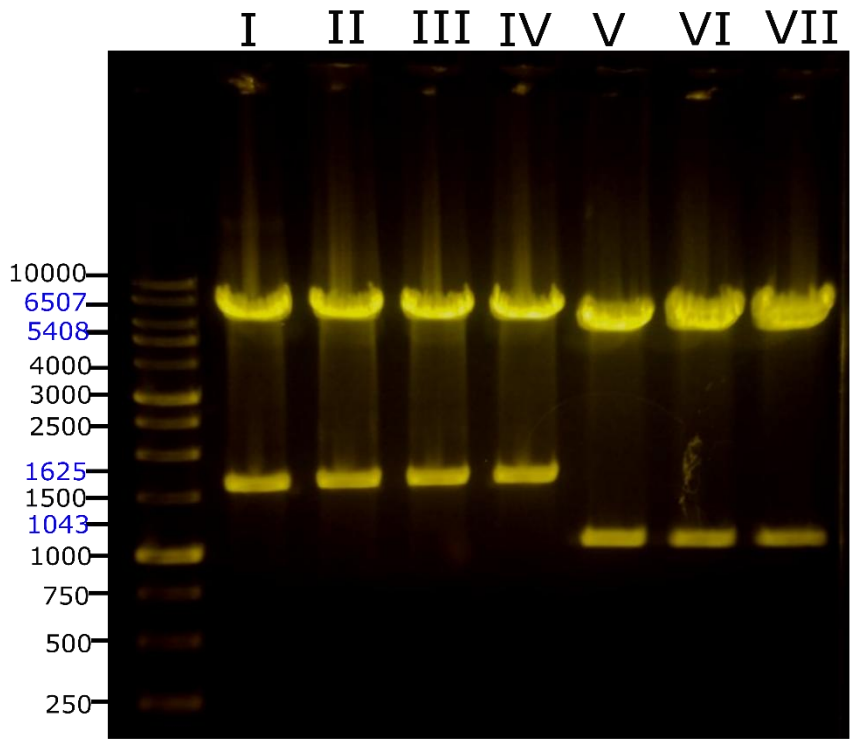

Figure 13. Agarose gel electrophoresis of recombinant *Ascaris lumbricoides* STIM constructs.
Agarose gel (0.8%) showing restriction analysis of recombinant clones. Lanes I–IV correspond to full-length *A. lumbricoides* STIM lacking the predicted signal peptide, revealing the expected insert size of ~1,625 bp. Lanes V–VII correspond to the C-terminal STIM construct (*Al*STIM-CT), displaying the expected fragment of ~1,043 bp. DNA size markers (bp) are shown on the left. All constructs were confirmed by sequencing.

The generation of the chimeric STIM construct was validated by restriction analysis and agarose gel electrophoresis (Figure 14). In this construct, the C-terminal region of *Schistosoma mansoni* STIM was replaced by the corresponding C-terminal domain from *Ascaris lumbricoides* and cloned into the pCMV6-XL5 expression vector. Digestion with HindIII and XhoI released a DNA fragment of approximately 1,625 bp, consistent with the expected size of the chimeric STIM insert. As shown in the gel, samples subjected to double digestion displayed a clear band at the predicted molecular size, confirming successful incorporation of the *A. lumbricoides* C-terminal region into the *Sm*STIM backbone. The absence of additional non-specific bands supports the specificity of the cloning strategy and indicates correct assembly of the chimeric construct, which was subsequently confirmed by sequencing.

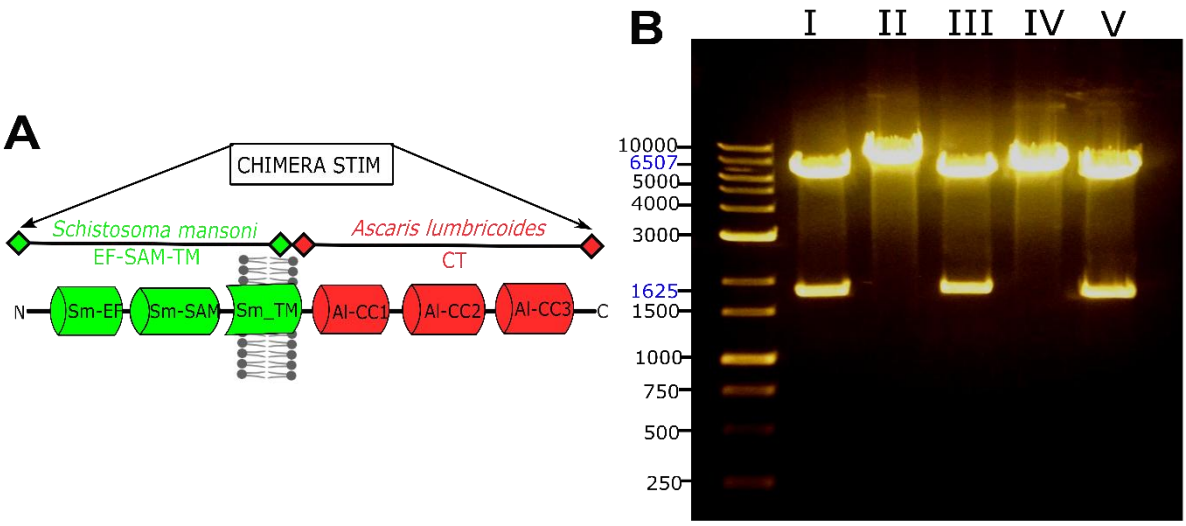

Figure 14. Agarose gel electrophoresis of recombinant chimeric STIM constructs.
(**A**) Schematic representation of the chimeric STIM protein, composed of the EF–SAM, transmembrane, and proximal cytosolic regions of *S. mansoni* STIM fused to the C-terminal domain of *A. lumbricoides* STIM. (**B**) Agarose gel (0.8%) showing restriction analysis of the chimeric construct. Double digestion with HindIII and XhoI released an insert of approximately 1,625 bp, detected in lanes II and IV, consistent with the expected size of the chimeric STIM sequence. Lanes I, III, and V correspond to undigested control samples (no restriction enzymes added), showing the intact plasmid. DNA size markers (bp) are shown on the left.

In contrast to the STIM-based constructs, we were unable to amplify the *Schistosoma mansoni* Orai isoform 2. This isoform encodes a markedly short protein of only 168 amino acids. In addition, truncated or non-canonical Orai isoforms may represent alternatively spliced or non-functional variants, which could further account for the lack of successful sequence amplification. Consequently, this isoform was excluded from subsequent functional analyses.

Table 7. Summary of recombinant STIM and Orai constructs generated in this study.
The table summarizes the cloning strategy, insert size, vector backbone, and validation status of each construct based on restriction analysis and sequencing.

Construct	Species	Protein / Domain	Vector	Expected insert size (bp)	Sequencing confirmation	Outcome
*Al*STIM (Δ signal peptide)	*Ascaris lumbricoides*	Full-length STIM	pCMV6-XL5	~1,625	Yes	Successfully cloned
*Al*STIM-CT	*Ascaris lumbricoides*	C-terminal domain (CT)	pcDNA3.1	~1,043	Yes	Successfully cloned
Chimeric STIM (*Sm*STIM–*Al*CT)	*S. mansoni* / *A. lumbricoides*	SmSTIM backbone + AlSTIM C-terminus	pCMV6-XL5	~1,625	Yes	Successfully cloned
*Sm*Orai (isoform 2)	*Schistosoma mansoni*	Orai isoform 2 (168 aa)	pGEM	~523	No	Not confirmed

4.3. Confocal imaging of STIM–Orai coupling and puncta formation

Confocal imaging was used to evaluate the ability of *Ascaris lumbricoides* STIM (*Al*STIM) to undergo puncta formation upon endoplasmic reticulum (ER) Ca^{2+} store depletion. HEK293 cells transiently expressing EGFP-*Al*STIM exhibited a predominantly diffuse distribution of the protein, mainly associated with intracellular membranes of the ER, under resting conditions (Figure 15B). Notably, treatment with thapsigargin (TG, 1 μM) for up to 40 minutes failed to induce the formation of discrete STIM puncta at ER–plasma membrane (ER–PM) junctions, as evidenced by the absence of punctate structures following stimulation (Figure 15C).

In humans, puncta formation represents a hallmark early step in CRAC channel activation, reflecting STIM oligomerization and its accumulation at endoplasmic reticulum–plasma membrane (ER–PM) contact sites, where STIM physically couples to Orai channels in the plasma membrane. This process is

critically supported by the polybasic domain (PBD) located at the C-terminus of human STIM1, which mediates electrostatic interactions with plasma membrane phosphoinositides and stabilizes STIM positioning at ER–PM junctions (Cohen et al., 2023). In contrast, *Ascaris lumbricoides* STIM (AlSTIM) lacks a canonical C-terminal polybasic region, a structural feature that is also absent in STIM homologs from several invertebrate species.

Studies in *Caenorhabditis elegans* have shown that STIM can display atypical spatial distributions, including pre-assembled peripheral puncta at resting state; however, such puncta are not sufficient to activate Orai or induce CRAC currents in the absence of ER Ca^{2+} depletion (Gao et al., 2009). In contrast, recent work in *Schistosoma mansoni* has demonstrated that the CRAC channel is constitutively active when expressed in HEK293 cells, a behavior attributed to structural features within the C-terminal region of SmSTIM that promote stable ER–plasma membrane coupling (Zeraik et al., Submitted article). In this context, the absence of puncta formation observed for *Al*STIM after TG treatment suggests that, unlike *Sm*STIM or human STIM1, *Al*STIM alone is unable to efficiently reorganize into functional ER–PM contact sites. Collectively, these observations indicate that puncta formation and CRAC activation are tightly regulated, species-dependent processes, in which structural differences within the STIM C-terminal region critically determine spatial dynamics and coupling competence.

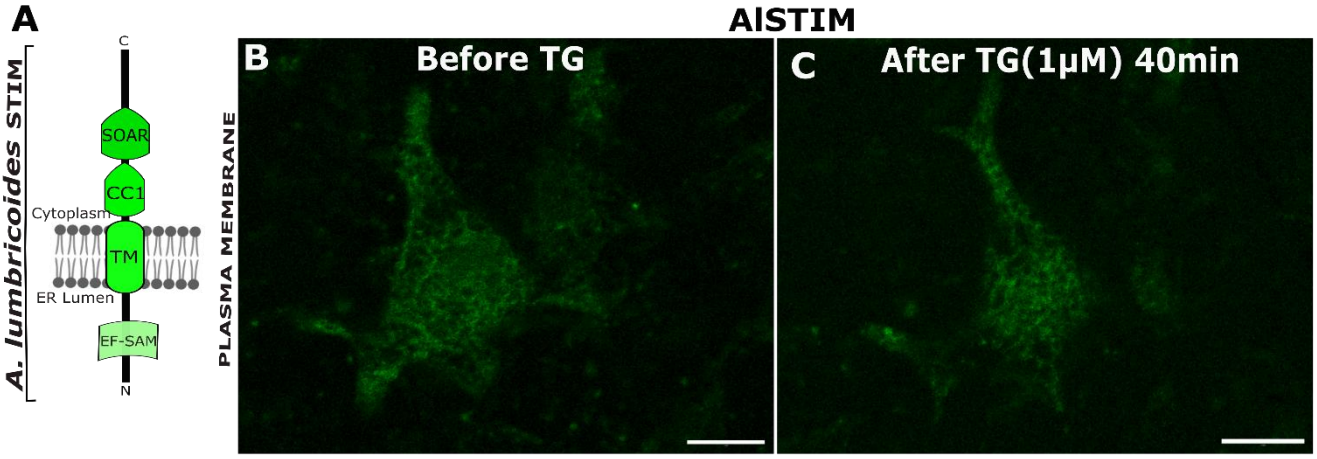

Figure 15. Confocal analysis of EGFP-*Al*STIM distribution in HEK293 cells following ER Ca^{2+} store depletion.
(**A**) Schematic representation of *A. lumbricoides* STIM highlighting the absence of a polybasic domain at the C-terminal region. (**B**) Confocal images of HEK293 cells expressing EGFP-*Al*STIM

under basal conditions, showing a diffuse intracellular distribution. (**C**) After treatment with thapsigargin (TG, 1 µM) for 40 min, EGFP-*Al*STIM does not reorganize into punctate structures at ER–PM contact sites, indicating a lack of puncta formation upon ER Ca^{2+} depletion. Scale bars = 10 µm.

Co-expression of EGFP-tagged *Ascaris lumbricoides* STIM (*Al*STIM) together with mCherry-tagged *A. lumbricoides* Orai (*Al*Orai) revealed a marked change in STIM spatial organization upon endoplasmic reticulum (ER) Ca^{2+} store depletion. In HEK293 cells co-transfected with both proteins, treatment with thapsigargin (TG, 1 µM) for 40 min induced the formation of discrete puncta at ER–plasma membrane (ER–PM) junctions (Figure 16C), in contrast to the diffuse distribution observed when *Al*STIM was expressed alone. The absence of the red channel corresponding to mCherry-*Al*Orai is due to a malfunction of the microscope's red laser; consequently, only the green fluorescence signals could be reported throughout this document.

The inability of *Al*STIM to form puncta in the absence of *Al*Orai is consistent with the lack of a canonical C-terminal polybasic domain (PBD), which in mammalian STIM1 mediates electrostatic interactions with plasma membrane phosphoinositides and stabilizes ER–PM contact sites (Cohen et al., 2023; Liou et al., 2005). Multiple sequence alignment of STIM orthologs confirms the absence of conserved polybasic residues in the C-terminal region of *Al*STIM, in contrast to vertebrate STIM1 and several invertebrate homologs (Figure 16D), a feature that has been shown to critically influence membrane tethering and puncta stability (Gao et al., 2009). In agreement with these observations, structural representations of the STIM polybasic domain reveal a positively charged helical motif that is absent in A. lumbricoides STIM (Figure 16E), providing a structural explanation for its limited intrinsic membrane-anchoring capacity (Stathopulos et al., 2013).

In this context, the presence of *Al*Orai appears to compensate for the absence of a PBD in *Al*STIM by providing a binding and anchoring platform that enables STIM clustering at ER–PM junctions. This interpretation is supported by studies demonstrating that direct interactions between the SOAR/CAD region of STIM and cytosolic domains of Orai can stabilize puncta formation and promote channel gating even when membrane lipid interactions are weakened (Baraniak et

al., 2020; Yuan et al., 2009). Together, these findings support a model in which puncta formation and CRAC channel activation in *A. lumbricoides* are strictly dependent on productive STIM–Orai coupling rather than on intrinsic STIM-driven membrane tethering alone.

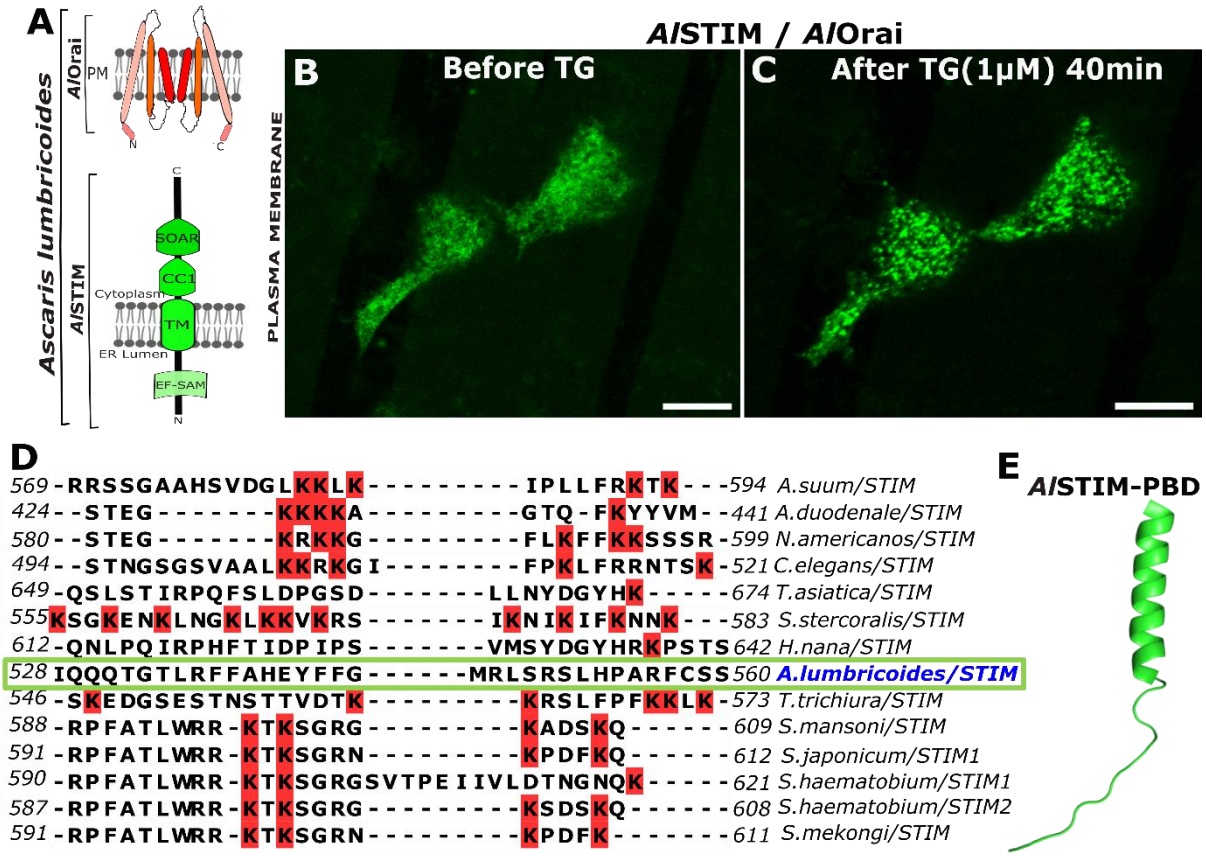

Figure 16. Orai-dependent puncta formation and CRAC channel activation mediated by *Al*STIM in HEK293 cells.
(**A**) Schematic representation of *A. lumbricoides* STIM, lacking a C-terminal polybasic domain (PBD), and the corresponding Orai protein. (**B**) Confocal images of HEK293 cells co-transfected with EGFP-*Al*STIM and mCherry-*Al*Orai under basal conditions, showing a predominantly diffuse distribution prior to stimulation. (**C**) Following ER Ca^{2+} store depletion with thapsigargin (TG, 1 μM) for 40 min, robust puncta formation is observed at ER–plasma membrane junctions, indicating functional STIM–Orai coupling and CRAC channel activation. (**D**) Multiple sequence alignment of the C-terminal region of STIM orthologs highlighting the absence of conserved polybasic residues in *A. lumbricoides* STIM. (E) Structural representation of the STIM polybasic domain illustrating a positively charged helical motif that is absent in *Al*STIM. Puncta formation in this system is dependent on the presence of *Al*Orai, compensating for the lack of a PBD in *Al*STIM. Scale bars = 10 μm.

To assess species specificity in STIM–Orai coupling, EGFP-tagged *Ascaris lumbricoides* STIM (*Al*STIM) was co-expressed with mCherry-tagged human Orai1 (*Hs*Orai1) in HEK293 cells. Under basal conditions, both proteins exhibited a diffuse distribution, predominantly associated with the plasma membrane. Notably,

ER Ca^{2+} store depletion induced by thapsigargin (TG, 1 µM) for 40 min failed to promote puncta formation or STIM reorganization at ER–plasma membrane (ER–PM) contact sites (Figure 17C), indicating the absence of functional CRAC channel activation in this heterologous combination.

Productive CRAC activation requires direct and structurally compatible interactions between the SOAR/CAD region of STIM and the cytosolic domains of Orai, which stabilize the STIM–Orai complex and enable channel gating (Stathopulos et al., 2013; Yuan et al., 2009). Previous studies have shown that even subtle mismatches in STIM–Orai interfaces across species can impair coupling efficiency and abolish Ca^{2+} influx, despite the individual functionality of each component in its native context (Liou et al., 2005; Prakriya et al., 2006). Consistent with this model, the inability of *Al*STIM to activate *Hs*Orai1 supports the notion that CRAC channel activation in *A. lumbricoides* depends on a cognate, species-specific STIM–Orai interaction, rather than on Orai presence alone.

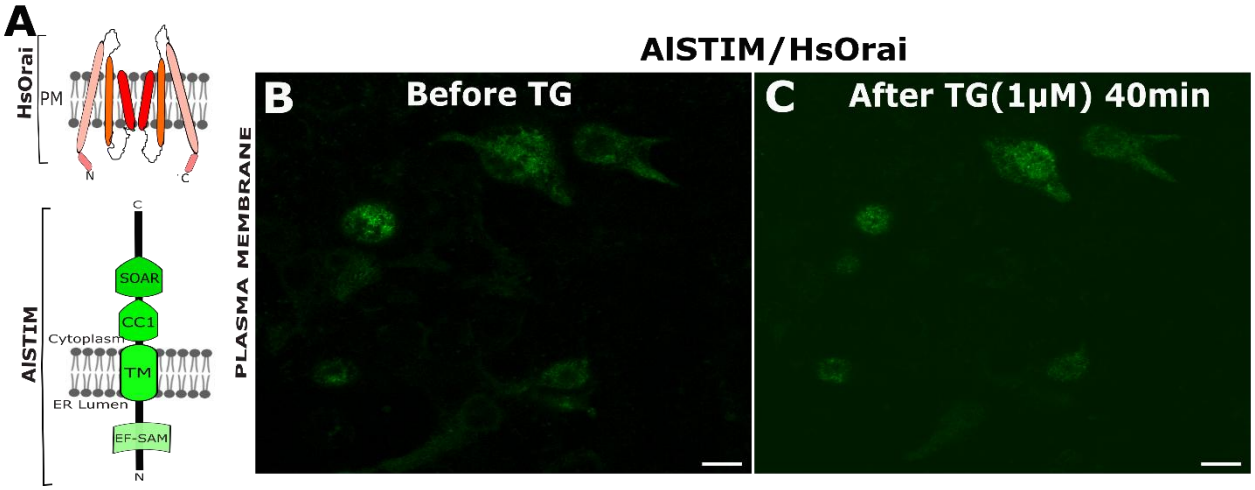

Figure 17. Lack of puncta formation and CRAC activation in the *Al*STIM–*Hs*Orai combination.
(**A**) Schematic representation of *A. lumbricoides* STIM, lacking a C-terminal polybasic domain, and human Orai1. (**B**) Confocal images of HEK293 cells co-transfected with EGFP-AlSTIM and mCherry-*Hs*Orai1 under basal conditions, showing a diffuse distribution of both proteins prior to stimulation. (**C**) Following ER Ca^{2+} store depletion with thapsigargin (TG, 1 µM) for 40 min, no puncta formation or STIM reorganization at ER–PM contact sites is observed, indicating ineffective STIM–Orai coupling and lack of CRAC channel activation. Scale bars = 10 µm.

To further evaluate the specificity of STIM–Orai coupling among phylogenetically related helminths, EGFP-tagged *Ascaris lumbricoides* STIM

(*Al*STIM) was co-expressed with mCherry-tagged *Schistosoma mansoni* Orai (*Sm*Orai) in HEK293 cells. Despite the evolutionary proximity between *A. lumbricoides* and *S. mansoni*, ER Ca^{2+} store depletion induced by thapsigargin (TG, 1 µM) for 40 min failed to trigger puncta formation or STIM reorganization at ER–plasma membrane (ER–PM) contact sites (Figure 18C), indicating ineffective STIM–Orai coupling in this heterologous helminth–helminth combination.

Previous studies have demonstrated that productive CRAC channel activation relies on highly specific molecular interfaces between STIM and Orai, particularly involving the SOAR/CAD region of STIM and conserved cytosolic helices of Orai that mediate direct binding and channel gating (Stathopulos et al., 2013; Yuan et al., 2009). Although *Sm*Orai is functional and capable of supporting CRAC currents when paired with its cognate STIM in mammalian cells, structural divergence within the C-terminal region of *Al*STIM—most notably the absence of a canonical polybasic domain likely impairs its ability to recognize and stably engage *Sm*Orai (Zeraik et al., Submitted article). This interpretation is further supported by comparative analyses indicating that even subtle sequence variations in STIM–Orai interaction surfaces can abolish coupling across species boundaries (Gao et al., 2009; Prakriya et al., 2006). Taken together with the lack of functional coupling observed in the *Al*STIM–*Hs*Orai combination (Figure 17 and Figure 18), these findings demonstrate that *Al*STIM supports CRAC channel activation exclusively in the presence of its cognate *Al*Orai. This strict specificity suggests the existence of parasite-selective molecular determinants within *Al*STIM that prevent productive interaction with Orai proteins from other organisms. Importantly, such species-restricted coupling provides a conceptual framework for rational drug design, as pharmacological targeting of helminth-specific STIM–Orai interfaces could enable selective modulation of parasite Ca^{2+} signaling without interfering with host CRAC channels.

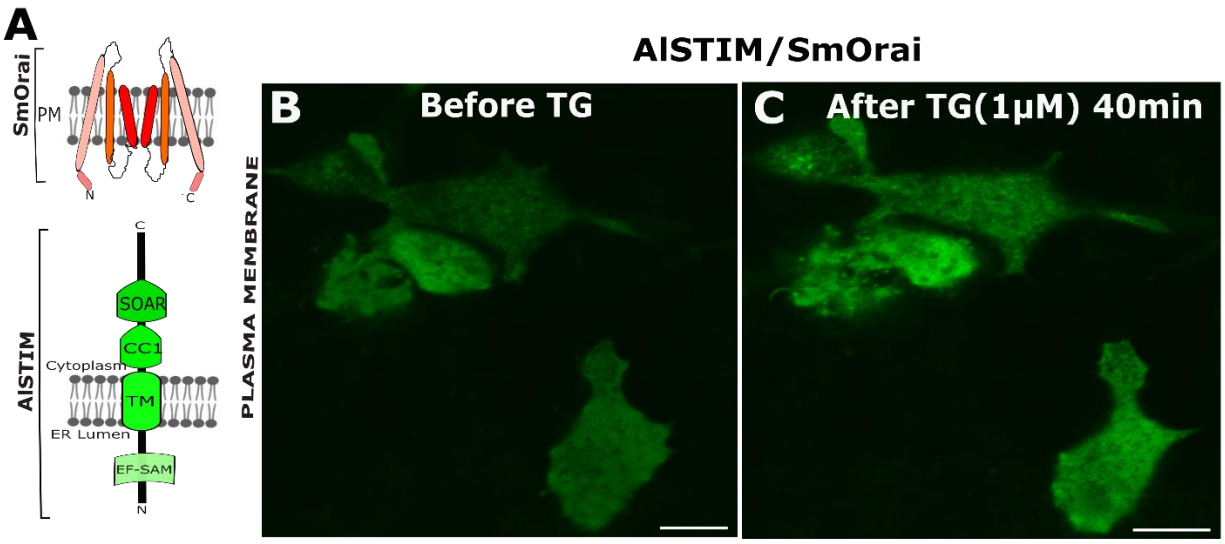

Figure 18. Absence of puncta formation and CRAC activation in the AlSTIM–SmOrai combination.
(**A**) Schematic representation of *A. lumbricoides* STIM, lacking a C-terminal polybasic domain, and *S. mansoni* Orai. (**B**) Confocal images of HEK293 cells co-transfected with EGFP-*Al*STIM and mCherry-SmOrai under basal conditions, showing a diffuse intracellular distribution of both proteins. (**C**) Following ER Ca^{2+} store depletion with thapsigargin (TG, 1 μM) for 40 min, no puncta formation or STIM reorganization at ER–PM contact sites is observed, indicating ineffective STIM–Orai coupling and absence of CRAC channel activation. Scale bars = 10 μm.

A chimeric construct was generated in which the luminal EF–SAM domain, transmembrane segment, and proximal cytosolic regions of *Schistosoma mansoni* STIM were fused to the C-terminal region of *Ascaris lumbricoides* STIM and co-expressed with *A. lumbricoides* Orai. This strategy was based on the hypothesis that the STIM C-terminus, which contains the SOAR/CAD activation domain, could function as a modular element capable of restoring constitutive or store depletion–dependent Ca^{2+} activation from the endoplasmic reticulum (ER). However, confocal microscopy analysis revealed a predominantly diffuse intracellular distribution under both basal conditions and following ER Ca^{2+} depletion induced by thapsigargin, with no evidence of puncta formation or redistribution to ER–plasma membrane contact sites (Figure 19). These results indicate that isolated replacement of the STIM C-terminal region is not sufficient to support productive STIM–Orai coupling, suggesting that additional domains and allosteric interactions between structural regions are essential for proper STIM activation. The absence of puncta formation further supports the notion that STIM function relies on a finely tuned global architecture, in which coordinated interactions among luminal, transmembrane, and cytosolic domains are required to effectively transmit ER Ca^{2+} depletion signals to Orai

channels. Overall, this chimeric approach highlights the limitations of considering the *A. lumbricoides* STIM C-terminus as an autonomous activation module.

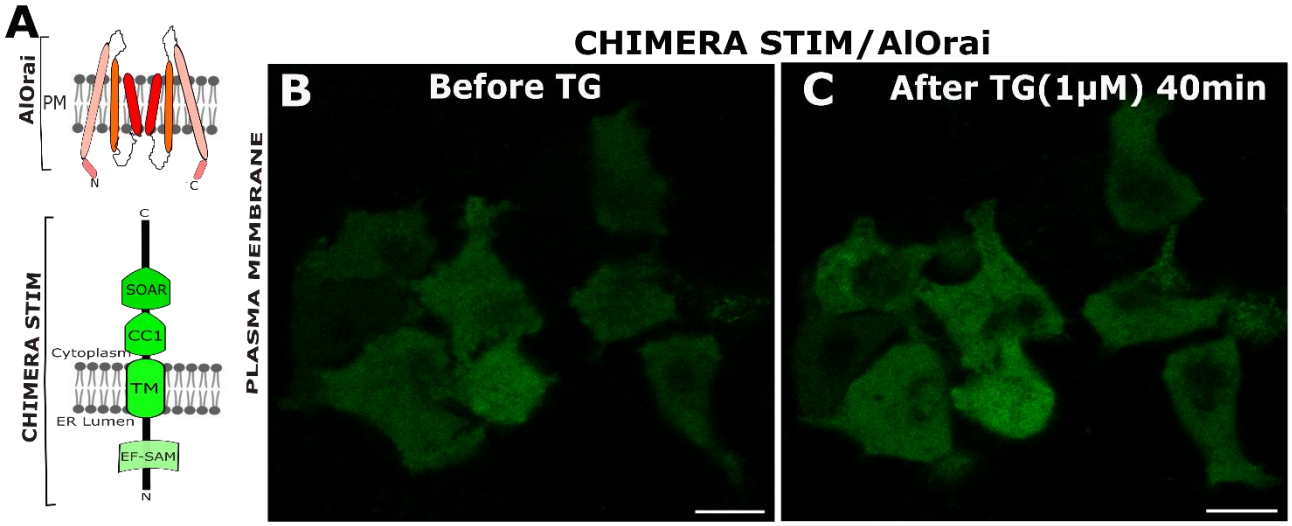

Figure 19. Chimeric STIM–*Al*Orai construct fails to induce puncta formation upon ER Ca^{2+} depletion.
(**A**) Schematic representation of the chimeric STIM protein, composed of the luminal EF–SAM domain, transmembrane segment, and proximal cytosolic regions of Schistosoma mansoni STIM fused to the C-terminal region of Ascaris lumbricoides STIM, co-expressed with *A. lumbricoides* Orai. (**B**) Confocal images of HEK293 cells expressing the chimeric STIM/AlOrai combination under basal conditions, showing a predominantly diffuse intracellular distribution. (**C**) Following ER Ca^{2+} store depletion with thapsigargin (TG, 1 µM) for 40 min, no puncta formation or reorganization at ER–plasma membrane contact sites is observed. These results indicate that the chimeric STIM construct is unable to support puncta formation and functional CRAC channel activation, highlighting the critical requirement for an intact and species-specific STIM C-terminal architecture for productive STIM–Orai coupling. Scale bars = 10 µm.

4.4. Functional assessment of CRAC channel activation by NFAT nuclear translocation

To functionally validate CRAC channel activation mediated by the *Ascaris lumbricoides* STIM–Orai complex, NFAT nuclear translocation was employed as a Ca^{2+}-dependent downstream readout of sustained store-operated calcium entry (SOCE). HEK293 cells were co-transfected with EGFP-tagged *A. lumbricoides* STIM (*Al*STIM), mCherry-tagged *A. lumbricoides* Orai (*Al*Orai), and a GFP-tagged NFAT reporter. Under basal conditions, NFAT fluorescence was predominantly localized in the cytoplasm, consistent with its phosphorylated and inactive state (Figure 20B,D). Depletion of endoplasmic reticulum Ca^{2+} stores by treatment with thapsigargin (TG, 1 µM) for 40 min induced robust STIM–Orai puncta formation at ER–plasma membrane junctions (Figure 20C), indicating effective coupling

between *Al*STIM and *Al*Orai. However, under Ca^{2+}-free extracellular conditions, NFAT remained cytoplasmic, demonstrating that ER Ca^{2+} depletion alone is insufficient to trigger NFAT activation in the absence of Ca^{2+} influx. Subsequent addition of extracellular $CaCl_2$ (2 mM) resulted in a pronounced translocation of GFP-NFAT from the cytoplasm to the nucleus within 15 min (Figure 20E). Higher extracellular Ca^{2+} concentrations may promote activation of endogenous STIM–Orai channels in HEK293 cells, which natively express functional CRAC components; therefore, 2 mM $CaCl_2$ was selected to limit this contribution and ensure that NFAT translocation predominantly reflects the activity of the heterologously expressed *A. lumbricoides* STIM–Orai complex (Gwack et al., 2007; Prakriya & Lewis, 2015). This provides direct functional evidence of Ca^{2+} entry through a STIM–Orai–dependent CRAC channel formed by *A. lumbricoides* proteins. This nuclear accumulation of NFAT reflects sustained Ca^{2+} signaling sufficient to activate the Ca^{2+}/calmodulin–calcineurin pathway, leading to NFAT dephosphorylation and nuclear import.

NFAT nuclear translocation is widely recognized as a sensitive and integrative functional readout of CRAC channel activity, as it specifically requires prolonged Ca^{2+} influx rather than transient Ca^{2+} release events (Hogan & Rao, 2015; Prakriya & Lewis, 2015). Previous studies in mammalian systems have firmly established that CRAC-mediated Ca^{2+} entry is both necessary and sufficient to drive NFAT-dependent transcriptional responses (Feske et al., 2006; Liou et al., 2005). More recently, NFAT-based assays have been successfully applied to indirectly quantify CRAC channel activity in heterologous expression systems and immune cells (Carretta et al., 2018).

Importantly, functional STIM–Orai coupling and SOCE have previously been demonstrated in the helminth *Schistosoma mansoni* using heterologous expression approaches, providing the first evidence of a bona fide CRAC channel in a parasitic flatworm (Zeraik et al., Submitted article). The present results extend these findings to a parasitic nematode and demonstrate, for the first time, that *A. lumbricoides* STIM and Orai proteins assemble into a functional CRAC channel capable of supporting Ca^{2+}-dependent transcriptional signaling. Taken together, the coordinated observation of STIM–Orai puncta formation and NFAT nuclear translocation establishes that the *A. lumbricoides* CRAC channel is not only

structurally competent but also functionally active. These findings provide a critical functional validation of CRAC channel activity in *A. lumbricoides* and support the broader concept that SOCE represents an evolutionarily conserved signaling mechanism in helminth parasites with potential relevance for parasite physiology and therapeutic targeting.

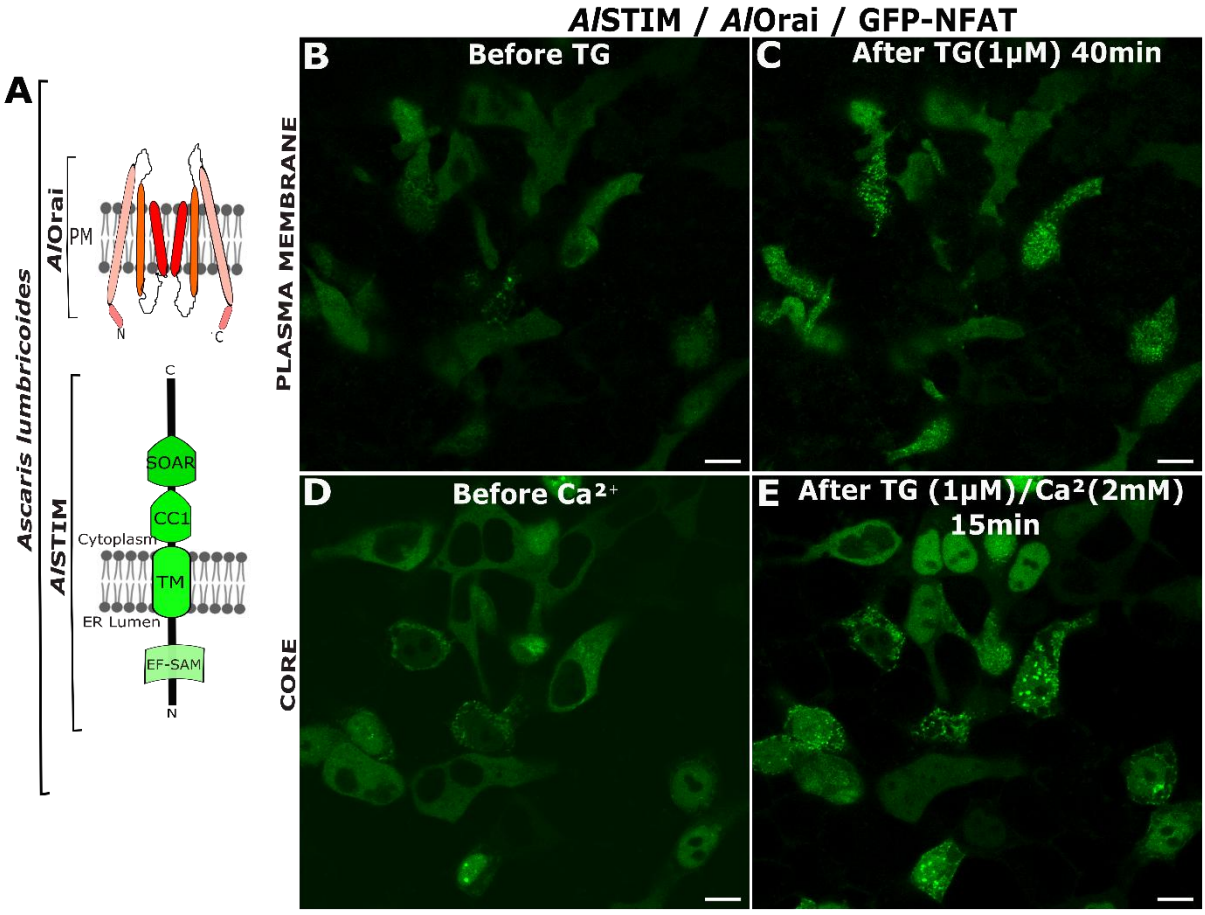

Figure 20. Indirect measurement of Ca^{2+} influx through NFAT nuclear translocation in the *Ascaris lumbricoides* CRAC channel.
(**A**) Schematic representation of *A. lumbricoides* STIM and Orai proteins. (**B,D**) Confocal images correspond to the same cells acquired at different focal planes. Panel B shows the superficial plane at the plasma membrane, whereas panel D corresponds to a deeper focal plane centered on the nucleus to assess NFAT subcellular localization. HEK293 cells co-transfected with EGFP-AlSTIM (1 μg), mCherry-AlOrai (1 μg), and GFP-NFAT (0.5 μg) showing basal subcellular localization of the proteins prior to stimulation, with NFAT predominantly cytoplasmic. (**C**) After endoplasmic reticulum Ca^{2+} store depletion by thapsigargin (TG, 1 μM) for 40 min, STIM–Orai puncta formation is observed, indicating CRAC channel assembly. (**E**) Subsequent addition of extracellular $CaCl_2$ (2 mM) induces Ca^{2+} influx and results in robust nuclear translocation of GFP-NFAT within 15 min, demonstrating functional CRAC channel activity mediated by *A. lumbricoides* STIM–Orai coupling. Scale bars = 10 μm.

To further evaluate the specificity and directionality of STIM–Orai coupling, human STIM1 (*Hs*STIM) was co-expressed with *Ascaris lumbricoides* Orai (*Al*Orai)

in HEK293 cells, together with a GFP-tagged NFAT reporter. Under basal conditions, NFAT remained predominantly cytoplasmic, indicating an inactive signaling state. Depletion of ER Ca^{2+} stores with thapsigargin (TG, 1 µM) induced rapid formation of STIM puncta at ER–plasma membrane junctions (Figure 21C), demonstrating efficient recruitment and clustering of *Hs*STIM in the presence of *Al*Orai. Subsequent addition of extracellular $CaCl_2$ (2 mM) resulted in robust nuclear translocation of GFP-NFAT within 15 min (Figure 21E), providing functional evidence of Ca^{2+} influx through *AlOrai* gated by human STIM1. These results indicate that *A. lumbricoides* Orai constitutes a fully competent CRAC channel pore capable of supporting sustained Ca^{2+} signaling and downstream NFAT activation. In contrast with the non-functional *Al*STIM–*Hs*Orai combination, this finding highlights a directional compatibility in which human STIM can productively activate parasite Orai, reinforcing the notion that species-specific constraints are primarily encoded within STIM, while the pore-forming properties of *Al*Orai are evolutionarily conserved.

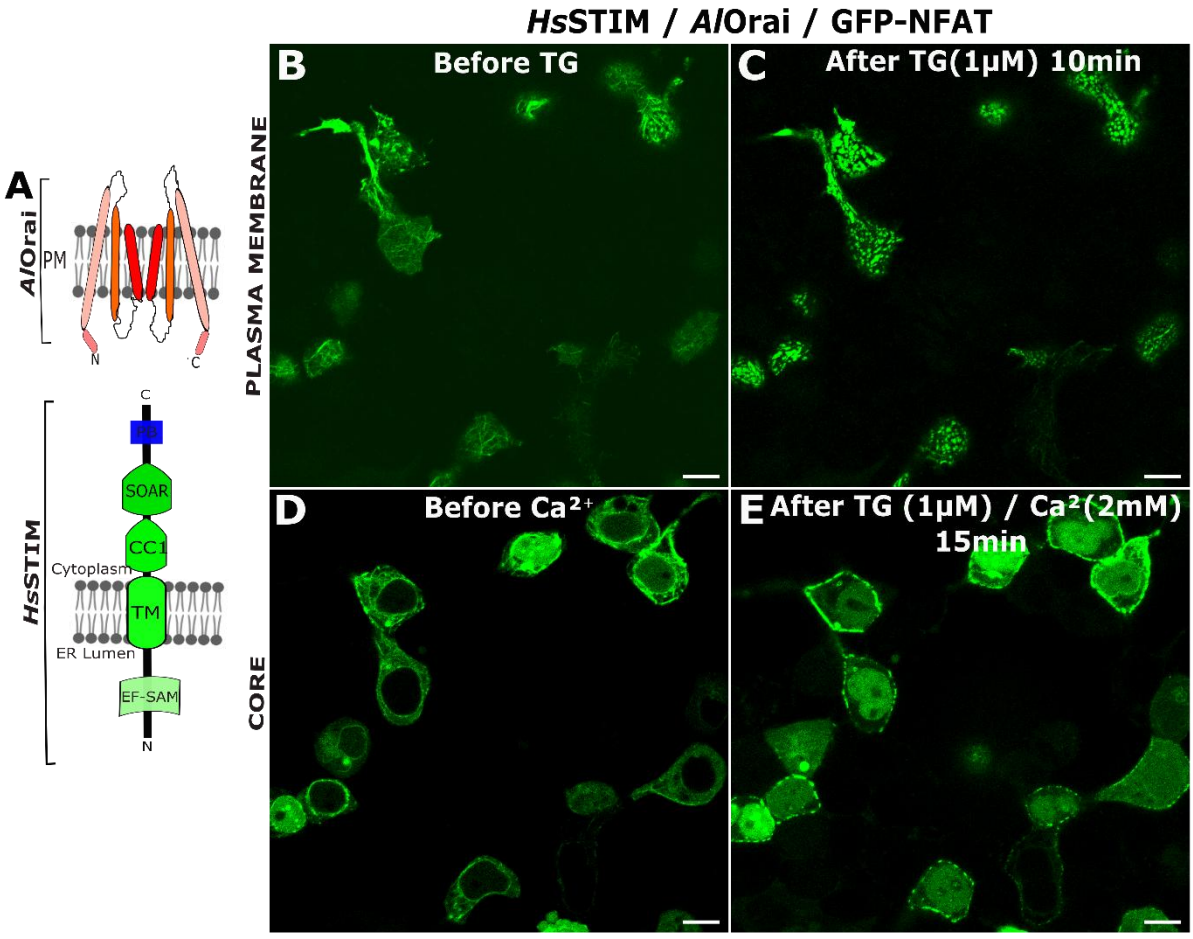

Figure 21. Functional reconstitution of CRAC channel activity by human STIM1 and *Ascaris lumbricoides* Orai assessed by NFAT nuclear translocation.

(**A**) Schematic representation of human STIM1 (*Hs*STIM), containing a canonical C-terminal polybasic domain, and *A. lumbricoides* Orai (*Al*Orai). (**B,D**) HEK293 cells co-transfected with EGFP-*Hs*STIM (1 µg), mCherry-*Al*Orai (1 µg), and GFP-NFAT (0.5 µg) showing basal subcellular localization of STIM and NFAT prior to stimulation, with NFAT predominantly cytoplasmic. (**C**) Following ER Ca^{2+} store depletion with thapsigargin (TG, 1 µM) for 10 min, *Hs*STIM redistributes into discrete puncta at ER–plasma membrane junctions, indicative of CRAC channel assembly. (**E**) Subsequent addition of extracellular $CaCl_2$ (2 mM) induces Ca^{2+} influx and results in robust nuclear translocation of GFP-NFAT within 15 min, demonstrating functional CRAC channel activation mediated by the *Hs*STIM–*Al*Orai interaction. Scale bars = 10 µm.

To evaluate whether the isolated C-terminal region of *A. lumbricoides* STIM is sufficient to promote CRAC channel activation independently of endoplasmic reticulum Ca^{2+} store depletion, the *Al*STIM-CT construct was co-expressed with *A. lumbricoides* Orai and GFP-NFAT. Under basal conditions, NFAT displayed a predominantly cytosolic localization, consistent with low intracellular Ca^{2+} levels. Upon addition of extracellular $CaCl_2$, a pronounced nuclear translocation of GFP-NFAT was observed, indicating Ca^{2+} influx mediated by constitutively active CRAC channels (Figure 22). These results demonstrate that the C-terminal region of *Al*STIM is capable of activating Orai independently of Ca^{2+} store depletion, consistent with the presence of the SOAR/CAD activation domain within this region. In contrast to the chimeric STIM construct, which failed to induce puncta formation or functional coupling, the isolated *Al*STIM-CT region retains the ability to activate Orai, highlighting the functional competence of the *A. lumbricoides* STIM C-terminal domain when released from the constraints imposed by the full-length protein architecture. Collectively, these findings support a model in which the AlSTIM C-terminal domain is sufficient to induce constitutive CRAC channel activation.

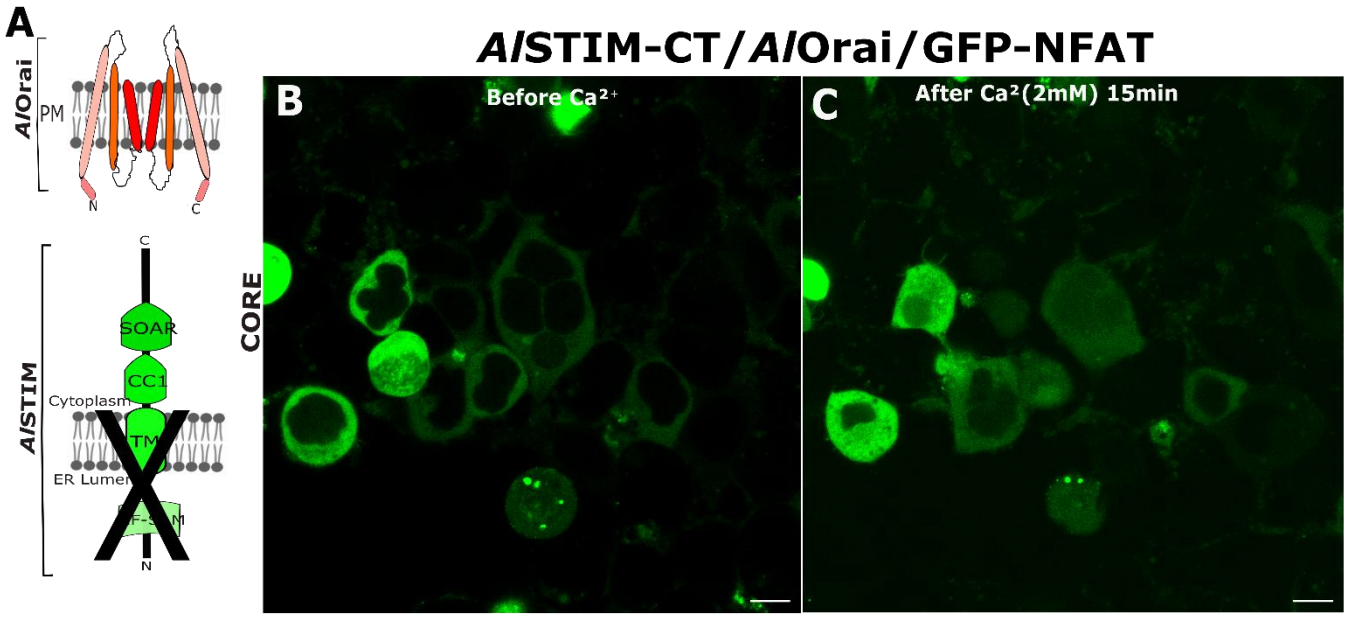

Figure 22.Constitutive CRAC channel activation mediated by the C-terminal domain of *Ascaris lumbricoides* STIM (*Al*STIM-CT).
(**A**) Schematic representation of *Al*Orai and the isolated C-terminal region of *Al*STIM (*Al*STIM-CT), lacking the luminal EF–SAM Ca^{2+}-sensing domain. (**B**) HEK293 cells co-transfected with *Al*STIM-CT, *Al*Orai, and GFP-NFAT showing basal NFAT localization in the absence of extracellular Ca^{2+}. (**C**) Addition of extracellular $CaCl_2$ (2 mM) for 15 min induces Ca^{2+} influx and nuclear translocation of GFP-NFAT, indicating constitutive CRAC channel activation mediated by AlSTIM-CT. Scale bars = 10 µm.

The results of puncta formation and Ca^2-dependent NFAT nuclear translocation assays, obtained with different STIM and Orai combinations, are summarized in Table 8.

Table 8.Summary of STIM–Orai constructs and combinations evaluated for CRAC channel activation.
This table summarizes the STIM and Orai constructs experimentally tested in this study and their functional outcomes, assessed by STIM–Orai puncta formation and Ca^{2+}-dependent NFAT nuclear translocation.

Construct / Combination	Organism(s)	STIM–Orai puncta formation	NFAT nuclear translocation	Functional CRAC channel
EGFP-AlSTIM	*Ascaris lumbricoides*	No	-	**No**
EGFP-*Al*STIM + mCherry -*Al*Orai	*Ascaris lumbricoides*	Yes (after TG-induced ER Ca^{2+} depletion)	-	**Yes**
EGFP-*Al*STIM + mCherry -*Al*Orai + GFP-NFAT	*Ascaris lumbricoides*	Yes (after TG)	Yes (after Ca^{2+} addition)	**Yes**
EGFP-*Al*STIM-CT + mCherry-*Al*Orai + GFP-NFAT	*Ascaris lumbricoides*	Yes (after TG)	Yes (after Ca^{2+} addition)	**Yes**
EGFP-*Al*STIM + mCherry -*Hs*Orai	*Ascaris lumbricoides* / *Homo sapiens*	No	-	**No**
EGFP-*Al*STIM + mCherry -*Sm*Orai	*Ascaris lumbricoides* / *Schistosoma mansoni*	No	-	**No**
EGFP-CHIMERA STIM + mCherry-*Al*Orai	*Ascaris lumbricoides* / *Homo sapiens*	No	-	**No**
EGFP-*Hs*STIM1 + mCherry-*Al*Orai + GFP-NFAT	*Homo sapiens* / *Ascaris lumbricoides*	Yes (after TG)	Yes (after Ca^{2+} addition)	**Yes**

* STIM–Orai puncta formation reflects clustering at ER–plasma membrane junctions following ER Ca^{2+} store depletion. NFAT nuclear translocation indicates sustained Ca^{2+} influx mediated by functional CRAC channel activity. Constitutive activation by *Al*STIM-CT occurs independently of ER Ca^{2+} depletion.

4.5. STIM function as an intracellular pH sensor

To validate our experimental approach and establish a reliable positive control, we first evaluated the pH-dependent behavior of the human STIM–Orai complex, a mechanism that has been characterized in previous studies (Y. Chen et al., 2024). HEK293 cells were co-transfected with EGFP-tagged human STIM1 (*Hs*STIM1) and mCherry-tagged human Orai1 (*Hs*Orai1), and intracellular pH was clamped using nigericin-based buffers at defined pH values. As expected, intracellular alkalinization triggered a robust relocalization of STIM1 from a diffuse endoplasmic reticulum distribution toward discrete puncta at ER–plasma membrane (ER–PM) contact sites, indicative of STIM activation. STIM activation became evident at pH 7.2 and was markedly enhanced at higher pH values, consistent with its function as a molecular pH sensor (Figure 23). This pH sensitivity is mediated by protonation–deprotonation events involving conserved histidine residues within the SOAR/CAD domain, which act as intracellular pH-sensing elements that regulate STIM oligomerization and coupling to Orai channels. Consequently, intracellular alkalinization acts as a molecular trigger for CRAC channel activation and calcium entry (Y. Chen et al., 2024).

Given that this mechanism is well established in the literature, the present experiment was performed exclusively as a positive control and therefore is not discussed in further detail. This validation was essential prior to extending the analysis to *Ascaris lumbricoides* STIM proteins, where pH-dependent regulation is addressed in subsequent sections.

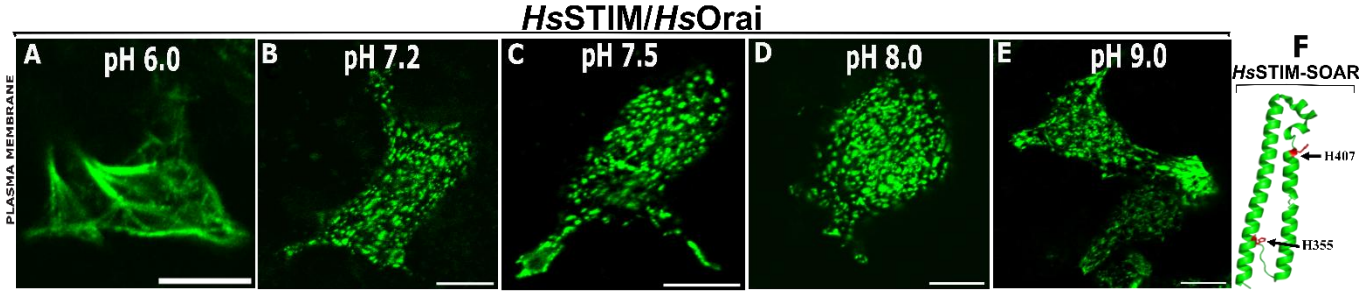

Figure 23. pH-dependent activation of the human STIM–Orai complex.
Confocal microscopy images of HEK293 cells co-expressing EGFP–HsSTIM1 and mCherry–HsOrai1 under controlled intracellular pH conditions. Cells were exposed to nigericin-containing buffers adjusted to pH 6.0 (**A**), 7.2 (**B**), 7.5 (**C**), 8.0 (**D**), and 9.0 (**E**). Progressive intracellular alkalinization induces STIM1 relocalization and puncta formation at ER–plasma membrane contact sites, indicative of STIM activation. The schematic representation highlights conserved histidine residues within the SOAR domain implicated in pH sensing. Scale bars = 10 µm.

We next evaluated the pH-dependent behavior of the *Ascaris lumbricoides* STIM–Orai pair. HEK293 cells were co-transfected with EGFP-tagged *Al*STIM and mCherry-tagged *Al*Orai, and intracellular pH was clamped using nigericin-containing buffers. Under acidic and near-neutral conditions (pH 6.0–7.5), *Al*STIM exhibited a predominantly diffuse cytosolic and reticular distribution, with no clear puncta formation (Figure 24A–C). In contrast, intracellular alkalinization induced a detectable, albeit weaker, relocalization of *Al*STIM toward punctate structures, which became more evident at pH 8.0 and was most pronounced at pH 9.0 (Figure 24D–E).

Compared to the human STIM1 response, the pH sensitivity of *Al*STIM appears shifted toward more alkaline values, suggesting a reduced or altered proton-sensing capacity. Structural analysis of the *Al*STIM C-terminal region revealed that histidine residues implicated in pH sensing are not conserved within the canonical SOAR/CAD α-helical core (Y. Chen et al., 2024). Instead, six histidine residues are located within flexible loop regions, while only a single histidine is positioned within the α-helical segment of the polybasic domain (Figure 24F). Previous studies have demonstrated that histidine residues embedded within structured α-helices are critical for effective protonation-dependent conformational transitions, whereas histidines located in disordered or loop regions contribute less efficiently to pH sensing and long-range allosteric coupling to Orai channels (Fahrner et al., 2018). This structural organization likely underlies the attenuated puncta formation observed for *Al*STIM, as flexible loop-localized histidines may exhibit reduced capacity to stabilize STIM oligomerization and ER–PM trapping upon alkalinization. Nevertheless, the persistence of puncta formation at pH 9.0 indicates that *Al*STIM retains intrinsic pH responsiveness, supporting its role as an intracellular pH sensor. The shifted activation range may reflect physiological adaptation of *A. lumbricoides* to its host environment, where intracellular and extracellular pH conditions differ substantially from those encountered by humans. Collectively, these data demonstrate that while the pH-sensing function of STIM is evolutionarily conserved, the molecular determinants and effective pH window for activation are species-specific (Y. Chen et al., 2024; Fahrner et al., 2018).

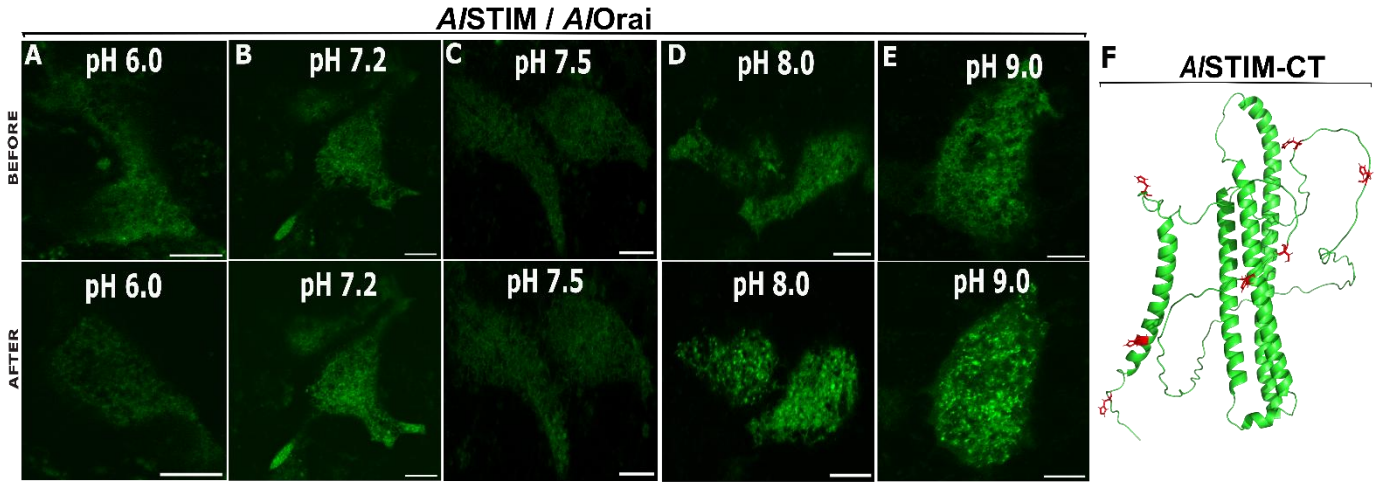

Figure 24. pH-dependent activation of *Ascaris lumbricoides* STIM–Orai complex.
Confocal microscopy images of HEK293 cells co-expressing EGFP–*Al*STIM and mCherry–*Al*Orai before and after intracellular pH clamping using nigericin. Cells were exposed to buffers adjusted to pH 6.0 (**A**), 7.2 (**B**), 7.5 (**C**), 8.0 (**D**), and 9.0 (**E**). AlSTIM displays a predominantly diffuse distribution at acidic and near-neutral pH, whereas intracellular alkalinization induces weak but detectable puncta formation, which is most evident at pH 9.0. (**F**) Structural model of the *Al*STIM C-terminal region highlighting histidine residues (red), predominantly localized in loop regions rather than within the α-helical SOAR core. Scale bars = 10 μm.

4.6. Structural modeling and identification of potential inhibitors of *Ascaris lumbricoides* Orai

Once the homohexameric model of *Ascaris lumbricoides* Orai was generated and structurally stabilized through energy minimization, as described in Figure 25, we next evaluated the druggability of the channel pore using structure-based cavity detection. Druggable site prediction was performed with the Fpocket analysis pipeline (FPocketWeb, n.d.), which identifies and ranks putative ligand-binding cavities based on geometric and physicochemical descriptors.

As shown in Figure 26, analysis of the minimized Orai homohexamer from both lateral and extracellular top views revealed the presence of two prominent pharmacologically relevant cavities located within the central pore region. These cavities exhibited the highest druggability scores among all detected pockets, indicating an increased potential for small-molecule binding. The first cavity (Pocket 1), represented by cyan spheres, displayed a drug score of 0.66, while the second cavity (Pocket 2), represented by magenta spheres, showed a drug score of 0.45. Importantly, both cavities are positioned within the pore lumen and at interfaces formed by the transmembrane helices, making them highly accessible

to small molecules approaching from the extracellular side. The localization of these high-scoring pockets within the ion-conducting pathway is particularly relevant, as previous structural and functional studies have demonstrated that small molecules and pore-blocking inhibitors targeting the Orai transmembrane region can directly interfere with channel architecture and Ca^{2+} permeation (Hou et al., 2012a, 2020b; Tiffner et al., 2021; Yeung et al., 2020). Indeed, several CRAC channel inhibitors have been shown to bind within or near the pore region, stabilizing non-conductive conformations or physically occluding ion flow (Bergsmann et al., 2011; McNally & Prakriya, 2012; Waldherr et al., 2020).

In this context, the identification of druggable cavities within the central pore of *A. lumbricoides* Orai provides a strong structural basis for pharmacological inhibition of the parasite CRAC channel. These findings support the suitability of the refined Orai model for subsequent structure-based virtual screening and reinforce the central pore as a functionally relevant and druggable target for the development of parasite-selective CRAC channel inhibitors.

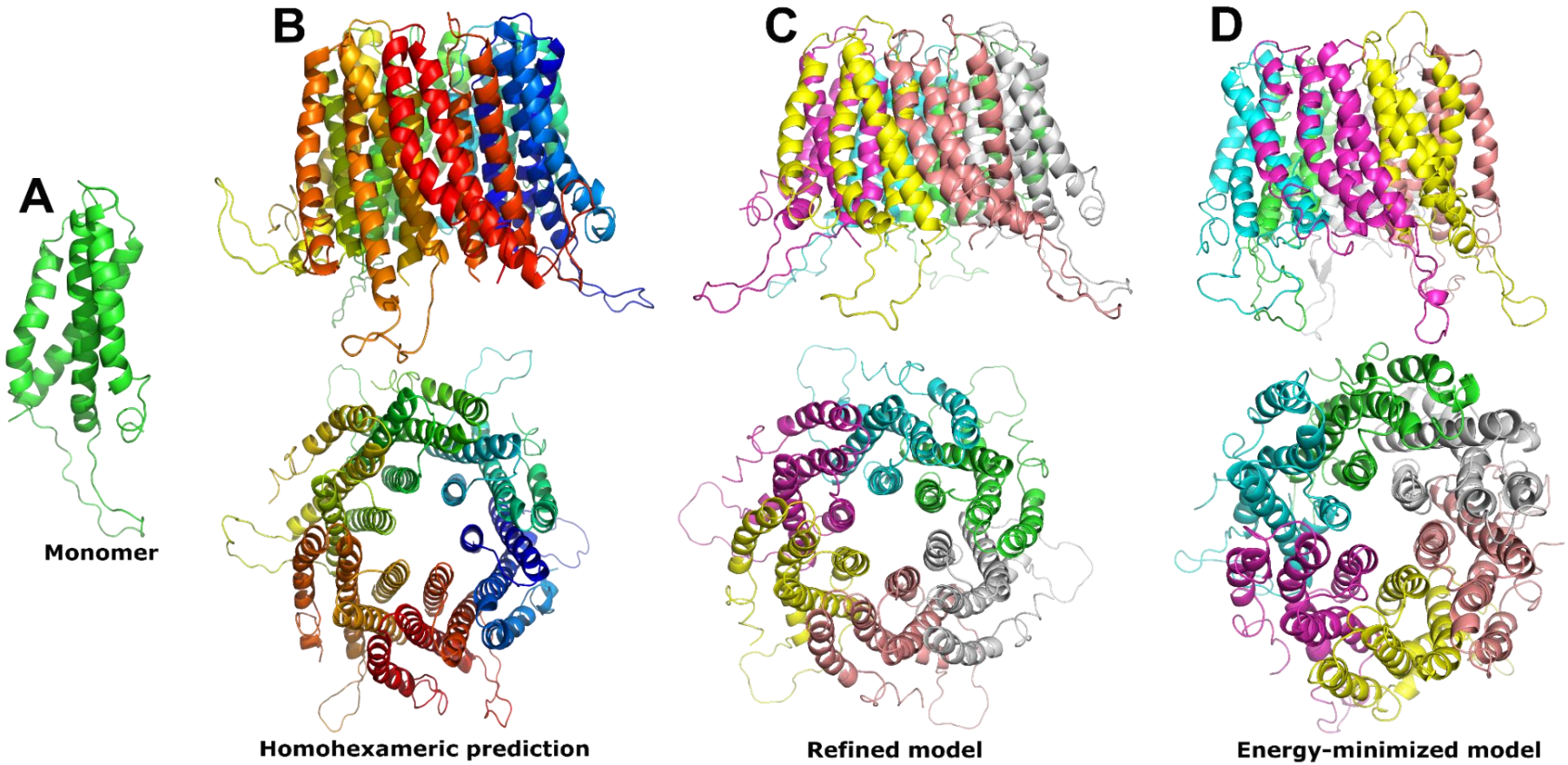

Figure 25. Structural modeling workflow of the homohexameric Orai channel from *Ascaris lumbricoides*.
This annex illustrates the stepwise generation and refinement of the three-dimensional structural model of *Ascaris lumbricoides* Orai. (**A**) The Orai monomer was generated by homology modeling using MODELLER, employing the open-state structure of *Drosophila melanogaster* Orai (PDB ID: 7KR5) as a template. (**B**) Homohexameric pore assembly was constructed from the monomeric units, revealing a central ion-conducting pore and flexible cytosolic and extracellular loop regions, some of which extend laterally toward the membrane bilayer. (**C**) Structural refinement was performed to reposition disordered loop regions away from the membrane surface, allowing them to adopt outward-facing conformations that minimize steric interference and facilitate stable channel dynamics. (**D**) The refined homohexameric model was subsequently subjected to energy minimization and molecular dynamics relaxation for 50 ns using Desmond-Maestro, yielding a structurally stable conformation suitable for downstream membrane-embedded simulations and structure-based drug discovery analyses.

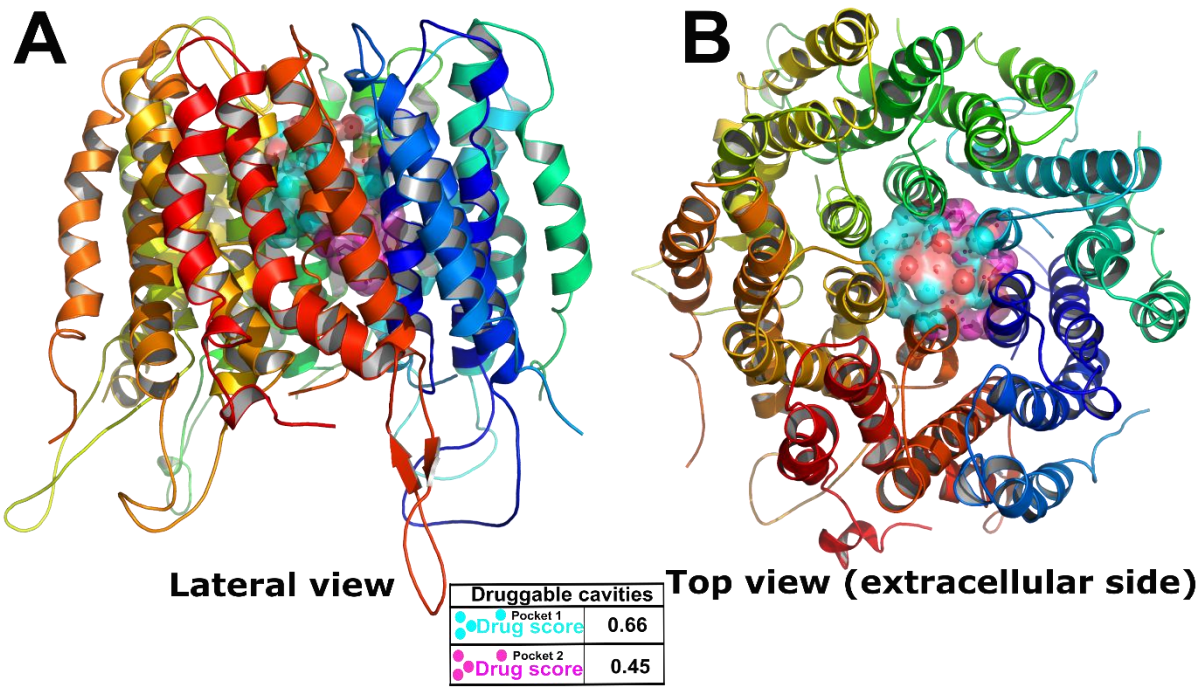

Figure 26. Identification of druggable cavities in the homohexameric Orai channel from *Ascaris lumbricoides*.
Structural representation of the energy-minimized Orai homohexamer showing predicted druggable cavities identified by Fpocket analysis. (**A**) Lateral view of the channel embedded in the membrane, highlighting cavities located along the pore axis. (**B**) Top view from the extracellular side, illustrating the spatial distribution of the cavities within the central pore. Pocket 1 (cyan spheres) exhibits a drug score of 0.66, while Pocket 2 (magenta spheres) shows a drug score of 0.45. Higher drug scores indicate increased druggability potential and accessibility for small-molecule binding within the ion-conducting pathway.

Following the identification of druggable cavities within the central pore of the *Ascaris lumbricoides* Orai channel, a structure-based virtual screening was performed to prioritize small molecules with high binding affinity toward the predicted pharmacological sites. Docking calculations were carried out using AutoDock Vina against the minimized homohexameric Orai model (Trott & Olson, 2010), focusing on the pore region identified by Fpocket as highly druggable (Ferreira et al., 2015). From the initial virtual screening dataset, ligands were ranked according to their predicted binding energy (kcal/mol). Based on this ranking, three compounds identified as ligands 209, 212, and 1005—were selected for further analysis, as they consistently exhibited the most favorable binding affinities among the screened molecules. These ligands showed binding energies ranging from −12.2 to −11.1 kcal/mol, indicating a strong predicted interaction with the Orai pore region (Table 9). Importantly, beyond their favorable binding energies, the selected ligands displayed docking poses that were spatially consistent with the high-scoring druggable cavities previously identified within the

ion-conducting pathway. This convergence between energetic ranking and structural localization provided a robust criterion for prioritizing these three ligands for subsequent refinement and redocking analyses.

To further refine ligand–channel interactions and assess pose reproducibility, a focused redocking analysis was performed for the three selected ligands. For each compound, 30 independent docking runs were conducted using AutoDock Vina, restricting the search space to the druggable cavity region identified in the virtual screening step. The final binding pose for each ligand was selected based on the lowest binding energy and the consistency of the docking orientation across multiple runs. Notably, the lowest-energy poses obtained during redocking consistently localized within the same druggable cavities identified by Fpocket, further validating these regions as structurally and pharmacologically relevant binding sites. This redocking strategy increased confidence in both ligand selection and binding mode reliability, providing a refined structural basis for subsequent molecular dynamics simulations and inhibitor optimization (McNally & Prakriya, 2012; Yeung et al., 2020).

Table 9. Prioritized ligands identified through structure-based virtual screening and redocking against *Ascaris lumbricoides* Orai.

The table summarizes the three ligands selected based on their favorable binding energies obtained from virtual screening using AutoDock Vina and subsequent redocking analyses. All selected compounds exhibited strong predicted affinities and consistent binding poses within the central pore region of the Orai channel, corresponding to the high-scoring druggable cavities identified by Fpocket.

Ligand	Compound name	PubChem CID	Best binding affinity (kcal/mol)	Docking strategy	Target site
209	Pyrrolidinyl-4-pyrimidinyl	145705968	−12.2	Virtual screening + redocking	Central pore
212	Golvatinib	16118392	−12.0	Virtual screening + redocking	Central pore
1005	Revastinib	25066467	−11.1	Virtual screening + redocking	Central pore

Following the structure-based virtual screening, molecular dynamics (MD) simulations were performed for the Orai–ligand complex containing the pyrrolidinyl-4-pyrimidinyl compound (ligand 209), selected based on its favorable binding affinity and consistent localization within the predicted druggable cavity. As shown (Figure 27A), the ligand remains stably positioned within the central pore

region during the MD simulation, occupying the same binding site identified by Fpocket and refined through redocking. This observation supports the structural relevance of the selected cavity and confirms the reliability of the docking-derived binding pose. Analysis of protein–ligand interactions (Figure 27B) revealed that the complex is primarily stabilized by hydrophobic and π–alkyl interactions involving residues lining the pore lumen. Such nonpolar interactions are commonly reported as key contributors to ligand stabilization within ion channel pores, particularly in transmembrane environments where hydrophobic packing plays a dominant role (Hou et al., 2012b; Yeung et al., 2020).

The temporal evolution of the root mean square deviation (RMSD) further supports the stability of the complex (Figure 27C). While moderate fluctuations are observed for the ligand, its RMSD remains within a stable range throughout the simulation, indicating sustained retention within the binding site without dissociation. In parallel, the protein RMSD reaches a plateau after an initial equilibration phase, suggesting overall structural stability of the Orai channel in the presence of the bound ligand. Similar RMSD behaviors have been widely used as indicators of stable ligand binding in MD-based drug discovery studies (Hollingsworth & Dror, 2018).

Residue-level flexibility analysis (RMSF) showed that the largest fluctuations occur predominantly in external loop regions, whereas residues directly involved in ligand binding exhibit reduced mobility (Figure 27D). This pattern indicates a locally rigid binding environment, which is often associated with favorable ligand retention and specificity (Kuzmanic & Zagrovic, 2010). The reduced flexibility of pore-lining residues further supports the functional relevance of the identified binding site. Finally, the interaction fraction analysis (Figure 27E) highlights persistent contacts between the ligand and key pore residues throughout the MD trajectory, reinforcing the notion that the ligand–channel complex is dynamically stable. Collectively, these results demonstrate that ligand 209 not only exhibits favorable docking scores but also maintains a stable and well-defined binding mode during molecular dynamics, thereby strengthening its candidacy as a potential inhibitor of the *Ascaris lumbricoides* CRAC channel.

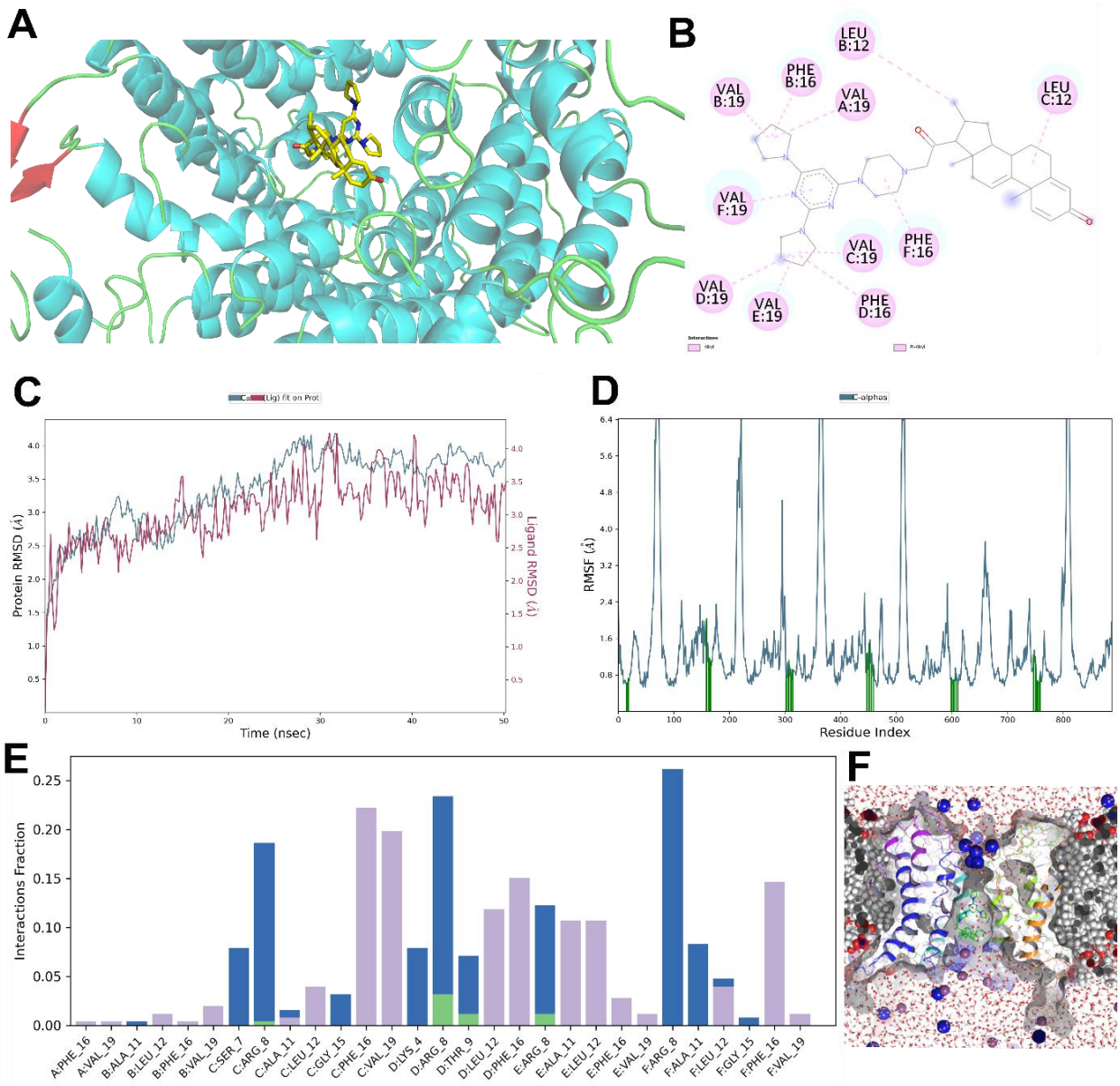

Figure 27. Redocking and molecular dynamics analysis of the *Ascaris lumbricoides* Orai–pyrrolidinyl-4-pyrimidinyl (209) complex.
(**A**) Representative binding pose of ligand 209 within the central pore of *Ascaris lumbricoides* Orai after redocking and molecular dynamics refinement. (**B**) Two-dimensional interaction map highlighting key hydrophobic and π–alkyl interactions between the ligand and pore-lining residues. (**C**) RMSD profiles of the protein backbone and ligand throughout the MD simulation. (**D**) RMSF per residue showing increased flexibility in external loop regions and reduced mobility of ligand-interacting residues. (**E**) Interaction fraction analysis summarizing persistent protein–ligand contacts during the MD simulation. (**F**) Three-dimensional view of the Orai–ligand complex embedded in a membrane-mimetic environment, illustrating the stable positioning of ligand 209 within the central pore in the context of the lipid bilayer and solvent. Collectively, these analyses indicate a stable and well-defined binding mode of ligand 209 within the Orai pore.

Molecular dynamics simulations were next performed for the Orai–Golvatinib (ligand 212) complex in order to evaluate the stability and persistence of ligand binding within the central pore of Ascaris lumbricoides Orai. As shown in (Figure

28A), Golvatinib remains stably positioned within the pore region during the MD simulation, occupying the same binding site identified during redocking and overlapping with the high-scoring druggable cavity predicted by Fpocket. This spatial consistency supports the robustness of the docking-derived binding pose. The two-dimensional interaction map (Figure 28B) reveals that Golvatinib engages in a combination of hydrophobic, π–alkyl, and hydrogen-bond interactions with pore-lining residues. Notably, a persistent interaction with residue ARG D:8 is observed, which is maintained during both the redocking stage and throughout the MD simulation. The involvement of positively charged residues such as arginine in stabilizing ligands within ion channel pores has been previously reported, as these residues can contribute to electrostatic anchoring and orientation of ligands within the conduction pathway (Hou et al., 2012b; Yeung et al., 2020).

RMSD analysis further supports the stability of the Orai–Golvatinib complex (Figure 28C). After an initial equilibration phase, the protein backbone RMSD reaches a stable plateau, indicating global structural stability of the channel. Although the ligand RMSD exhibits moderate fluctuations, Golvatinib remains confined within the pore region without evidence of dissociation. Such RMSD behavior is commonly interpreted as indicative of a stable yet dynamically adaptable binding mode(Hollingsworth & Dror, 2018).

Residue-level flexibility analysis (RMSF) shows that the highest fluctuations are primarily localized in external loop regions, while residues involved in ligand binding—including ARG D:8—display reduced mobility (Figure 28D). This reduction in local flexibility suggests the formation of a relatively rigid interaction network around the ligand, which is often associated with enhanced binding stability and specificity(Kuzmanic & Zagrovic, 2010). Consistent with these observations, interaction fraction analysis (Figure 28E) highlights sustained contacts between Golvatinib and several pore-lining residues throughout the MD trajectory, with ARG D:8 exhibiting one of the highest interaction occupancies. The persistence of this interaction from redocking through MD strongly suggests that ARG D:8 plays a key role in anchoring Golvatinib within the Orai pore. Collectively, these results demonstrate that Golvatinib adopts a stable and well-defined binding mode within the central pore of *A. lumbricoides* Orai, reinforcing its potential as a pharmacological modulator of the parasite CRAC channel.

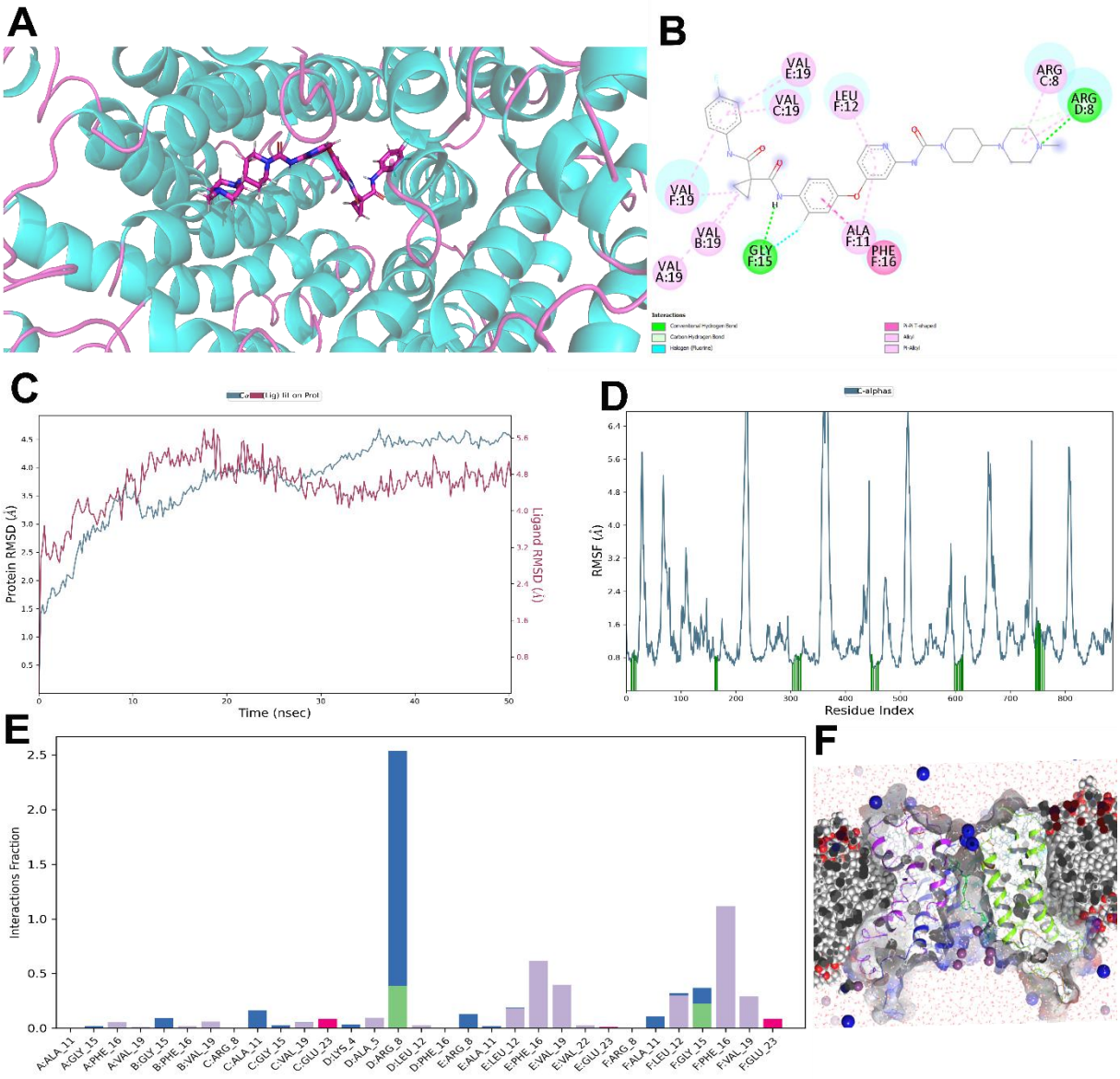

Figure 28. Redocking and molecular dynamics analysis of the *Ascaris lumbricoides* Orai–Golvatinib (212) complex.
Representative binding pose of Golvatinib within the central pore of *Ascaris lumbricoides* Orai after redocking and molecular dynamics refinement. (**B**) Two-dimensional interaction map showing hydrophobic, π–alkyl, and hydrogen-bond interactions between Golvatinib and pore-lining residues, highlighting the persistent interaction with ARG D:8. (**C**) RMSD profiles of the protein backbone and Golvatinib throughout the MD simulation. (**D**) RMSF per residue indicating increased flexibility in external loop regions and reduced mobility of ligand-interacting residues. (**E**) Interaction fraction analysis summarizing persistent protein–ligand contacts during the MD simulation. (**F**) Three-dimensional view of the Orai–Golvatinib complex embedded in a membrane-mimetic environment, illustrating stable ligand positioning within the central pore.

Molecular dynamics simulations were subsequently performed for the Orai–Revastinib (ligand 1005). As illustrated in (Figure 29A), Revastinib remains consistently positioned within the pore region throughout the MD simulation, occupying the same binding site identified during redocking and coinciding with the

high-scoring druggable cavity predicted by Fpocket. This spatial agreement further supports the reliability of the docking-derived binding pose. The two-dimensional interaction analysis (Figure 29B) shows that Revastinib establishes a network of hydrophobic and π–alkyl interactions with residues lining the pore lumen. Notably, interactions with ARG C:8 and LEU F:12 are conserved from the redocking stage and maintained throughout the MD simulation. The persistence of contacts involving positively charged residues such as arginine and hydrophobic residues such as leucine has been described as a key determinant of ligand stabilization within ion channel pores, contributing to both electrostatic anchoring and hydrophobic packing (Hou et al., 2012a; Yeung et al., 2020).

RMSD analysis (Figure 29C) indicates that the protein backbone rapidly reaches a stable plateau, reflecting overall structural stability of the Orai channel in the presence of Revastinib. The ligand RMSD exhibits moderate fluctuations but remains confined within the pore region without dissociation events, a behavior commonly associated with stable binding in membrane-embedded protein–ligand complexes (Hollingsworth & Dror, 2018).

Residue-level flexibility analysis (RMSF) reveals that the largest fluctuations occur predominantly in external loop regions, while residues directly involved in ligand binding—particularly ARG C:8 and LEU F:12 display reduced mobility (Figure 29D). This reduced flexibility suggests the formation of a locally rigid interaction environment, which is often correlated with enhanced ligand retention and binding specificity (Kuzmanic & Zagrovic, 2010). Consistent with these findings, interaction fraction analysis (Figure 29E) highlights sustained contacts between Revastinib and key pore-lining residues throughout the MD trajectory. The high interaction occupancy observed for ARG C:8 and LEU F:12 further supports their central role in anchoring Revastinib within the Orai pore. Collectively, these results demonstrate that Revastinib adopts a stable and well-defined binding mode within the central pore of *A. lumbricoides* Orai, reinforcing its potential as a pharmacological modulator of the parasite CRAC channel.

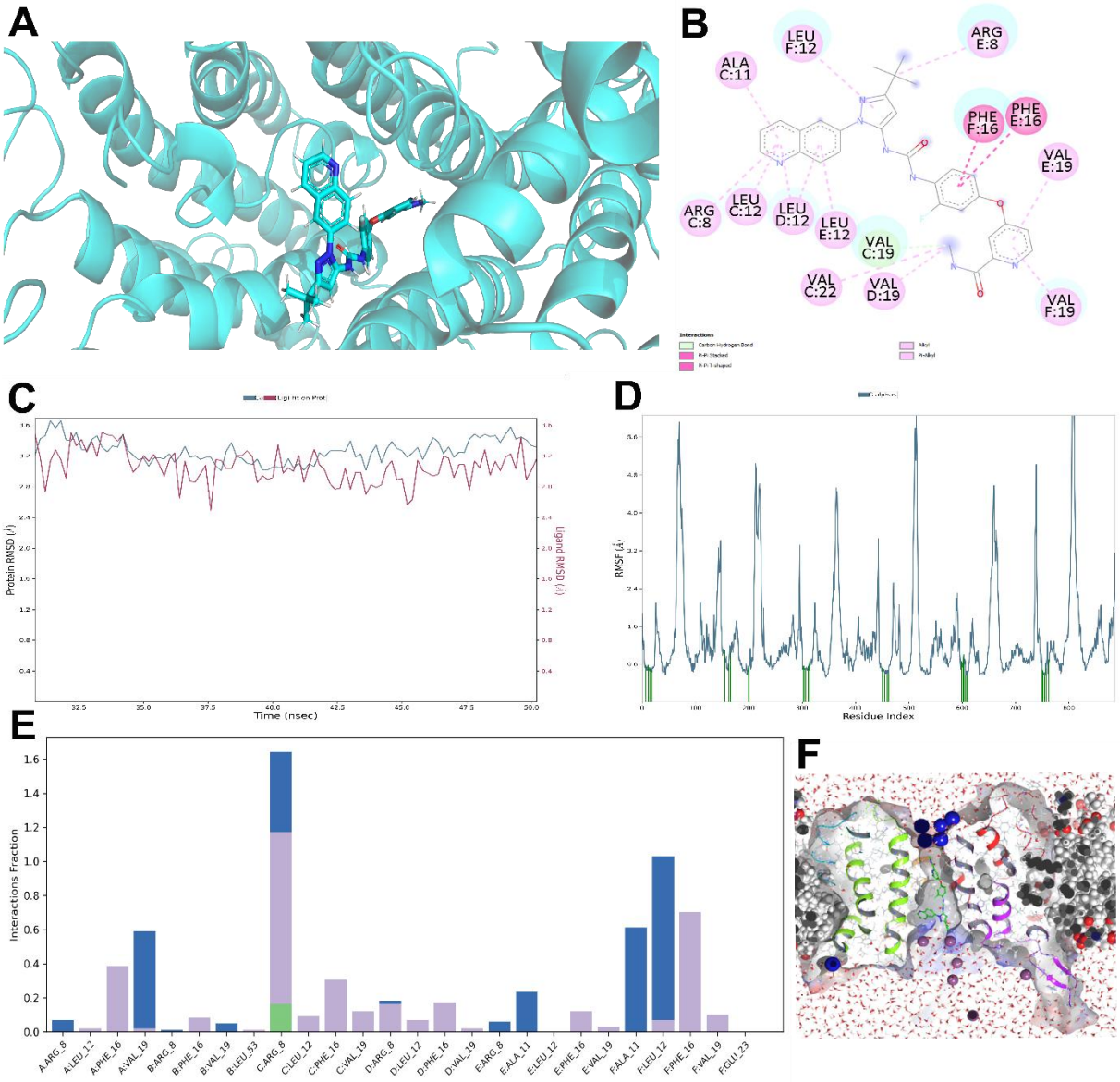

Figure 29. Redocking and molecular dynamics analysis of the *Ascaris lumbricoides* Orai–Revastinib (1005) complex.
(**A**) Representative binding pose of Revastinib within the central pore of *Ascaris lumbricoides* Orai after redocking and molecular dynamics refinement. (**B**) Two-dimensional interaction map highlighting hydrophobic and π–alkyl interactions between Revastinib and pore-lining residues, emphasizing conserved contacts with ARG C:8 and LEU F:12. (**C**) RMSD profiles of the protein backbone and Revastinib throughout the MD simulation. (**D**) RMSF per residue showing increased flexibility in external loop regions and reduced mobility of ligand-interacting residues. (**E**) Interaction fraction analysis summarizing persistent protein–ligand contacts during the MD simulation. (**F**) Three-dimensional view of the Orai–Revastinib complex embedded in a membrane-mimetic environment, illustrating stable ligand positioning within the central pore.

A comparative analysis of the three prioritized ligands pyrrolidinyl-4-pyrimidinyl (209), Golvatinib (212), and Revastinib (1005)—reveals both shared and distinct binding features that provide important insights into their potential as pharmacological modulators of the *Ascaris lumbricoides* CRAC channel. All three compounds consistently occupy the central pore region of Orai, overlapping with

the high-scoring druggable cavity identified by Fpocket, and remain stably associated with the channel throughout redocking and molecular dynamics simulations. This convergence strongly supports the central pore as a structurally and functionally relevant target for small-molecule inhibition, in agreement with previous structural and pharmacological studies on Orai channels (Hou et al., 2012a; Yeung et al., 2020).

Despite these shared features, clear differences emerge in the nature and persistence of ligand–protein interactions. Ligand pyrrolidinyl-4-pyrimidinyl (209) exhibits a predominantly hydrophobic binding mode, characterized by stable π–alkyl and nonpolar contacts with pore-lining residues. While this interaction pattern supports good retention within the pore, its relative lack of persistent polar or electrostatic interactions may render binding more sensitive to local conformational fluctuations of the channel, a limitation commonly observed for hydrophobically driven ligands in membrane proteins (Hollingsworth & Dror, 2018). In contrast, Golvatinib (212) and Revastinib (1005) display more complex interaction networks that combine hydrophobic packing with persistent electrostatic or polar contacts. Notably, Golvatinib maintains a conserved interaction with ARG D:8, while Revastinib preserves interactions with both ARG C:8 and LEU F:12 from redocking through molecular dynamics. The involvement of positively charged residues such as arginine has been previously implicated in anchoring ligands within the Orai pore and contributing to binding orientation and stability (Hou et al., 2012a; Tiffner et al., 2021; Tiffner & Derler, 2020). The persistence of these interactions during MD suggests that Golvatinib and Revastinib may achieve more robust anchoring within the conduction pathway compared to Pyrrolidinyl-4-pyrimidinyl.

Importantly, RMSD and RMSF analyses indicate that, for all three complexes, ligand binding is associated with reduced mobility of pore-lining residues, while higher flexibility is retained in external loop regions. This pattern is consistent with a binding mode that stabilizes the pore architecture without globally rigidifying the channel, a feature that may be advantageous for selective inhibition without complete structural collapse (Kuzmanic & Zagrovic, 2010). However, it must be emphasized that the present simulations capture equilibrium stability rather than functional inhibition per se, and do not directly address ion permeation or conductance changes.

Taken together, these results suggest that while ligand Pyrrolidinyl-4-pyrimidinyl represents a strong hydrophobic pore binder, Golvatinib and Revastinib may offer enhanced binding robustness due to conserved electrostatic anchoring interactions. Nonetheless, all three ligands should be regarded as structural leads rather than confirmed inhibitors, and their predicted binding modes warrant further validation through extended molecular dynamics, free-energy calculations, and experimental functional assays. This comparative analysis provides a rational framework for prioritizing compounds and guiding future structure-based optimization of parasite-selective CRAC channel inhibitors.

5. CONCLUSION

Based on multiple sequence alignment and comparative sequence analysis, STIM and Orai proteins from *Ascaris lumbricoides* and *Schistosoma mansoni* were shown to preserve the essential structural architecture required for CRAC channel activation, despite exhibiting only moderate overall sequence identity with metazoan orthologs. The strong conservation of the EF–SAM Ca^{2+}-sensing domain, the single transmembrane helix, and the SOAR/CC2–CC3 activation region in STIM, together with the preservation of the four transmembrane helices (TM1–TM4) forming the Orai pore, indicates that the fundamental mechanisms of Ca^{2+} detection and STIM–Orai coupling are evolutionarily conserved in helminths. In contrast, the greater divergence observed in regulatory and low-complexity regions, including the CC1/PBD segments of STIM and non-transmembrane regions of Orai, suggests that parasite-specific modulation occurs predominantly at the regulatory level rather than through alterations of the core functional machinery of the channel. Collectively, these results provide a robust amino acid sequence–based framework for subsequent evaluation of the functional conservation of CRAC signaling in helminths and identify divergent regions as potential determinants of species-specific regulation and targets for selective inhibition.

Confocal imaging demonstrated that STIM–Orai coupling in helminths is functionally competent but highly dependent on molecular context and cognate partner recognition. When expressed alone in HEK293 cells, EGFP-tagged *Ascaris lumbricoides* STIM (*Al*STIM) failed to form puncta following ER Ca^{2+} depletion, in contrast to the behavior of human STIM1. This inability to cluster was

attributed to the absence of a C-terminal polybasic domain (PBD) in *Al*STIM, a region that is essential for plasma membrane anchoring in mammalian STIM proteins. In contrast, co-expression with the cognate mCherry-*Al*Orai resulted in robust puncta formation at ER–plasma membrane junctions, providing direct evidence of productive STIM–Orai coupling and efficient CRAC channel activation. These results indicate that, in *A. lumbricoides*, direct interaction with Orai compensates for the reduced intrinsic membrane-anchoring capacity of STIM, thereby enabling functional clustering. Critically, combinations (*Al*STIM with human Orai1 or *Schistosoma mansoni* Orai) failed to induce puncta formation, demonstrating that *Al*STIM supports CRAC channel activation exclusively in the presence of its cognate *Al*Orai. This strict specificity strongly suggests the existence of parasite-selective molecular determinants within *Al*STIM that prevent productive interactions with Orai proteins from other organisms, reinforcing the concept of species restricted STIM–Orai coupling in helminths.

NFAT nuclear translocation assays demonstrated that helminth STIM–Orai complexes are capable of sustaining functional CRAC channel activation and downstream Ca^{2+}-dependent signaling, but only under conditions of productive and species-matched STIM–Orai coupling. Co-expression of EGFP-tagged STIM from *Ascaris lumbricoides* with its cognate mCherry-tagged Orai induced a clear and robust accumulation of NFAT in the nucleus, indicating sustained Ca^{2+} entry consistent with CRAC channel opening. Collectively, these results establish that functional CRAC signaling in helminths strictly depends on species-specific STIM–Orai interactions, and that the integrity of regulatory interfaces governing coupling efficiency is essential to translate Ca^{2+} influx into transcriptional responses. Importantly, NFAT activation provides the first functional evidence that the CRAC channel in *A. lumbricoides* is operational, demonstrating that helminth STIM–Orai complexes are not only structurally conserved but also functionally competent, while simultaneously revealing parasite-selective constraints on channel activation that may be exploited for targeted inhibitory strategies.

Intracellular pH modulation revealed that STIM from *Ascaris lumbricoides* functions as a pH-sensitive regulator of CRAC channel activation, albeit with an activation profile shifted toward more alkaline conditions compared to human STIM1. Structural analysis indicates that histidine residues implicated in proton

sensing are largely excluded from the canonical SOAR/CAD α-helical core and are predominantly located within flexible loop regions of the C-terminal domain, with only a single histidine embedded in an α-helical segment of the polybasic region. This organization likely reduces the efficiency of protonation dependent conformational transitions and contributes to the attenuated puncta formation observed under moderate pH changes. Nevertheless, the persistence of puncta formation at highly alkaline pH demonstrates that *Al*STIM retains intrinsic pH responsiveness, supporting its role as an intracellular pH sensor. Collectively, these findings indicate that while pH-dependent regulation of STIM is evolutionarily conserved, the molecular determinants and effective pH window for activation are species-specific, likely reflecting physiological adaptation of *A. lumbricoides* to its host environment.

The homohexameric three-dimensional model of *Ascaris lumbricoides* Orai provided a coherent structural framework to identify pharmacologically relevant transmembrane cavities and prioritize candidate inhibitors through structure-based virtual screening, redocking, and molecular dynamics (MD). Fpocket analysis highlighted druggable pockets within/adjacent to the conduction pathway, and screening of an FDA-approved–focused library yielded three prioritized ligands (pyrrolidinyl-4-pyrimidinyl/209, Golvatinib/212, and Revastinib/1005). Redocking supported pose reproducibility, while MD trajectories consistently indicated stable ligand retention in the pore region with conserved engagement of pore-lining residues (including persistent contacts involving Arg8 and hydrophobic residues such as Leu12), and with flexibility remaining largely confined to peripheral loop regions rather than the binding core. Collectively, these results support the feasibility of targeting helminth Orai through pore-associated transmembrane pockets and define concrete ligand–residue interaction hypotheses; however, they remain in silico predictions that require experimental validation to confirm true inhibitory potency and parasite selectivity.

6. REFERENCES

Almagro Armenteros, J. J., Tsirigos, K. D., Sønderby, C. K., Petersen, T. N., Winther, O., Brunak, S., von Heijne, G., & Nielsen, H. (2019). SignalP 5.0 improves signal peptide predictions using deep neural networks. *Nature Biotechnology 2019 37:4*, *37*(4), 420–423. https://doi.org/10.1038/s41587-019-0036-z

Amcheslavsky, A., Wood, M. L., Yeromin, A. V., Parker, I., Freites, J. A., Tobias, D. J., & Cahalan, M. D. (2015). Molecular biophysics of Orai store-operated Ca2+ channels. *Biophysical Journal*, *108*(2), 237–246. https://doi.org/10.1016/J.BPJ.2014.11.3473

Baraniak, J. H., Zhou, Y., Nwokonko, R. M., & Gill, D. L. (2020). The Intricate Coupling Between STIM Proteins and Orai Channels. *Current Opinion in Physiology*, *17*, 106–114. https://doi.org/10.1016/J.COPHYS.2020.07.018

Bateman, A., Martin, M. J., Orchard, S., Magrane, M., Ahmad, S., Alpi, E., Bowler-Barnett, E. H., Britto, R., Bye-A-Jee, H., Cukura, A., Denny, P., Dogan, T., Ebenezer, T. G., Fan, J., Garmiri, P., da Costa Gonzales, L. J., Hatton-Ellis, E., Hussein, A., Ignatchenko, A., … Zhang, J. (2023). UniProt: the Universal Protein Knowledgebase in 2023. *Nucleic Acids Research*, *51*(D1), D523–D531. https://doi.org/10.1093/NAR/GKAC1052

Bergsmann, J., Derler, I., Muik, M., Frischauf, I., Fahrner, M., Pollheimer, P., Schwarzinger, C., Gruber, H. J., Groschner, K., & Romanin, C. (2011). Molecular determinants within N terminus of orai3 protein that control channel activation and gating. *Journal of Biological Chemistry*, *286*(36), 31565–31575. https://doi.org/10.1074/jbc.M111.227546

BIOVIA. (n.d.). *Scientific Software: Accelerate Your Scientific Innovation | Dassault Systèmes*. Retrieved January 13, 2026, from https://www.3ds.com/products/biovia

Brooker, S., Clements, A. C. A., & Bundy, D. A. P. (2006). Global Epidemiology, Ecology and Control of Soil-Transmitted Helminth Infections. *Advances in Parasitology*, *62*, 221–261. https://doi.org/10.1016/S0065-308X(05)62007-6

Carretta, M. D., Hidalgo, M. A., & Burgos, R. A. (2018). Indirect Measurement of CRAC Channel Activity Using NFAT Nuclear Translocation by Flow Cytometry in Jurkat Cells. *Methods in Molecular Biology (Clifton, N.J.)*, *1843*, 83–94. https://doi.org/10.1007/978-1-4939-8704-7_7

CDC. (2019, July). *CDC - DPDx - Ascariasis*. https://www.cdc.gov/dpdx/ascariasis/index.html?utm_source=

CDC. (2024a). *About Ascariasis | Soil-Transmitted Helminths | CDC*. https://www.cdc.gov/sth/about/ascariasis.html?utm_source=

CDC. (2024b, January 17). *About Schistosomiasis | Schistosomiasis | CDC*. https://www.cdc.gov/schistosomiasis/about/?CDC_AAref_Val=https://www.cdc.gov/parasites/schistosomiasis/index.html

CDC. (2024c, July 7). *CDC - DPDx - Schistosomiasis Infection*. https://www.cdc.gov/dpdx/schistosomiasis/index.html

CDC - DPDx - Ascariasis. (2019, July 19). *CDC - DPDx - Ascariasis - Laboratory Identificaction of Parasites of Public Health Concern*. https://www.cdc.gov/dpdx/ascariasis/index.html

CDC - DPDx - Schistosomiasis. (2024, June 7). *CDC - DPDx - Schistosomiasis Infection- Laboratory Identification of Parasites of Public Health Concern*. https://www.cdc.gov/dpdx/schistosomiasis/index.html

Chang, C. L., Chen, Y. J., Quintanilla, C. G., Hsieh, T. S., & Liou, J. (2018). EB1 binding restricts STIM1 translocation to ER–PM junctions and regulates store-operated Ca2+ entry. *The Journal of Cell Biology*, *217*(6), 2047. https://doi.org/10.1083/JCB.201711151

Chen, J., Gong, Y., Chen, Q., Li, S., & Zhou, Y. (2024). Global burden of soil-transmitted helminth infections, 1990–2021. *Infectious Diseases of Poverty 2024 13:1*, *13*(1), 77-. https://doi.org/10.1186/S40249-024-01238-9

Chen, Y., Liu, P., Zhong, Z., Zhang, H., Sun, A., & Wang, Y. (2024). STIM1 functions as a proton sensor to coordinate cytosolic pH with store-operated calcium entry. *Journal of Biological Chemistry*, *300*(12), 107924. https://doi.org/10.1016/J.JBC.2024.107924/ATTACHMENT/FF3A4E18-12FA-4999-A1B3-94B09F891EEC/MMC1.PDF

Cohen, H. A., Zomot, E., Nataniel, T., Militsin, R., & Palty, R. (2023). The SOAR of STIM1 interacts with plasma membrane lipids to form ER-PM contact sites. *Cell Reports*, *42*(3), 112238. https://doi.org/10.1016/j.celrep.2023.112238

Colley, D. G., Bustinduy, A. L., Secor, W. E., & King, C. H. (2014). Human schistosomiasis. *Lancet (London, England)*, *383*(9936), 2253–2264. https://doi.org/10.1016/S0140-6736(13)61949-2

Conterno, L. O., Turchi, M. D., Corrêa, I., & Monteiro de Barros Almeida, R. A. (2020). Anthelmintic drugs for treating ascariasis. *The Cochrane Database of Systematic Reviews*, *4*(4). https://doi.org/10.1002/14651858.CD010599.PUB2

Derler, I., Schindl, R., Fritsch, R., Heftberger, P., Riedl, M. C., Begg, M., House, D., & Romanin, C. (2013). The action of selective CRAC channel blockers is affected by the Orai pore geometry. *Cell Calcium*, *53*(2), 139–151. https://doi.org/10.1016/J.CECA.2012.11.005

Despommier, D. D. ., Griffin, D. O. ., Gwadz, R. W. ., Hotez, P. J. ., Knirsch, C. A. ., & Katz, Michael. (2019). *Parasitic diseases* (7th edition). Parasites Without

Borders, Inc. https://parasiteswithoutborders.com/wp-content/uploads/2020/02/PD7thEditionLowResVersion5-11-2019.pdf?utm_source=

Doenhoff, M. J., Kusel, J. R., Coles, G. C., & Cioli, D. (2002). Resistance of Schistosoma mansoni to praziquantel: is there a problem? *Transactions of the Royal Society of Tropical Medicine and Hygiene*, *96*(5), 465–469. https://doi.org/10.1016/S0035-9203(02)90405-0

Eliza Zeraik, A., Gabriel Fontes, M., Luiz Souza Lopes, J., Paula, A., Araujo, U., & DeMarco, R. (2016). STIM-Orai Interaction in Schistosoma Mansoni Indicates the Existence of Functional Store-Operated Calcium Entry in the Parasite. *Biophysical Journal*, *110*(3), 264a. https://doi.org/10.1016/j.bpj.2015.11.1441

Expasy ProtParam. (n.d.). *Expasy - ProtParam*. Retrieved January 16, 2026, from https://web.expasy.org/protparam/

Fahrner, M., Stadlbauer, M., Muik, M., Rathner, P., Stathopulos, P., Ikura, M., Müller, N., & Romanin, C. (2018). A dual mechanism promotes switching of the Stormorken STIM1 R304W mutant into the activated state. *Nature Communications 2018 9:1*, *9*(1), 825-. https://doi.org/10.1038/s41467-018-03062-w

Ferreira, L. G., Dos Santos, R. N., Oliva, G., & Andricopulo, A. D. (2015). Molecular Docking and Structure-Based Drug Design Strategies. *Molecules 2015, Vol. 20, Pages 13384-13421*, *20*(7), 13384–13421. https://doi.org/10.3390/MOLECULES200713384

Feske, S., Gwack, Y., Prakriya, M., Srikanth, S., Puppel, S. H., Tanasa, B., Hogan, P. G., Lewis, R. S., Daly, M., & Rao, A. (2006). A mutation in Orai1 causes immune deficiency by abrogating CRAC channel function. *Nature 2006 441:7090*, *441*(7090), 179–185. https://doi.org/10.1038/nature04702

FPocketWeb. (n.d.). *FPocketWeb – Durrant Lab*. Retrieved January 20, 2026, from https://durrantlab.pitt.edu/fpocketweb-download/

Friedrichs, M. S., Eastman, P., Vaidyanathan, V., Houston, M., Legrand, S., Beberg, A. L., Ensign, D. L., Bruns, C. M., & Pande, V. S. (2009). Accelerating molecular dynamic simulation on graphics processing units. *Journal of Computational Chemistry*, *30*(6), 864–872. https://doi.org/10.1002/JCC.21209;JOURNAL:JOURNAL:1096987X;WGROUP:STRING:PUBLICATION

Fröhlich, M., Söllner, J., & Derler, I. (2024). Insights into the dynamics of the Ca2+ release-activated Ca2+ channel pore-forming complex Orai1. *Biochemical Society Transactions*, *52*(2), 747–760. https://doi.org/10.1042/BST20230815

Gao, S., Fan, Y., Chen, L., Lu, J., Xu, T., & Xu, P. (2009). Mechanism of different spatial distributions of Caenorhabditis elegans and human STIM1 at resting state. *Cell Calcium*, *45*(1), 77–88. https://doi.org/10.1016/J.CECA.2008.06.005

Greenberg, R. M. (2005). Ca2+ signalling, voltage-gated Ca2+ channels and praziquantel in flatworm neuromusculature. *Parasitology*, *131*(S1), S97–S108. https://doi.org/10.1017/S0031182005008346

Gwack, Y., Feske, S., Srikanth, S., Hogan, P. G., & Rao, A. (2007). Signalling to transcription: Store-operated Ca2+ entry and NFAT activation in lymphocytes. *Cell Calcium*, *42*(2), 145–156. https://doi.org/10.1016/J.CECA.2007.03.007

Higginbotham, T., Meier, K., Ramírez, J., & Garaizar, A. (2025). Predicting Drug-Polymer Compatibility in Amorphous Solid Dispersions by MD Simulation: On the Trap of Solvation Free Energies. *Molecular Pharmaceutics*, *22*(2), 760–770. https://doi.org/10.1021/ACS.MOLPHARMACEUT.4C00810

Hogan, P. G., & Rao, A. (2015). Store-operated calcium entry: Mechanisms and modulation. *Biochemical and Biophysical Research Communications*, *460*(1), 40–49. https://doi.org/10.1016/J.BBRC.2015.02.110

Hollingsworth, S. A., & Dror, R. O. (2018). Molecular Dynamics Simulation for All. *Neuron*, *99*(6), 1129–1143. https://doi.org/10.1016/J.NEURON.2018.08.011

Hotez, P. J., Brindley, P. J., Bethony, J. M., King, C. H., Pearce, E. J., & Jacobson, J. (2008). Helminth infections: the great neglected tropical diseases. *The Journal of Clinical Investigation*, *118*(4), 1311–1321. https://doi.org/10.1172/JCI34261

Hou, X., Outhwaite, I. R., Pedi, L., & Long, S. B. (2020a). Cryo-em structure of the calcium release-activated calcium channel orai in an open conformation. *ELife*, *9*, 1–27. https://doi.org/10.7554/ELIFE.62772

Hou, X., Outhwaite, I. R., Pedi, L., & Long, S. B. (2020b). Cryo-em structure of the calcium release-activated calcium channel orai in an open conformation. *ELife*, *9*, 1–27. https://doi.org/10.7554/ELIFE.62772

Hou, X., Pedi, L., Diver, M. M., & Long, S. B. (2012a). Crystal structure of the calcium release-activated calcium channel orai. *Science*, *338*(6112), 1308–1313. https://doi.org/10.1126/SCIENCE.1228757;WEBSITE:WEBSITE:AAAS-SITE;JOURNAL:JOURNAL:SCIENCE;WGROUP:STRING:PUBLICATION

Hou, X., Pedi, L., Diver, M. M., & Long, S. B. (2012b). Crystal structure of the calcium release-activated calcium channel orai. *Science*, *338*(6112), 1308–1313. https://doi.org/10.1126/SCIENCE.1228757;WEBSITE:WEBSITE:AAAS-SITE;JOURNAL:JOURNAL:SCIENCE;WGROUP:STRING:PUBLICATION

Irwin, J. J., Tang, K. G., Young, J., Dandarchuluun, C., Wong, B. R., Khurelbaatar, M., Moroz, Y. S., Mayfield, J., & Sayle, R. A. (2020). ZINC20—A Free Ultralarge-

Scale Chemical Database for Ligand Discovery. *Journal of Chemical Information and Modeling*, *60*(12), 6065–6073. https://doi.org/10.1021/ACS.JCIM.0C00675

Jumper, J., Evans, R., Pritzel, A., Green, T., Figurnov, M., Ronneberger, O., Tunyasuvunakool, K., Bates, R., Žídek, A., Potapenko, A., Bridgland, A., Meyer, C., Kohl, S. A. A., Ballard, A. J., Cowie, A., Romera-Paredes, B., Nikolov, S., Jain, R., Adler, J., … Hassabis, D. (2021). Highly accurate protein structure prediction with AlphaFold. *Nature 2021 596:7873*, *596*(7873), 583–589. https://doi.org/10.1038/s41586-021-03819-2

King, C. H. (2019). Helminthiasis Epidemiology and Control: Scoring Successes and Meeting the Remaining Challenges. *Advances in Parasitology*, *103*, 11–30. https://doi.org/10.1016/BS.APAR.2018.08.001

Krogh, A., Larsson, B., Von Heijne, G., & Sonnhammer, E. L. L. (2001). Predicting transmembrane protein topology with a hidden markov model: application to complete genomes. *Journal of Molecular Biology*, *305*(3), 567–580. https://doi.org/10.1006/JMBI.2000.4315

Krücken, J., Fraundorfer, K., Mugisha, J. C., Ramünke, S., Sifft, K. C., Geus, D., Habarugira, F., Ndoli, J., Sendegeya, A., Mukampunga, C., Bayingana, C., Aebischer, T., Demeler, J., Gahutu, J. B., Mockenhaupt, F. P., & von Samson-Himmelstjerna, G. (2017). Reduced efficacy of albendazole against Ascaris lumbricoides in Rwandan schoolchildren. *International Journal for Parasitology. Drugs and Drug Resistance*, *7*(3), 262–271. https://doi.org/10.1016/J.IJPDDR.2017.06.001

Kuzmanic, A., & Zagrovic, B. (2010). Determination of ensemble-average pairwise root mean-square deviation from experimental B-factors. *Biophysical Journal*, *98*(5), 861–871. https://doi.org/10.1016/j.bpj.2009.11.011

Leles, D., Gardner, S. L., Reinhard, K., Ĩiguez, A., & Araujo, A. (2012). Are Ascaris lumbricoides and Ascaris suum a single species? *Parasites & Vectors 2012 5:1*, *5*(1), 42-. https://doi.org/10.1186/1756-3305-5-42

Letunic, I., & Bork, P. (2025). SMART v10: three decades of the protein domain annotation resource. *Nucleic Acids Research*. https://doi.org/10.1093/NAR/GKAF1023

Li, X., Wu, G., Yang, Y., Fu, S., Liu, X., Kang, H., Yang, X., Su, X. C., & Shen, Y. (2017). Calmodulin dissociates the STIM1-Orai1 complex and STIM1 oligomers. *Nature Communications*, *8*(1), 1–14. https://doi.org/10.1038/S41467-017-01135-W;SUBJMETA

Liou, J., Kim, M. L., Won, D. H., Jones, J. T., Myers, J. W., Ferrell, J. E., & Meyer, T. (2005). STIM is a Ca2+ sensor essential for Ca2+-store- depletion-triggered Ca2+ influx. *Current Biology*, *15*(13), 1235–1241. https://doi.org/10.1016/j.cub.2005.05.055

Lupas, A. (1997). Predicting coiled-coil regions in proteins. *Current Opinion in Structural Biology*, *7*(3), 388–393. https://doi.org/10.1016/S0959-440X(97)80056-5

Ma, G., Wei, M., He, L., Liu, C., Wu, B., Zhang, S. L., Jing, J., Liang, X., Senes, A., Tan, P., Li, S., Sun, A., Bi, Y., Zhong, L., Si, H., Shen, Y., Li, M., Lee, M. S., Zhou, W., … Zhou, Y. (2015). Inside-out Ca2+ signalling prompted by STIM1 conformational switch. *Nature Communications 2015 6:1*, *6*(1), 7826-. https://doi.org/10.1038/ncomms8826

Maia, C. V. de A., Hassum, I. C., & Valladares, G. S. (2015). PARASITOSES INTESTINAIS EM USUÁRIOS DO SUS EM LIMOEIRO DO NORTE, CEARÁ, ANTES DE EXPANSÃO DE SISTEMA DE ESGOTAMENTO SANITÁRIO. *HOLOS*, *2*, 98–109. https://doi.org/10.15628/HOLOS.2015.1973

McNally, B. A., & Prakriya, M. (2012). Permeation, selectivity and gating in store-operated CRAC channels. *Journal of Physiology*, *590*(17), 4179–4191. https://doi.org/10.1113/JPHYSIOL.2012.233098;CTYPE:STRING:JOURNAL

McVeigh, P. (2020). Post-genomic progress in helminth parasitology. *Parasitology*, *147*(8), 835–840. https://doi.org/10.1017/S0031182020000591

Melo, M. do C. B. de, Klem, V. G. Q., Mota, J. A. C., & Penna, F. J. (2004). Parasitoses intestinais. *Rev. Méd. Minas Gerais*, 3–12.

Ministério da Saúde do Brasil. (n.d.). *Esquistossomose — Ministério da Saúde*. Retrieved January 9, 2026, from https://www.gov.br/saude/pt-br/assuntos/saude-de-a-a-z/e/esquistossomose

Molehin, A. J. (2020). Schistosomiasis vaccine development: Update on human clinical trials. *Journal of Biomedical Science*, *27*(1), 1–7. https://doi.org/10.1186/S12929-020-0621-Y/TABLES/1

Morris, G. M., Ruth, H., Lindstrom, W., Sanner, M. F., Belew, R. K., Goodsell, D. S., & Olson, A. J. (2009). Software news and updates AutoDock4 and AutoDockTools4: Automated docking with selective receptor flexibility. *Journal of Computational Chemistry*, *30*(16), 2785–2791. https://doi.org/10.1002/JCC.21256;PAGE:STRING:ARTICLE/CHAPTER

Murray, P. R. ., Rosenthal, K. S. ., & Pfaller, M. A. . (2005). *Medical microbiology*. Elsevier Mosby. chrome-extension://efaidnbmnnnibpcajpcglclefindmkaj/https://parabolasdocotidiano.wordpress.com/wp-content/uploads/2011/10/microbiologia_murray.pdf

Narayanasamy, S., Ong, H. L., & Ambudkar, I. S. (2024). A Deep Dive into the N-Terminus of STIM Proteins: Structure–Function Analysis and Evolutionary Significance of the Functional Domains. *Biomolecules 2024, Vol. 14, Page 1200*, *14*(10), 1200. https://doi.org/10.3390/BIOM14101200

Oliveira de Freitas, E., & Oliveira, D. F. G. T. (2015). *Imunologia, parasitologia e hematologia aplicadas à biotecnologia - Minha Biblioteca*. https://minhabiblioteca.com.br/catalogo/livro/74545/imunologia-parasitologia-e-hematologia-aplicadas-biotecnologia/

Park, S. K., Gunaratne, G. S., Chulkov, E. G., Moehring, F., McCusker, P., Dosa, P. I., Chan, J. D., Stucky, C. L., & Marchant, J. S. (2019). The anthelmintic drug praziquantel activates a schistosome transient receptor potential channel. *Journal of Biological Chemistry*, *294*(49), 18873–18880. https://doi.org/10.1074/JBC.AC119.011093

Prakriya, M., Feske, S., Gwack, Y., Srikanth, S., Rao, A., & Hogan, P. G. (2006). Orai1 is an essential pore subunit of the CRAC channel. *Nature 2006 443:7108*, *443*(7108), 230–233. https://doi.org/10.1038/nature05122

Prakriya, M., & Lewis, R. S. (2015). Store-Operated Calcium Channels. *Https://Doi.Org/10.1152/Physrev.00020.2014*, *95*(4), 1383–1436. https://doi.org/10.1152/PHYSREV.00020.2014

Princen, K., Van Dooren, T., van Gorsel, M., Louros, N., Yang, X., Dumbacher, M., Bastiaens, I., Coupet, K., Dupont, S., Cuveliers, E., Lauwers, A., Laghmouchi, M., Vanwelden, T., Carmans, S., Van Damme, N., Duhamel, H., Vansteenkiste, S., Prerad, J., Pipeleers, K., … Griffioen, G. (2024). Pharmacological modulation of septins restores calcium homeostasis and is neuroprotective in models of Alzheimer's disease. *Science*, *384*(6699). https://doi.org/10.1126/SCIENCE.ADD6260/SUPPL_FILE/SCIENCE.ADD6260_MDAR_REPRODUCIBILITY_CHECKLIST.PDF

PyMOL. (2025, June). *PyMOL | pymol.org*. https://www.pymol.org/

Sayers, E. W., Beck, J., Bolton, E. E., Bourexis, D., Brister, J. R., Canese, K., Comeau, D. C., Funk, K., Kim, S., Klimke, W., Marchler-Bauer, A., Landrum, M., Lathrop, S., Lu, Z., Madden, T. L., O'Leary, N., Phan, L., Rangwala, S. H., Schneider, V. A., … Sherry, S. T. (2021). Database resources of the National Center for Biotechnology Information. *Nucleic Acids Research*, *49*(D1), D10–D17. https://doi.org/10.1093/NAR/GKAA892

Schindelin, J., Arganda-Carreras, I., Frise, E., Kaynig, V., Longair, M., Pietzsch, T., Preibisch, S., Rueden, C., Saalfeld, S., Schmid, B., Tinevez, J. Y., White, D. J., Hartenstein, V., Eliceiri, K., Tomancak, P., & Cardona, A. (2012). Fiji: an open-source platform for biological-image analysis. *Nature Methods 2012 9:7*, *9*(7), 676–682. https://doi.org/10.1038/nmeth.2019

Schoch, C. L., Ciufo, S., Domrachev, M., Hotton, C. L., Kannan, S., Khovanskaya, R., Leipe, D., McVeigh, R., O'Neill, K., Robbertse, B., Sharma, S., Soussov, V., Sullivan, J. P., Sun, L., Turner, S., & Karsch-Mizrachi, I. (2020a). NCBI Taxonomy: A comprehensive update on curation, resources and tools. *Database*, *2020*. https://doi.org/10.1093/DATABASE/BAAA062

Schoch, C. L., Ciufo, S., Domrachev, M., Hotton, C. L., Kannan, S., Khovanskaya, R., Leipe, D., McVeigh, R., O'Neill, K., Robbertse, B., Sharma, S., Soussov, V., Sullivan, J. P., Sun, L., Turner, S., & Karsch-Mizrachi, I. (2020b). NCBI Taxonomy: A comprehensive update on curation, resources and tools. *Database*, *2020*. https://doi.org/10.1093/DATABASE/BAAA062

Silva Teixeira, A. G., Barbosa Santos, F., Rodrigues Santos, G., De Sousa Santos, M. do R., & Meira Rodrigues, G. (2018). *OS EFEITOS DO SANEAMETO BÁSICO PRECÁRIO PARA O AUMENTO DA ASCARIS LUMBRICOIDES | Teixeira | Revista Brasileira de Pesquisa em Ciências da Saúde*. https://revistas.icesp.br/index.php/RBPeCS/article/view/169

Siqueira, B. R., Patrícia Gomez, A., Silva Santos, S., & Alberto Santana, L. (2020). *Parasitologia - fundamentos e prática clínica* (Guanabara Koogan).

Stathopulos, P. B., Schindl, R., Fahrner, M., Zheng, L., Gasmi-Seabrook, G. M., Muik, M., Romanin, C., & Ikura, M. (2013). STIM1/Orai1 coiled-coil interplay in the regulation of store-operated calcium entry. *Nature Communications 2013 4:1*, *4*(1), 2963-. https://doi.org/10.1038/ncomms3963

Stathopulos, P. B., Zheng, L., Li, G. Y., Plevin, M. J., & Ikura, M. (2008). Structural and Mechanistic Insights into STIM1-Mediated Initiation of Store-Operated Calcium Entry. *Cell*, *135*(1), 110–122. https://doi.org/10.1016/j.cell.2008.08.006

Strange, K., Yan, X., Lorin-Nebel, C., & Xing, J. (2007). Physiological roles of STIM1 and Orai1 homologs and CRAC channels in the genetic model organism Caenorhabditis elegans. *Cell Calcium*, *42*(2), 193–203. https://doi.org/10.1016/J.CECA.2007.02.007

Thomas, C. M., & Timson, D. J. (2018). The Mechanism of Action of Praziquantel: Six Hypotheses. *Current Topics in Medicinal Chemistry*, *18*(18), 1575–1584. https://doi.org/10.2174/1568026618666181029143214

Thomas, P., & Smart, T. G. (2005). HEK293 cell line: A vehicle for the expression of recombinant proteins. *Journal of Pharmacological and Toxicological Methods*, *51*(3), 187–200. https://doi.org/10.1016/J.VASCN.2004.08.014

Tiffner, A., & Derler, I. (2020). Molecular Choreography and Structure of Ca2+ Release-Activated Ca2+ (CRAC) and KCa2+ Channels and Their Relevance in Disease with Special Focus on Cancer. *Membranes 2020, Vol. 10, Page 425*, *10*(12), 425. https://doi.org/10.3390/MEMBRANES10120425

Tiffner, A., Maltan, L., Weiß, S., & Derler, I. (2021). The Orai Pore Opening Mechanism. *International Journal of Molecular Sciences 2021, Vol. 22, Page 533*, *22*(2), 533. https://doi.org/10.3390/IJMS22020533

Trott, O., & Olson, A. J. (2010). AutoDock Vina: Improving the speed and accuracy of docking with a new scoring function, efficient optimization, and multithreading.

Journal of Computational Chemistry, *31*(2), 455–461. https://doi.org/10.1002/JCC.21334;CTYPE:STRING:JOURNAL

UniProt AlOrai. (n.d.). *Protein orai - Ascaris lumbricoides (Giant roundworm) | UniProtKB | UniProt*. Retrieved January 16, 2026, from https://www.uniprot.org/uniprotkb/A0A0M3IB65/entry

UniProt AlSTIM. (n.d.). *SAM domain-containing protein - Ascaris lumbricoides (Giant roundworm) | UniProtKB | UniProt*. Retrieved January 16, 2026, from https://www.uniprot.org/uniprotkb/A0A0M3HP42/entry

UniProt SmOrai. (n.d.). *Zgc: - Schistosoma mansoni (Blood fluke) | UniProtKB | UniProt*. Retrieved January 16, 2026, from https://www.uniprot.org/uniprotkb/G4VF37/entry

UniProt SmSTIM. (n.d.). *SAM domain-containing protein - Schistosoma mansoni (Blood fluke) | UniProtKB | UniProt*. Retrieved January 16, 2026, from https://www.uniprot.org/uniprotkb/A0A5K4F914/entry#sequences

Urbano, F. M. (2020). *Parasitologia Contemporânea*. Guanabara Koogan. https://integrada.minhabiblioteca.com.br/reader/books/9788527737166/epubcfi/6/46[%3Bvnd.vst.idref%3Dchapter13]!/4/90[fig13-10]/2%4051:26

Utzinger, J., & Keiser, J. (2004). Schistosomiasis and soil-transmitted helminthiasis: common drugs for treatment and control. *Expert Opinion on Pharmacotherapy*, *5*(2), 263–285. https://doi.org/10.1517/14656566.5.2.263

Waldherr, L., Tiffner, A., Mishra, D., Sallinger, M., Schober, R., Frischauf, I., Schmidt, T., Handl, V., Sagmeister, P., Köckinger, M., Derler, I., Üçal, M., Bonhenry, D., Patz, S., & Schindl, R. (2020). Blockage of Store-Operated Ca2+ Influx by Synta66 is Mediated by Direct Inhibition of the Ca2+ Selective Orai1 Pore. *Cancers 2020, Vol. 12, Page 2876*, *12*(10), 2876. https://doi.org/10.3390/CANCERS12102876

Waterhouse, A. M., Procter, J. B., Martin, D. M. A., Clamp, M., & Barton, G. J. (2009). Jalview Version 2—a multiple sequence alignment editor and analysis workbench. *Bioinformatics*, *25*(9), 1189–1191. https://doi.org/10.1093/BIOINFORMATICS/BTP033

Webb, B., & Sali, A. (2016). Comparative protein structure modeling using MODELLER. *Current Protocols in Bioinformatics*, *2016*(1), 5.6.1-5.6.37. https://doi.org/10.1002/CPBI.3;JOURNAL:JOURNAL:1934340X;WGROUP:STRING:PUBLICATION

WHO. (2011). *Helminth control in school-age children : a guide for managers of control programmes*. World Health Organization.

WHO. (2023a). Effect of preventive chemotherapy with praziquantel on schistosomiasis among school-aged children in sub-Saharan Africa: a

spatiotemporal modelling study. *The Lancet Infectious Diseases*, *22*(1), 136–149. https://doi.org/10.1016/S1473-3099(21)00090-6

WHO. (2023b). *Soil-transmitted helminth infections*. https://www.who.int/news-room/fact-sheets/detail/soil-transmitted-helminth-infections?utm_source=

WHO. (2024). *Schistosomiasis | World Health Organization*. https://apps.who.int/neglected_diseases/ntddata/sch/sch.html

Yeung, P. S. W., Yamashita, M., & Prakriya, M. (2020). Molecular basis of allosteric Orai1 channel activation by STIM1. *Journal of Physiology*, *598*(9), 1707–1723. https://doi.org/10.1113/JP276550;REQUESTEDJOURNAL:JOURNAL:14697793;WEBSITE:WEBSITE:PHYSOC;JOURNAL:JOURNAL:14697793;ISSUE:ISSUE:DOI

Yuan, J. P., Zeng, W., Dorwart, M. R., Choi, Y. J., Worley, P. F., & Muallem, S. (2009). SOAR and the polybasic STIM1 domains gate and regulate Orai channels. *Nature Cell Biology 2009 11:3*, *11*(3), 337–343. https://doi.org/10.1038/ncb1842

Zeibig, E. (2014). *Parasitologia Clínica - Uma Abordagem Clínico-Laboratorial* (Guanabara Koogan, Ed.; 2ª Edición).

Zeraik, A. E., Gudlur, A., Stauderman, K. A., Veliçelebi, G., Ulian de Araujo, P., & Hogan, P. G. (n.d.). *Mechanisms determining Schistosoma mansoni CRAC channel activation*.